Tomas Bata University in Zlín
Faculty of Technology

Doctoral Thesis

Vlastnosti polymerních kompozitů pohlcující elektromagnetické vlny

Electromagnetic wave absorbing properties of polymer composites

Author: **Ing. Marek Gořalík**

Degree programme: Chemistry and Materials Technology (P2808)

Degree course: Technology of Macromolecular Compounds (2808V006)

Supervisor: Prof. Ing. Jarmila Vilčáková, Ph.D.

Consultant: Professor Extraordinary, MSc. Natalia Kazantseva, CSc.

External examiners: doc. Ing. et Ing. Ivo Kuřitka, Ph.D. et Ph.D.

                        doc. Dr. Ing. Vladimír Pavlínek

                        Prof. RNDr. Miroslav Raab, CSc.

Zlín, October 2022

Klíčová slova: *polymerní kompozitní materiály, elektrické a magnetické vlastnosti, reflexní ztráty, radioabsorbéry*

Keywords: *polymer composite materials, electrical and magnetic properties, reflection loss, radio-absorber*

Full text of the doctoral thesis is available in the Library of TBU in Zlín.

ABSTRACT

This work is focused on the optimization of electromagnetic and mechanical properties of magnetic polymer composites for electromagnetic interference (EMI) applications as radio absorbers (RAs). Polymer composites with a dual-phase polymer matrix, vinyl-terminated polydimethylsiloxane (PDMS) in epoxy resin (ER), acrylonitrile-butadiene rubber (NBR), and a propylene-based thermoplastic elastomer (TPE) matrix were investigated for the fabricating of highly filled manganese-zinc ferrite (MnZn), carbonyl iron (CI), carbon black (CB) and carbon nanotube (CNT) composites with the goals of enhanced radio-absorption and mechanical properties. The dielectric and magnetic properties of the composites were determined by the type, concentration, and polymer matrix composition. Increasing the filler and PDMS concentration leads to an increase in magnetic losses due to a decrease in the demagnetizing field. The electromagnetic properties of the composites were investigated in the radio-frequency (RF) band using the impedance method (1 MHz $-$ 3 GHz). Based on the complex permittivity ($\varepsilon*$) and complex permeability ($\mu*$), the reflection loss RL (dB) of single-layer RAs was calculated. The RAs with a MnZn ferrite and CI demonstrated better bandwidth performance in comparison with RAs based on carbon fillers, due to a proper ratio between $\varepsilon*$ and $\mu*$. According to the dynamic-mechanical analysis (DMA) and Charpy impact strength, the significant increase of stiffness up to 125% and the impact strength up to 150% was achieved due to the optimal composition of the polymer matrix and the filler. The results obtained in the study indicate the possibilities of the preparation of ER and elastomeric magnetic composites able to shield an electromagnetic field by absorption mechanisms.

3

ABSTRAKT

Tato práce je zaměřena na optimalizaci elektromagnetických a mechanických vlastností magnetických polymerních kompozitů jako radioabsorbérů pro aplikace v oblasti elektromagnetické interference (EMI). Polymerní kompozity s dvoufázovou polymerní matricí, obsahující polydimethylsiloxan (PDMS) v epoxidové pryskyřici (ER) byly využity pro výrobu vysoce plněných kompozitů s mangano-zinečnatým feritem (MnZn) a karbonylovým železem (CI) s ohledem na radioabsorpční a mechanické vlastnosti. Dále byly připraveny elastomerní kompozity s matricí akrylonitril-butadienového kaučuku (NBR) a termoplastického elastomeru na bázi propylenu (TPE) s plnivem sazí (CB), uhlíkových nanotrubiček (CNT), MnZn a CI. Dielektrické a magnetické vlastnosti kompozitů byly určeny typem, koncentrací a složením polymerní matrice. Zvýšení plniva a koncentrace PDMS vedlo ke zvýšení magnetických ztrát v důsledku poklesu demagnetizačního pole. Elektromagnetické vlastnosti kompozitů byly sledovány v radio-frekvenčním (RF) pásmu s pomocí impedanční metody (1 MHz – 3 GHz). Na základě komplexní permitivity ($\varepsilon*$) a komplexní permeability ($\mu*$) byla vypočtena ztráta odrazem RL (dB) jednovrstvých radioabsorbérů. Kompozity plněné MnZn a CI prokázaly větší poměr šířky operačního pásma k tloušťce ve srovnání s radioabsorbérem na bázi CB a CNT, a to díky správnému poměru mezi komplexní permitivitou $\varepsilon*$ a permeabilitou $\mu*$. Při optimálním složení polymerní matrice (ER/PDMS) a plniva bylo dosaženo výrazného zvýšení tuhosti (125 %) a rázové houževnatosti (150 %) na základě dynamicko-mechanické analýzy (DMA) a rázové zkoušky ve srovnání čistou pryskyřicí. Výsledky, které byly získané při řešení práce poukazují na možnost přípravy magnetických kompozitů na bázi ER a elastomerní matrice, schopných stínit elektromagnetické záření absorpčními mechanismy.

CONTENTS

1. THEORETICAL BACKGROUND

1.1 Introduction to EMI shielding composites

The high-frequency electromagnetic wave has increasingly attracted attention due to the rapid development of telecommunication devices for supporting 4G/5G wireless systems and aircraft applications. Various communication devices such as smartphones, router and electronic components are capable of producing a high-frequency electromagnetic wave, which emits into the surroundings. The electromagnetic wave may interrupt electronic devices, leak information, and threaten public health [1, 2]. To reduce the harmful effects of electromagnetic waves, it is necessary to (1) prevent unwanted radiation from electronics and the formation of radiation smog, and (2) protect sensitive electronics from external radiation.

In the high-frequency and microwave regions, thermal effects occur that lead to heating of living tissue. These effects are given by the conversion of radiation into heat after absorption by tissues. The faster the substance heats up, the more conductive it is (the heating factor is referred to as permittivity and dielectric loss coefficient). A substance with a high heating factor results in a small penetration depth of microwaves, because the energy is converted into heat already in its outer layers. The specific absorption rate (SAR) is an important indicator of the influence of EMI on the human body. The maximum permissible specific absorbed power of electromagnetic radiation for the whole body, which was set by organizations dealing with protection against non-ionizing radiation, is equal to the value of 0.4 W/kg. Hirata (2010) [2] argues that a whole-body averaged SAR below 0.08 W/kg is not hazardous to human health. The International Commission on Non-Ionizing Radiation Protection (ICNIRP), which is currently dealing with the effects of EM fields on living organisms, has determined that electrical devices that can be used without endangering health must meet certain limits, i.e., they must be electromagnetically compatible [3].

Previously, metal plates were used as screens due to their high electrical conductivity. However, problems in processing and manipulation, as well as low flexibility and heaviness, limit the use of metal-based screens [4]. The high performance of electromagnetic polymer composites (EPC) is the result of low weight and density along with high strength and toughness. EPCs can be used to obtain radio-absorbing material (RAM), reducing the reflection of incident electromagnetic waves due to dielectric and/or magnetic losses. It represents a layer (layers) of RAM placed on a highly-conductive surface. For EMI shielding materials based on polymer composites, the desired effect is often achieved due to a high filler concentration or an increase in the coating thickness, which inevitably leads to an increase in the weight of the absorbers [5]. The standard objective for the design of RAMs is to obtain an absorber of minimal thickness that has the lowest possible reflectance within the widest possible operating

bandwidth (bandwidth with the reflection loss RL ≤ 10 dB). To optimize the use of the RAMs in a design, there are sets of parameters that should be taken into account simultaneously: electromagnetic, mechanical and application. From the point of view of electrodynamics, a more efficient absorption of electromagnetic radiation can be achieved by using RAMs with high permeability, high magnetic loss, a favourable form of frequency dependence of complex permeability ($\mu*$) and complex permittivity ($\varepsilon*$), and a proper ratio between the permeability and the permittivity in a certain frequency range [6]. The physical performance guidelines are implied by the mechanical properties, the environmental resistance and the lifespan of RAMs. The application dictates the RAM type and the choice of materials and technology for its design. Common RAMs used for RAs are plastics and elastomers, as well as composites containing conductive and magnetic fillers [7]. RAMs operate in a limited frequency band. The usual method for expanding the operating frequency band of an RA consists of using multilayer structures (such as gradient index materials) instead of single-layer (the Dallenbubach screen) [8]. However, this increases the thickness and the weight of the RAMs, and moreover the design of multilayer absorbers may be highly sensitive to the material parameters in each layer. Thus, designing and fabricating single-layer magnetic type RAMs is still preferable [9, 10].

Currently, there is a tendency to use nanomaterials for fabricating RAs, regardless of the fact that it is a time-consuming and costly process that imposes restrictions for scale production [11]. The common technology for RAM preparation remains as mixing polymers with micron-sized magnetic and/or electrically-conductive fillers [12, 13]. The absorption of electromagnetic waves in RAMs is governed by various loss mechanisms related to the magnetization and electric polarization processes [14]. Taking into account the fact that the frequency dispersion of $\mu*$ and $\varepsilon*$ in these materials is structure-sensitive, one can manipulate the electromagnetic absorbing properties of a material over a wide frequency range by changing the structural-morphological properties of the filler, the volume fraction of the filler, and the microstructure of the composite. Processing the polymeric composites utilizes different techniques, however, more often it is compression moulding due to the simplicity of the operation and capability regarding the polymer matrix selection [7]. The primary function of the polymer in the composites is to bind the filler particles together and ensure the physical-and-mechanical properties. At the same time, depending on the filler type, the polymer can reduce the eddy current losses and facilitate the non-uniform magnetic flux distribution over the enclosed volume, thereby affecting the internal demagnetizing field [15]. Consequently, this results in a decrease in $\mu*$ and an uncontrolled variation of complex permeability as a function of the frequency [16, 17, 18].

The aim of this thesis is the optimization of electromagnetic and mechanical properties of magnetic polymer composites and elastomeric composites (NBR,

TPE), and composites for EMI applications in the radio-frequency band. To this end, highly filled magnetic polymer composites with a dual-phase polymer matrix, vinyl-terminated polydimethylsiloxane (PDMS) in epoxy resin (ER), an elastomeric (NBR) and thermoplastic (TPE) matrix were fabricated. MnZn, CI, CB and CNT fillers were used. RA composites have been investigated with respect to the bandwidth-to-thickness ratio and mechanical properties. The dielectric and magnetic properties of the composites were determined by type and concentration, as well as the polymer matrix composition. It was established that an increase of the filler and the PDMS concentration leads to an increase in magnetic losses due to a decrease in the demagnetizing fields. An elastomeric (NBR) composite filled with a combination of CB, CNT and MnZn ferrite leads to an improvement in the physical-mechanical properties. The electromagnetic properties of the composites were evaluated in the RF band using the impedance method (1 MHz – 3 GHz). Based on the complex permittivity ($\varepsilon*$) and the complex permeability ($\mu*$), the RL (dB) of single-layer RAs were calculated.

1.2 Electromagnetic polymer composites

A composite can be said to be an assembly containing at least two or more non-miscible materials forming a novel material with properties that are quite distinct from those of individual materials [19, 20]. The polymers that are intrinsically non-conducting in nature such as epoxy resin (ER), styrene-butadiene rubber (SBR), acrylonitrile-butadiene rubber (NBR), propylene-based thermoplastic elastomer (TPE), etc., can be made conducting or magnetic by loading then with fillers and thus using them as EMI shielding or radio-absorber materials. Such materials are categorized into two types: dielectric and magnetic, which means that the electromagnetic energy absorption is due to dielectric and/or magnetic losses [21].

A conductive polymer composite is defined as a multicomponent material comprising multiple different phase domains in which at least one type of phase domain is a continuous phase. Thus, a conductive polymer composite (CPC) consists of a nonconductive polymer matrix ($\sigma < 10^{-11}$ S cm^{-1}) and conductive fillers such as inorganic (metals) or organic CB, CNT, graphene or fullerene [22]. The total electrical conductivity of CPC is affected by 1) weight fraction of the filler, 2) the interface between the matrix and filler, at which these are chemically and mechanically combined and 3) processing conditions [23]. Besides, conducting polymers (polyaniline, polypyrrole, polythiophene) are also widely used as EMI shielding materials, magnetic field H_i.

Magnetic polymer composites are prepared by a judicious combination of micron, submicron, and nano-sized magnetic particles with dielectric and

conducting polymers by different methods. Such materials offer significant advantages over metals or ceramic materials due to low weight, high strength, high fatigue, corrosion resistance, and their ability to be easily fabricated into various shapes. Moreover, the combination of polymers with magnetic materials displays new and enhanced electromagnetic properties in specific cases. These properties are attributed to the polymer-filler interaction [24–26].

1.2.1 Polymer matrix

The primary purpose of the polymer matrix in composites is to bind the filler particles together, owing to its cohesive and adhesive characteristics, while the filler particles are responsible for the electromagnetic properties of the composite. However, both the physical-mechanical and electromagnetic properties of the composite significantly depend on how uniformly the filler particles are distributed in the composite [27].

The matrix plays two important roles: acts as a path for stress transfer between fillers and protects the reinforcements from an adverse environment. The matrix has a major influence on composite processing characteristics. Generally, polymer matrixes are classified as thermoplastic, thermosetting polymers and elastomers.

Thermoplastics consist of linear or branched chain molecules having strong intramolecular bonds but weak intermolecular bonds. They can be reshaped by application of heat and pressure and are either semicrystalline or amorphous in structure. They have higher fatigue resistance than most metals. The main disadvantages are faster degradation, and under high stress, fractures occur rather than deformations. Examples include polyethylene, polypropylene, polystyrene, nylons and polycarbonates. Fig. 1 shows the dependence of Young´s modulus (E) on the density (ρ) of materials (polymers, elastomers and composites). Polymers have the value of E in the range from 1 GPa to 20 GPa. Polymer composite materials have a higher stiffness and receive the value of E (12 – 200 GPa); the values of density are in the range (1300 – 1800 kg/m^3).
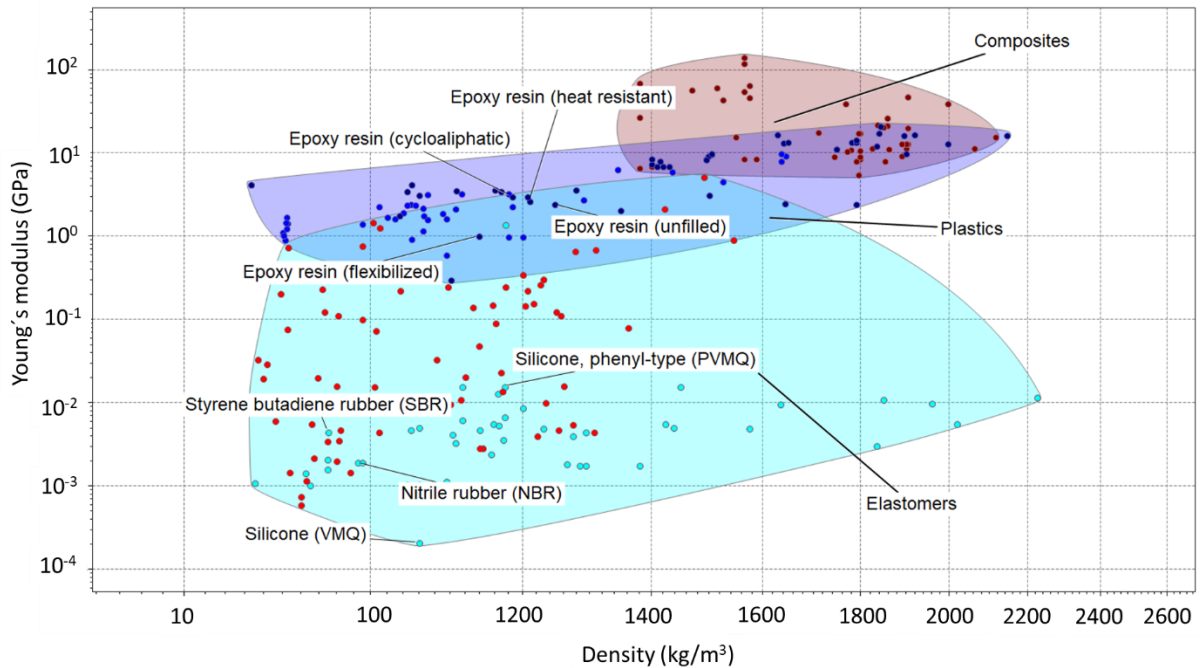
Figure 1: Dependence of Young´s modulus on density

Thermosets have cross-linked or network structures with covalent bonds among all molecules. They do not soften but decompose on heating. Once solidified by the cross-linking process, they cannot be reshaped. Common examples are epoxies, polyesters, phenolic, ureas, melamine resins, and silicone.

Epoxy resins (ER) are a group of viscous liquids containing a molecule epoxide group (oxirane) consisting of an oxygen atom attached to two connected carbon atoms. This group is quite reactive and can react with every compound containing reactive hydrogen. In this study, I concentrated on ERs of the glycidyl group – diglycidyl ether of bisphenol-A (DGEBA). ER enhances chemical resistance, heat resistance and structural integrity. They can improve the material's mechanical properties, and they are used for sealed products due to their resistance to deformation. The matrix is hard, rigid and often brittle. With regard to the low weight requirement of the composite, the epoxy resin reached the value of density in the interval from 1150 to 1250 kg/m^3, with value E (3 – 6 GPa). It therefore seems to be a suitable matrix for the preparation of magnetic polymer composites (Fig. 1).

Fig. 2 shows the dependence of tensile strength on price (CZK/kg) of materials. The price of epoxy resin is in the range of (50 – 80 CZK/kg), while maintaining a sufficiently high tensile strength with value (60 – 100 MPa). This matrix shows a good price-tensile strength ratio.
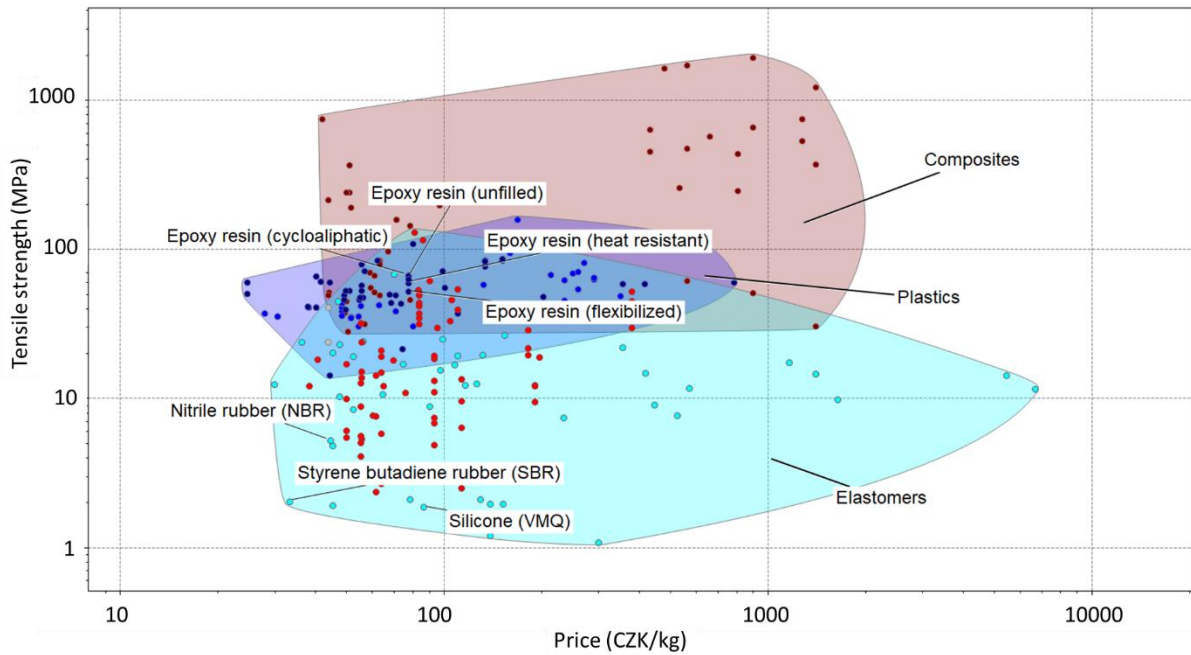
Figure 2: Dependence of tensile strength on price (CZK/kg)

Elastomers

Elastomers are polymers that are held together by weak intermolecular forces, generally (Figs. 1 and 2) exhibiting low Young's modulus (0.01 – 1 GPa) and tensile strength (1 – 100 MPa). They are also viscous and elastic, a property known as viscoelasticity. These plastics have unique properties that allow them to deform or stretch under extreme tensile and compressive loads then return to their original shape. Examples of elastomers include natural rubber, polyurethanes, polybutadiene, silicone, and neoprene.

Styrene-butadiene rubber (SBR)

Chemical formula:
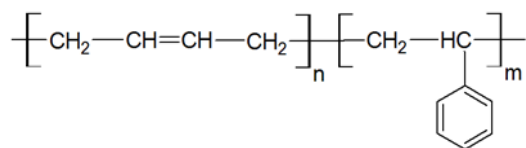
SBR is a mixture of approximately 75 percent butadiene and 25 percent styrene. *Operating temperature range*: -30 – 120°C; *Typical hardness*: Shore "A" 60 – 95. Typical applications include drive couplings, haul-off pads, conveyor belts, shoe soles and heels.

Advantages: resistant to heat and abrasion, and has a low temperature flexibility. SBR can be bonded to several different materials. It also has unique qualities such as good electrical insulation and resistance to alcohol, oxygenated solvents, and mild acids.

13

Limitations: poor when in contact with oils, fuels, strong acids, fat, and greases. Without additives, SBR is also vulnerable to ozone, oxygen, and sunlight.

Acrylonitrile-butadiene rubber (NBR)

Chemical formula:

$$\left[CH_2-CH=CH-CH_2 \right]_n \left[\begin{array}{c} CH-CH_2 \\ | \\ CN \end{array} \right]_m$$
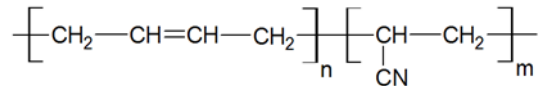
Operating temperature range: -50 – 150°C; *Typical hardness*: Shore "A" 66;

Advantages: Excellent resistance to oil and benzene; superior resistance to petroleum-based hydraulic fluids; good high-temperature performance; good resistance to sunlight and oxidation.

Limitations: Poor resistance to oxygenated solvents.

Poly (dimethylsiloxane)

Chemical formula:

$$\left[\begin{array}{c} CH_3 \\ | \\ O-Si \\ | \\ CH_3 \end{array} \right]_n$$
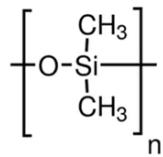
Operating temperature range: -60 – 370°C; *Typical hardness*: Shore "A" 60 – 70.

Advantages: Outstanding heat resistance; excellent flexibility at low temperature; excellent resistance to weather, ozone, sunlight, and oxidation.

Limitations: Fair resistance to oil benzene and solvents; poor resistance to abrasion, tear and cut growth.

Isostatic propylene (iPP)

Chemical formula:

$$\left[\begin{array}{c} CH_2-CH \\ | \\ CH_3 \end{array} \right]_n$$
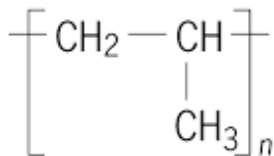
Operating temperature range: -30 – 130°C; *Typical hardness*: Shore "A" 67.

Advantages: Suitable for a wide range of blown and cast film applications, extrusion coating and lamination applications. Excellent adhesion to conventional or metallocene PP and PE. Good elasticity and toughness.

Limitations: degradation from exposure to heat and UV radiation such as that present in sunlight

1.3 Fillers

Fillers are a key component of composite material, not only for improving the stiffness of the composite. In the case of an electrical filler (based on carbon), there is a significant increase in its electrical conductivity, and the magnetic filler will significantly affect the electromagnetic properties.

1.3.1 Carbon-based fillers

Carbon-based fillers exhibit unique properties such as high permittivity, excellent electrical conductivity, low density, high mechanical, chemical and thermal stability, as well as excellent physical properties. Thanks to these attributes, they are suitable candidates for electromagnetic radiation shielding applications. In addition, due to their diverse structure, they have a greater or lesser reinforcing character and not only give the polymer matrices suitable shielding effects, but also improve their physico-mechanical and dynamic properties.

Carbon nanotubes

Carbon nanotubes (CNTs) are an allotropic modification of carbon. The hexagonal grid of carbon atoms provides several spatial arrangement options. The carbon nanotube has sp^2 hybridization, and its structure is achieved by rolling the graphite layer into a cylindrical or tubular shape. Thanks to their exceptional thermal conductivity, electrical and mechanical properties (high strength, stiffness and modulus of elasticity), they have found wide-ranging application in the preparation of nanocomposite materials, especially for the so-called "hi-tech" materials (e.g., aircraft parts, rockets, materials for the military and aerospace industry, and fillers for various types of polymer matrices). CNTs are a form of carbon having a high degree of constitutional organization. They exist in two fundamental forms: single-wall (SWNT) (Fig. 3a) and multi-wall (MWNT) (Fig. 3b). This efficient behaviour is caused by excellent electrical properties and high aspect ratios p (p=L/d, where L= length, 1 – 50 μm and d-diameter, 1-50 nm). They have electrical conductivity of 100 – 101 S/cm, low apparent density, high surface area, porosity, gas permeability and excellent mechanical properties: high tensile strength (13 – 53 GPa) and Young's modulus (1000 – 5000 GPa). CNTs are generally the strongest and hardest materials ever discovered. Due to low

weight, small diameter, high length ratio to aspect ratio, easy percolation, exceptional conductivity and good mechanical strength, CNTs have an advantage over conventional carbon-based fillers. High EMI shielding efficiency can be easily achieved with relatively low content in polymer matrices [50, 51].
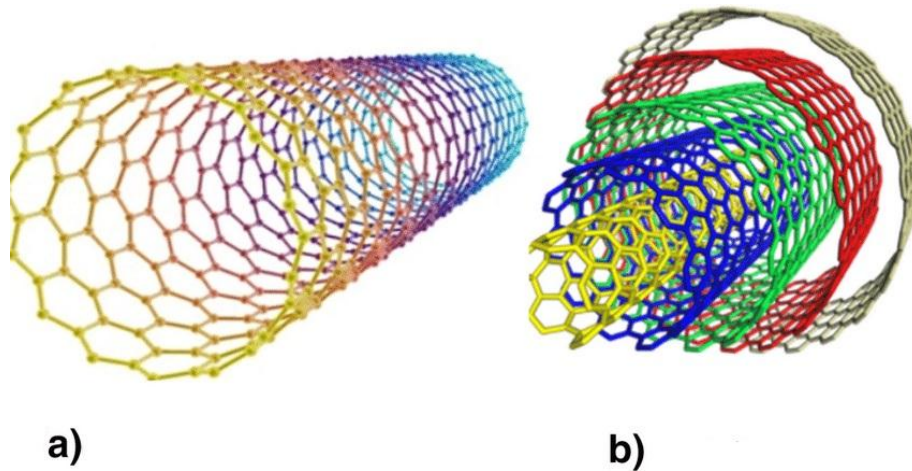

Figure 3: Structures of carbon nanotubes: a) SWCNT and b) MWCNT [52]

Carbon black

Carbon black (CB) is the most widely used carbon-based filler in the rubber industry, mainly due to its low cost, easy production and suitable physical properties. In addition, they absorb UV radiation excellently and protect polymer composites from the effects of UV radiation. CB is used as reinforcing filler in various products, such as tires, conveyor belts, cables, shoes or shock absorbers, and others. CB is produced by the imperfect combustion of gaseous and liquid hydrocarbons, which are mostly obtained from oil. Smaller CB particles together with their higher structure and low volatility (less chemically absorbed oxygen groups) shift the conductivity in polymer composites to higher values [53]. Conductive CB as a reinforcing filler help to improve the conductivity of polymer composites even at lower contents compared to conventional CB. The addition of fillers such as CB to polymeric composites also contributes to increasing the microwave absorption properties of the composite materials. In [54], CB in the amount of $1 - 15$ wt. % was mixed into silicone rubber, and the dielectric and microwave absorption properties as well as the overall shielding efficiency were monitored.

CB is a form of paracrystalline carbon that has a high surface area to volume ratio. It may be partially graphitic with onionskin structure, each layer being graphitic (hexagonal organization of carbon atoms). Domain structures of CB are: particle (~ 50 nm), aggregate (~ 1 μm) and agglomerate (~10 μm). Electrical conductivity of dry compressed CB is of the order 10^4 S/cm with density in the range $(1.7 - 1.9$ g/cm$^3)$. As far as the CB particles are concerned, the aggregate structure (Fig. 4), morphology and micro porosity of particles affect the electrical

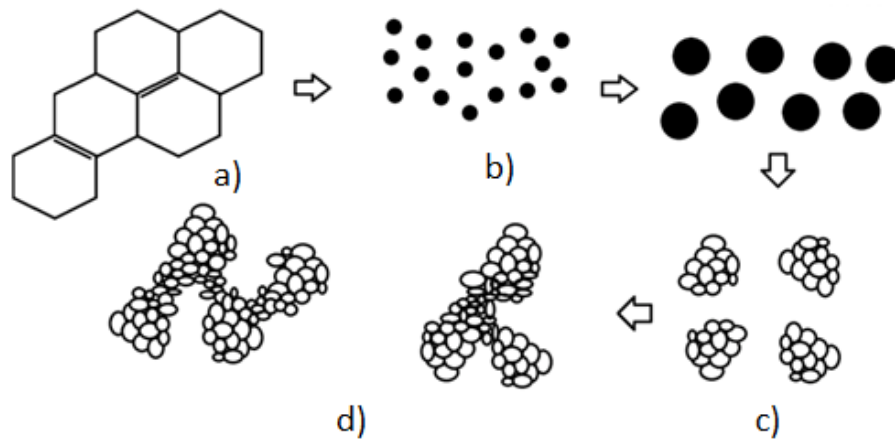conductivity of composite material and percolation threshold.

Figure 4: Carbon black structure: a) graphitic layer, b) primary particles, c) aggregates, d) agglomerates [33]

1.3.2 Ferrites

The ceramic method is one of the most used and oldest methods of ferrite preparation. First, iron oxide and other metal compounds (oxides, carbonates and chlorides) are mixed according to the required composition. The production of ferrites requires the processing of pure raw materials, oxides of the respective metals. The total impurity content must not exceed 0.2%, as the presence of impurities has a major impact on the properties of the final product. The presence of "ferrite poisons" Ba, Si and Na is particularly harmful. The particle size must also be taken into account in the preparation process. The quality of mixing, compression and the reaction of the individual components depend on the particle size. Therefore, it is desirable that all initially raw materials have approximately the same particle size.

The first step of the whole process consists in grinding and mixing the prepared and weighed raw materials in a steel ball mill. The main purpose of a ball (or sand) mill is to ensure that the components are evenly distributed. The process itself can be carried out dry, but mixing in water or ethanol, i.e., in a dispersive medium, is often used. In a ball mill, the whole mixing process takes several hours, after which the mixture is dehydrated by filtration and dried in an oven. After drying in an oven, the powder is subjected to calcination, which is firing in tunnel electric furnaces at a temperature of about 75% of the final sintering temperature, at about 900 to 1100° C. During calcination, cations and anions are pre-diffused, and ferrite grain nuclei are formed. This step is important mainly because carbonates decompose into oxides, removing impurities, thus reducing the possibility of cracking during cooling of the sintered product, which aids in homogenization [28-30]. The resulting calcine is ground again wet (in the presence of water) in a ball mill. This operation is similar to wet mixing, with the

only difference being that the milling time is 20 to 24 hours, instead of 8 hours, to reduce the particle size to 2 to 16 μm. After wet milling, the suspension is dried in an oven. During the grinding of calcine, we can influence not only physical properties such as density, but also magnetic properties. Too small a grain reduces permeability, while a large grain increases eddy current losses. With a homogeneous grain size and small porosity, we can achieve good ferrite quality.

The basic step in the preparation of ferrites is the sintering itself. During sintering between the compressed, partially reacted particles, which press against each other, cavities are formed. In the next step, due to heating, at temperatures above 1000° C, the crystals are completed, thus filling the free volume between the particles and increasing the density. The final state of the magnetic and electrical properties of ferrites strongly depends on the characteristics of the particles and the microstructure after the sintering process. It is known that small particles have a high free surface energy, which makes it possible to obtain higher density values at low calcination and sintering temperatures.

The microstructure of ferrite is determined by various factors: raw material quality, annealing temperature, annealing time and material composition. This is important because the microstructures developed during sintering are largely determined by the powder properties (crystal size and shape, distribution, particle size, and their porosity and agglomeration, chemical and phase composition), which are closely linked to the processing method [31, 32].

1.4 Properties of magnetic materials

Ferrites exhibit macroscopic magnetic properties that are similar to ferromagnetic metals such as iron, nickel, cobalt, and their alloys. For specific applications of these ferromagnets, it is necessary to know their magnetic properties under different operating conditions. Since in these materials the dependence of the magnetic induction B on the intensity of the magnetic field H is not linear, their magnetic properties are expressed mainly by magnetization curves. These magnetization curves are the dependences of the magnetic induction B (or magnetic polarization J) on the intensity of the external magnetic field H. They are obtained by measuring under defined conditions (time course of the magnetizing field, sample shape, etc.). They are most often expressed graphically in the form of the initial magnetization curve, resp. commutation curve and hysteresis loop. Characteristic quantities include, e.g., saturation magnetization (Bs), remanence (Br) and coercivity (Hc) [34]. Fig. 5 shows a hysteresis loop of ferromagnetic material.

In addition to magnetization curves, the properties of ferromagnets are characterized by the dependences of magnetization permeability or magnetic susceptibility on the intensity of the magnetic field. The ability of a substance to change its magnetic induction due to the intensity of the magnetic field is

characterized by the parameter magnetic permeability μ (H/m). Magnetic permeability in ferromagnets depends on the physical properties of the material and is also related to the geometry of the sample. From the point of view of magnetic properties, the dependence of magnetic susceptibility on temperature is also an important characteristic. All magnetic properties depend on the chemical composition and temperature, but not all of them depend on other external conditions, such as the intensity and direction of the magnetic field, structure, mechanical stress, etc. Based on this, the magnetic properties are divided into primary and secondary. Saturated magnetic polarization Js and Curie temperature Tc are among the primary properties. These properties do not depend on the structure and intensity of H, but only on the temperature and chemical composition. Secondary magnetic properties are structurally sensitive and can be classified as static or dynamic, depending on whether they show a frequency dependence of field changes. Magnetization curves, magnetic induction, coercivity, and permeability (susceptibility) are structurally sensitive, but also depend on mechanical stress, etc. [35].
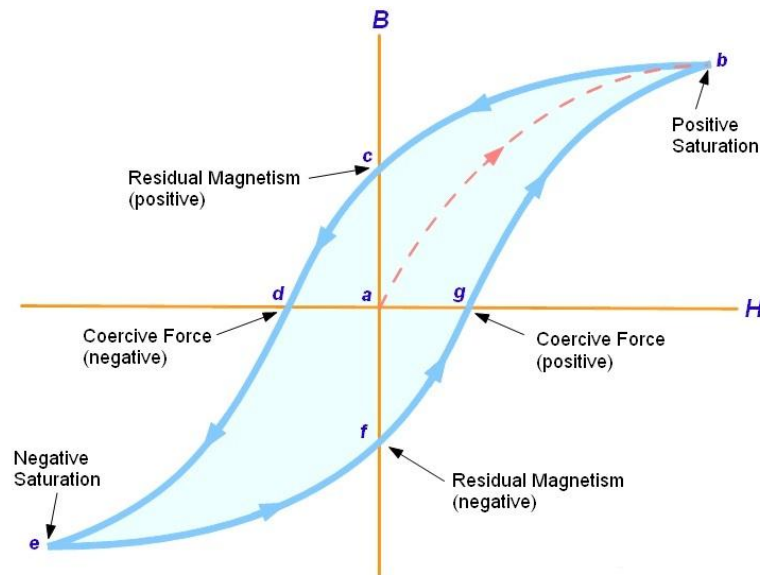
Figure 5: Hysteresis loop of ferromagnetic material [37]

Another important material characteristic of magnetic substances is the value of coercive force Hc [A/m]. According to this value, we usually divide magnetic materials into magnetically soft and magnetically hard. Magnetically soft materials have a narrow hysteresis loop with a corresponding value of Hc < 1000 A.m^{-1}. The small area under the hysteresis loop meets the requirement of small hysteresis losses in the magnets associated with its over magnetization in the alternating field. Magnetically hard materials, on the other hand, have a wide hysteresis loop with a corresponding Hc value > 1000 A/m and large hysteresis losses. During magnetization, part of the energy is converted into heat (domain

rotation). The wider the magnetization curve, the greater the losses, and these losses also increase with frequency [36].

1.4.1 Magnetic soft materials

These are materials that can be easily magnetized (even due to a weak magnetic field) and demagnetized, after the cancellation of the external magnetic field; their own magnetic field virtually disappears. Magnetically soft materials have a narrow hysteresis loop, high permeability, high saturation induction, low coercive intensity, low hysteresis losses, and eddy current losses when alternating magnetization. The production of these materials is demanding. Whether in solid or gaseous form, low impurity content and a defined crystalline structure with an anisotropic texture are required. These requirements are achieved by alloying with suitable additives, selecting raw materials and conducting the melting process so that the content of foreign impurities is reduced. By combining shaping processes with annealing operations, a suitable crystalline structure is achieved. For materials with top magnetic parameters, the final annealing of the formed parts is crucial. The annealing and cooling regime and the cleanliness of the protective atmosphere must be observed. Heated parts must no longer be mechanically formed or firmly clamped [28]. The types of magnetically soft materials used include:

a) Technical pure electrolytic Fe (Armco iron), which is used for the production of carbonyl cores of low-frequency and high-frequency coils on the basis of powder, which is enriched with shellac or resin. Ferrocard magnetic layer materials for recording tapes are obtained by alloying iron with a suitable additive.

b) Magnetically soft ferrites with a spinel structure of iron oxide Fe_2O_3 with nickel-zinc oxides (NiO-ZnO), manganese-zinc oxides (MnO-ZnO), resp. with oxides (Ni-Zn-M) O. Fe_2O_3, where M is one of the elements Cu, Mg, Mn, Pb and others, are characterized by a high value of maximum permeability when used for high-frequency coils with cut-off frequencies of the order of 10^1 to 10^2 MHz. Due to the fact that ferrites belong to magnetic oxides, their advantage over conventional magnets is that they are non-conductive, and therefore, especially at high frequencies, there are no losses due to eddy currents. They have a narrow to rectangular hysteresis loop. They are used in high-frequency electrical engineering (Mn-Zn, Ni-Zn), miniaturization in radio engineering and radio electronics, microwave technology (cores of high-frequency transformers, tape recorders, magnetic amplifiers, ferrite antennas, deflection rings for television cathode ray tubes, cores of broadband, intermediate frequency, output and pulse transformers) [28]. Substituted ferrite powders can be used as fillers in composite materials which are used, e.g., to shield unwanted interfering electromagnetic fields in the microwave frequency domain. A promising perspective in the field of medicine is also the treatment of cancerous tumours using the so-called

magnetic hyperthermia (thermotherapy). Its principle consists in the introduction of magnetic nanoparticles into the tumour tissue and subsequent local overheating by means of an alternating magnetic field with a suitably selected amplitude and frequency (microwave induction heating principle).

1.4.2 Magnetic hard materials

In technical practice, magnetically hard materials are used to produce permanent magnets, which, in the absence of an electric current, serve to create a magnetic field (unlike electromagnets). From a physical point of view, the basis of these properties is usually a defective structure, which makes premagnetization difficult. Another possibility is the use of single-domain particles in which only the effect of a strong external magnetic field can change the direction of spontaneous magnetization and the related direction of magnetic moments. These materials require high values of coercive intensity, remanence and energy product (BH)max [28]: The types of magnetically soft materials used include the following:

a) Al-Ni, Al-Ni-Co, Fe-Co, Mn-Bi and other powder materials suitable for the preparation of small magnets. On the basis of powder materials of cobalt with rare earth metals (Sm, Y, La, Ce, Pr, Nd, Gd, Yb), the most magnetically hardest materials with (BH)max greater than 250 $kJ.m^{-3}$ obtained so far.

b) Magnetically hard ferrites based on hexagonal barium ferrite $BaO.6Fe_2O_3$, in which part of the Ba ions is replaced by Co, Ni, Mg ions, used as cheap materials for permanent magnets of loudspeakers and in other constructions where a small value (BH)max, Br is sufficient, about 0.5 T, and at the same time a considerable temperature dependence is characteristic [38].

1.4.3 Magnetic fillers

These are materials with electric and/or magnetic dipoles suitable for screening applications, where absorption is the dominant screening mechanism. Electric dipoles involve high permittivity materials such as Fe_2O_3, ZrO_2, SiO_2, TiO_2, ZnO or $BaTiO_3$, while magnetic dipoles are present in high permeability materials (e.g., Fe_3O_4, various types of ferrite, mumetal, superpermealloy, etc.). Spinel ferrites with different compositions (e.g., Fe_3O_4, $NiFe_2O_4$, $CoFe_2O_4$, Mn-xZnxFe2O4 and others) are the most common fillers in polymer matrices due to their simple chemical composition and efficient preparation [100–104]. Sýkora et al. [90] investigated and compared the absorption shielding efficiency of prepared composites based on butadiene acrylonitrile rubber (NBR), which were filled with laboratory-prepared magnetically soft lithium ferrite (Li) and manganese-zinc ferrite (MnZn). The results showed that composites containing 27% by volume of fillers demonstrated sufficient absorbent shielding efficiency. NBR/Li ferrite

composites reached an absorption maximum of -30 dB at 1.1 GHz, and NBR/MnZn ferrite composites reached -35 dB at 0.9 GHz.

In addition to spinel ferrites, hexagonal ferrites of the M, X, Y, U, Z or W type are also interesting high-frequency materials absorbing microwave radiation, especially due to planar magnetic anisotropy and resonance in the GHz region [108]. M-types of ferrites such as strontium ferrite ($SrFe_{12}O_{19}$) and barium ferrite ($BaFe_{12}O_{19}$) are typical examples of a hexagonal group that exhibits significant uniaxial anisotropy, strong permeability, and high saturation magnetization [39 – 41].

The most widespread magnetic fillers in magneto-polymeric composites are soft and hard ferrites (MnZn, NiZn, Co_2Z, Co_2W, etc.), ferromagnetic alloys (permalloy, etc.), and CI powders, which are characterized by high saturation magnetization, high initial magnetic permeability, and a wide range of electrical properties.

Electrically conductive fillers, such as metal powder, CB [42, 43] and (CNT) [44] are used to achieve high electrical conductivity of the composite. Filler type and shape, aspect ratio, and dispersion degree of the filler in a polymer matrix significantly influence the total electrical conductivity and magnetic properties.

Manganese-zinc ferrite (MnZn)

Ferrite consists of 53.75 mol % of Fe_2O_3, 26.10 mol % of MnO, and 20.15 mol % of ZnO. This ferrite is characterized by the initial permeability $\mu_i \sim 3000\text{-}5000$, the Curie temperature $T_C = 473$ K [45], the conductivity $\sigma_f = 2\text{x}10^{-2}$ S/m, the density $\rho_f = 4.8$ g/cm^3), specific surface area (10.99 m^2/g), and cost-efficiency. It has high values of resistivity, permeability, and permittivity, and low power losses.

Carbonyl Iron (CI)

Soft magnetic, CI powders are widely used as a filler of radio and microwave absorbers due to their superior electric conductivity, saturation magnetization 1659 kA/m, high Curie-temperature, and broad bandwidth 2 – 18 GHz [46]. In particular, the relatively high density of CI (7.9 g/cm^3) makes it possible to achieve high filler content, and thus improve the electromagnetic absorbing properties of the composites. Meanwhile, the shape of the CI particles such as spherical and flaky may also affect absorption properties due to the different demagnetizing factor [47]. The disadvantage of CI is its rapid oxidation in the air, which affects its magnetic properties. To prevent oxidation, CI particles are modified by coating with SiO_2 or conducting polymers. Moreover, practical applications of CI-filled composites, as in EM wave absorbers, are restricted due to large eddy current effects and high permittivity [48]. From this point of view, eddy current effects of flake-like shaped CI particles are lower compared to spherical particles. Simultaneously, the high complex permittivity of flake-like CI

particles deteriorates the impedance matching between the absorber and free space, which have a significant effect on EM wave absorption [49].

1.5 Electromagnetic wave absorbers

Electromagnetic wave absorbers are devices that convert the energy of incident electromagnetic radiation to heat via conductive, dielectric, and/or magnetic losses. In general, the performance of EM wave absorbing materials depends on EM attenuation capability and impedance matching characteristics [55, 56]. Several types of EWA aborbers are used, as shown in Fig. 6.
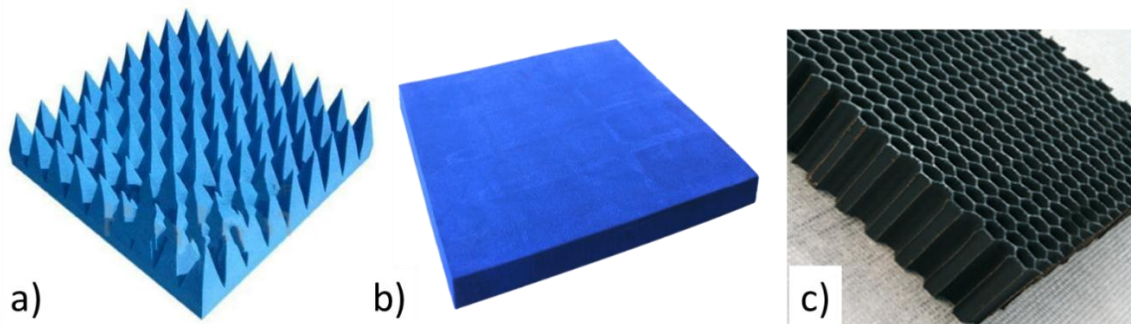

Figure 6: EWAs: a) pyramidal type, b) plane type, c) honeycomb type
[57, 85]

The efficiency of EWAs is normally estimated by two parameters: reflection loss and operating frequency bandwidth. Reflection loss (RL) is a parameter that characterizes the absorbing ability of EWAs in decibels (dB). The electromagnetic absorbing performance of any electromagnetic wave absorbing materials is linked to their intrinsic electromagnetic properties (i.e., conductivity, complex permittivity and permeability), which can be tailored through changing geometry, composition, morphology, and volume fraction of the filler particles, as well as extrinsic properties such as the thickness and working frequencies.

Classifications of EWAs

Electromagnetic wave absorbers can be divided into dielectric absorbers and magnetic absorbers. Dielectric absorbers (CB and CNT) are materials with a low permeability μ', and they are matched with free space by using the resonance thickness. The typical dielectric absorbers are composite materials consisting of a conductive filler. Ferrite is the most frequently used in RAM, due to the combination of electric loss and magnetic loss. Materials for electromagnetic (EM) wave absorbers, such as MnZn and CI, can be added in a polymer matrix to create microwave absorbing composites. The complex permeability of ferrites is frequency dependent. It is caused by the rotation of the magnetization vector and the movement of domain boundaries. The electric losses are caused by the

polarization processes and charge transport.

EWAs can be divided into absorptive and interference types. The choice of the thickness of such materials is defined by the wavelength and the real parts of permittivity and permeability of the composite material. The second type is a group of materials that can convert energy into Joule heat due to weak scattered currents, magnetic-hysteresis, and high-frequency dielectric losses. Often, both physical principles are used in the development of EWAs [107].

Classification by frequency

The level of RL equal to -10 dB corresponds to more than 90% absorption of incident energy. If the bandwidth cut by the level of -10 dB is assumed to be Δf, by dividing the bandwidth values Δf with the centre frequency f_0, the figure of merit can be defined as $\Delta f/f_0$. This characteristic is mainly classified into two types:

a) Narrowband-type Absorber

This is usually associated with the case of the characteristic that can be found in a single-layer wave absorber, or the like. In this case, if the figure of merit is expressed as a percentage, it is approximately $10 - 20\%$. When a narrow frequency band is needed, as in the case of a radar application, this type of absorber is used.

b) Broadband-type Absorber

Notice that the distinction between the case of the wideband and the narrowband types is not clearly defined. In a case where the percentage of $\Delta f/f_0$ is not less than 20%, the EM-wave absorbers often show a peak or twin-peak characteristic [108].

1.5.1 Application of electromagnetic wave absorbers

EM waves can be classified into extremely low frequency (ELF), radio frequency, and microwave radiation depending on the wavelength range (Fig. 7). Generally, EM wave frequencies in the range of 3 to 3000 Hz are generated from the electric wires and electronics used in workplaces and homes. ELF is also emitted from the high-voltage power lines that transmit electricity from the power plant to the areas where electricity is used (Barr et al., 2000) [106].

An electromagnetic field is emitted from devices such as radio, Wi-Fi systems, mobile phones, satellite communication systems, and TV stations. Many of these wireless communication devices are used in human life.

Examples of the main applications of the wave absorber and the related materials used therein are given in Tab. 1.

Table 1: Applications of electromagnetic wave absorbers

| Application examples	EM-wave absorber, and material used
For anechoic chamber (more than 30 MHz)	• Wave absorber of combination multilayer structure with carbon-based material and ferrite • Pyramid-type wave absorber material being produced by mixing carbon in urethane foam material
For electromagnetic interference prevention (for prevention of leakage wave of a microwave oven, wireless LAN measures) (2.45 and 5.2 GHz)	• Wave absorber using rubber ferrite • Wave absorber using resin ferrite • Wave absorber composed of carbon-based dielectric material and building materials
Countermeasure for electronic circuit noise (10 MHz to 5 GHz)	• Sheets composed of special magnetic materials and electrically conductive material • Insulation sheet which has ferrite powder mixed with polymer
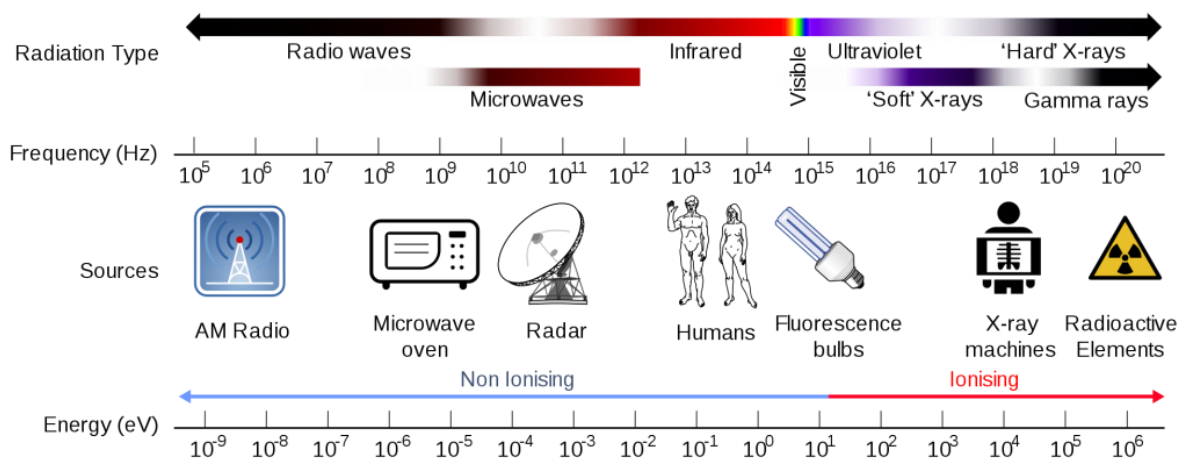
Figure 7: EM band applications in the (RF) and (MW) range [73]

The most promising use of the absorbers are in the field of defence and aeronautics, where they are employed in stealth technology [58, 59], avionics cover surfaces, RCS reduction [60, 61], electromagnetic protection against natural phenomena (lightning), electromagnetic compatibility of electronic devices, high-intensity radiated field protection, and radar absorbing materials [62]. The RF anechoic chambers are designed in such a way that they can completely absorb EM waves and their reflections by covering the interior surfaces (walls, floor, and ceiling) of the chamber with radiation absorber materials to simulate a free space environment. Other areas of applications of EWAs are in the field of consumer and industrial electronics, where they are used for the mitigation of EMI [63], enhancement of the EM compatibility [64] of the devices, subsystems, and systems as well as in EM shielding technology [65, 66]. Electronic circuits and devices that operate at higher frequencies are a major source of EM radiation and require the use of suitable shielding solutions to prevent spurious radiations arising either from their own components and circuitry or from nearby systems and devices.

1.6 EMI shielding mechanism

Shielding of electromagnetic radiation is achieved using three mechanisms: reflection, absorption and multi-reflection. However, shielding caused by reflection is in many cases undesirable due to the secondary interference of reflected EM radiation with the original radiation emitted from other electromagnetic sources, leading to the formation of a secondary EMI effect.

An effective EMI shielding material must meet two conditions: One is to reduce undesirable emissions and the other is to preserve the component from straying external signals. The reflection of radiation for EMI shielding is the primary reason for using charge carriers, which are directly related to the interaction of electromagnetic waves with a shielding material. A good reflector of electromagnetic waves is the conducting material with mobile charge carriers. Absorption of EM radiation is the second element for EMI shielding, the principle of which is that the material's electric and magnetic dipoles interact with the radiation [67]. The existing dipoles in the material interact with the electric and/or magnetic component of the penetrating electromagnetic waves, which transforms the electromagnetic energy to heat. Multiple reflections are another probable interaction of the electromagnetic waves with the material, which takes place when waves reflect from encountered surfaces. The interaction of electromagnetic waves with the material is illustrated in Fig. 8.
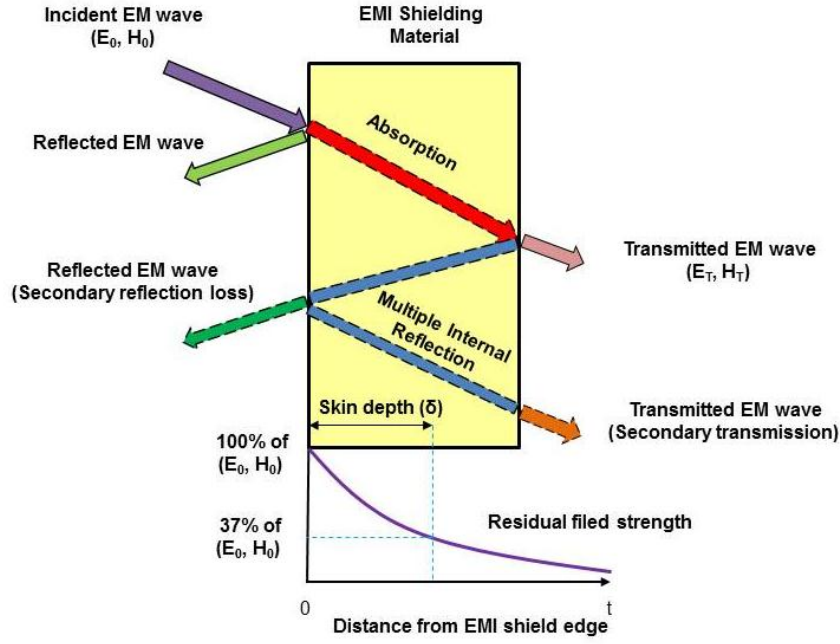
Figure 8: The interaction of electromagnetic waves with the material

1.6.1 Calculation of reflection loss

For a single-layer RA (Fig. 8), the absorption of electromagnetic energy is a function of frequency. Based on a generalized transmission line theory, the reflection loss (RL) can be evaluated from the measured magnetic and dielectric spectra and the RA thickness by the following equations:

$$\text{RL} = 20\log\left|\frac{Z-Z_0}{Z+Z_0}\right| \tag{1}$$

in which the normalized input impedance can be computed according to the transmission-line theory. To satisfy the minimum reflection loss, according to Eq.1, the perfect matching condition is,

$$Z = j\sqrt{\frac{\mu}{\varepsilon}}\tan\left(\frac{2\pi f}{c}\sqrt{\mu^*\varepsilon^*}d\right) \tag{2}$$

where Z is the input impedance of the layer, Z_0 is the wave impedance of the free space; f is the frequency; c is the velocity of the light; d is the layer thickness; ε^* and μ^* are complex relative permittivity and permeability.

If the condition Z=1 is fulfilled, the reflection from the RA is absent. To find these conditions in RAMs, a numerical procedure close to a graphical procedure is usually applied to find the matching frequency f_0 and the matching thickness d_0

27

[17]. The complex permittivity (ε' and ε'') and the complex permeability (μ' and μ'') are important EM parameters for evaluating the microwave absorption performance. The ε' and ε'' are related to the dielectric properties, and the μ' and μ'' are associated with the magnetic properties [68].

From Eq. (1) and (2)

$$d = d' + jd'' = \frac{c}{2\pi\sqrt{\mu^*\varepsilon^*}} \arctan\left(-j\sqrt{\frac{\mu^*}{\varepsilon^*}}\right) \tag{3}$$

Then, Eq. (3) was used to calculate the dependence of the complex parameter d on the frequency f and to find the minima of the ratio $\left|\frac{d''}{d}\right|$ from the obtained curve. Then, the minima for which $\left|\frac{d''}{d}\right| \leq 0.01$ are selected, and the thicknesses $d_0 = d'$ corresponding to these minima are determined. For the selected values of the parameter d_0, the frequency characteristics of the reflection loss are calculated with Eq. (1) and (2).

The electromagnetic waves at higher frequencies penetrate only near the surface of the conducting shield, and the magnitude of the field exponentially decays with thickness. The distance (i.e., the thickness of the shield) required for the electromagnetic wave to be diminished to 1/e or 37% is known as the skin depth (δ), which can be mathematically expressed by Eq. 4 [69].

$$\delta = \sqrt{\frac{1}{\pi f \sigma \mu}} \tag{4}$$

in which, μ – magnetic permeability, $\mu = \mu_0 \cdot \mu_r$, where μ_r is the relative permeability, μ_0 – permeability of free space ($\mu_0 = 4\pi 10^{-7}$ H/m), $\sigma = \omega\varepsilon_0\varepsilon''$ is the AC conductivity, and f is the frequency. Due to the skin effect, composites that contain conductive fillers with a small size are more effective for shielding compared to fillers with large sizes. It is reported that the size of fillers should be smaller or comparable to the surface thickness [70]. Therefore, filler with a size of 1 μm or less is preferred. Achieving good dispersion and distribution of small fillers in polymer matrices is often difficult. They tend to agglomerate, which leads to dispersion inhomogeneity. This can have a negative impact not only on the workability and physical-mechanical properties of composite materials, but also on their shielding effects.

1.6.2 Calculation of shielding effectiveness

The electromagnetic interference shielding refers to the attenuation of the transmitting electromagnetic waves by the shielding material. A high value of

electromagnetic interference (EMI) shielding effectiveness (SE) means less energy transmitted through the shielding material. For commercial applications, a shielding material that possesses the (SE) of 20 dB can block 99% of the incident electromagnetic waves. The electromagnetic shielding effectiveness (SE) can be expressed as the ratio of transmitted power corresponding to the incident power of the EM wave, as in Eq. (5)

$$SE\text{(dB)} = SE_R + SE_A + SE_M = 10\log\left(\frac{P_T}{P_I}\right) = 20\log\left(\frac{E_T}{E_I}\right) = 20\log\left(\frac{H_T}{H_I}\right) \quad (5)$$

where, P_T (E_T or H_T) and P_I (E_I or H_I) symbolize transmitted power and initial power (electric and magnetic field intensity) of the EM wave respectively. Here, SE_R and SE_A are the shielding effectiveness because of reflection and absorption, respectively. SE_M is the shielding effectiveness due to multiple reflections inside the material, which can be negligible when $SE_T > 10$dB. The total shielding effectiveness (SE_T) is given as:

$$SE_T\text{(dB)} = SE_R + SE_A \quad (6)$$

A vector network analyser is a highly demanded and widely utilized instrument to measure complex signals such as complex permittivity (ε_r) or complex permeability (μ_r). The reflected and transmitted waves in the two-port vector analyser, as displayed in Fig. 9 can be mathematically expressed by scattering S-parameters. The shielding effectiveness of the composite filled by MnZn, CI, CB and CNT can be evaluated on the basic of scattering parameters ($S_{11,} S_{21}, S_{21}, S_{22}$) by the following equations (7, 8, 9):

$$SE_R = 10\log_{10}\left(\frac{1}{1-R}\right) = 10\log_{10}\left(\frac{1}{1-|S_{11}|^2}\right) \quad (7)$$

$$SE_A = 10\log_{10}\left(\frac{1-R}{T}\right) = 10\log_{10}\left(\frac{1-|S_{11}|^2}{|S_{21}|^2}\right) \quad (8)$$

$$SE_T = 10\log_{10}\left(\frac{1}{T}\right) = 10\log_{10}\left(\frac{1}{|S_{21}|^2}\right) \quad (9)$$
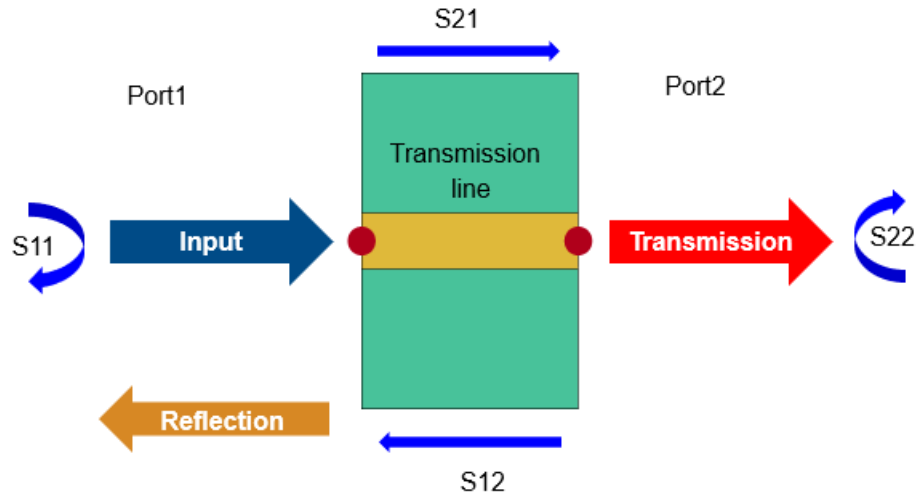
Figure 9: Schematic for the complex scattering parameters of an electromagnetic interference shielding material from a two-port vector network analyser [71]

When an EM wave approaches the shielding material's surface, the intrinsic impedance of which is different from the impedance of the EM wave propagating medium, the wave gets reflected away from the surface and also transmitted inside the material. The strength of the reflected and transmitted waves is governed by the impedance of the medium and material. Further, the strength of the transmitted waves will decrease exponentially as they travel inside the material.

1.7 Measurement techniques

1.7.1 Dielectric and magnetic properties

Absorbing properties of composites are determined by the electrodynamics characteristics of the materials. Magnetic permeability and dielectric permittivity related to a material´s dielectric and magnetic properties belong among the most important characteristics of RAM, and are directly joined with their absorbing properties, which are determine by the electrodynamics characteristics of the materials [72]. Magnetic properties of magnetic composites can be described by complex permeability ($\mu^* = \mu' - i\mu''$), where μ' is real permeability and μ'' is imaginary permeability. Both parts of μ^* increase with the concentration of magnetic filler in the composite. Real permeability (μ') and imaginary permeability (μ'') signify magnetic storage and losses, respectively. The amount of losses can be determined by evaluating the magnetic loss tangent ($\tan\delta_\mu$) and dielectric loss tangent ($\tan\delta_\varepsilon$). Dielectric properties are represented as $\varepsilon^* = \varepsilon' - i\varepsilon''$. In the above equation, parameter real permittivity (ε') signifies the charge storage (or dielectric constant) or electric energy storage capacity, whereas imaginary permittivity (ε'') represents an amount of dielectric dissipation or losses [14]. The values of these parameters can be obtained from measured values

30

of the transmission and reflection coefficients of the material. The establishment of μ^* and ε^* of a material is primarily based on measurements of complex electromagnetic parameters (*S-parameters*), and the reflection and transmission coefficients [74, 75].

1.7.2 Dielectric loss

Based on the Debye theory, the imaginary permittivity ε'' signifies the loss of the capability of electromagnetic energy. The dielectric loss tangent ($\tan\delta\varepsilon$) is the contribution of both polarization loss and conduction loss [76]. The polarization loss can be attributed to dipole orientation (due to bound charges) as well as electronic, ionic, and interfacial polarization (owing to the trapping of space charge). Electronic and ionic polarization contributes only at a very high frequency (above 1000 GHz); therefore, in the low microwave frequency region, their influence can be neglected [77]. Dipole polarization comes about due to the existence of the defects and the residual group in the material, which highly depend on the preparation approach and other preparation conditions, etc. [78]. The interfacial polarization and associated relaxation can be attributed to trapped space charges at the interfaces [14].

1.7.3 Magnetic loss

Magnetic loss generally originates from natural resonance, domain wall resonance, exchange resonance, eddy current loss, etc. [79, 80]. Domain wall resonance occurs under an ac magnetic field, $H = H_o e^{j\omega t}$, and parallel to the plane of the sample material, the domain wall will vibrate at its equilibrium position [81]. Generally, domain wall resonance has a relaxation type permeability spectrum (Debye-type spectrum) [82]. Natural resonance is associated with the magnetization vector that precesses about the static magnetic field, and the energy is absorbed highly from the ac transverse field when its energy is equal to the precessional frequency. It is called ferromagnetic resonance, which was first noticed by Griffiths in 1946 [14, 83].

1.7.4 S-parameters measurement

These techniques include free-space methods, open-ended coaxial-probe techniques, cavity resonators, dielectric-resonator techniques, magnetic material test fixture and transmission-line techniques (Fig. 10). Standard magnetic measurements are based on tests of standard toroid – typically using a toroidal core. Magnetic materials are characterized from an electrical perspective by the values of electrical conductivity, magnetic permeability and dielectric constant.

There are various types of electromagnetic interference shielding measurement arrangements.
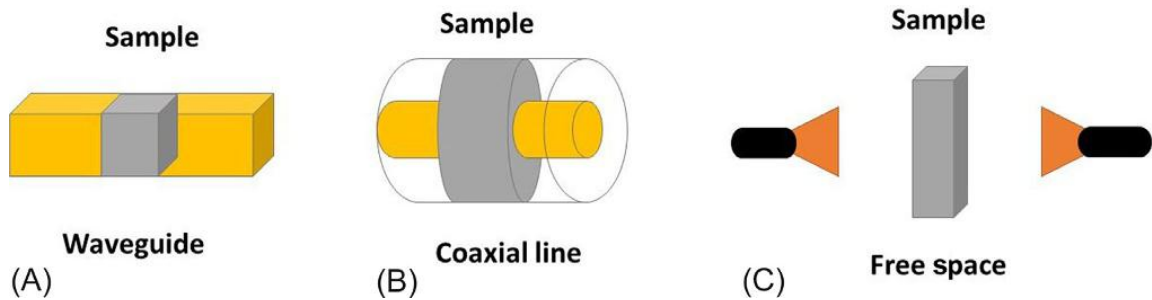

Figure 10: Various types of electromagnetic interference shielding measurement arrangements A) waveguide, B) coaxial line, and C) free space [14]

Impedance method (1 MHz – 3 GHz)

There are many measurement methods to choose from when measuring impedance, each of which has advantages and disadvantages. In measurements from 100 MHz to 3 GHz, the RF impedance method has the best measurement capability.

Free-space method (2 – 20 GHz)

The basic free space measurement system consists of a network analyser, a sample holder, two horn antennas and software. The free-space measurement technique has the advantages of allowing reflection and transmission measurements without any physical contact with the sample. Free-space methods use antennas to focus microwave energy, and a sample is placed perpendicular to the antenna axis. The concept of transmission and reflection FSM is shown in Fig. 11a, b, c. After the measurement, the *S-parameters* are used for extracting the electromagnetic properties of the sample.
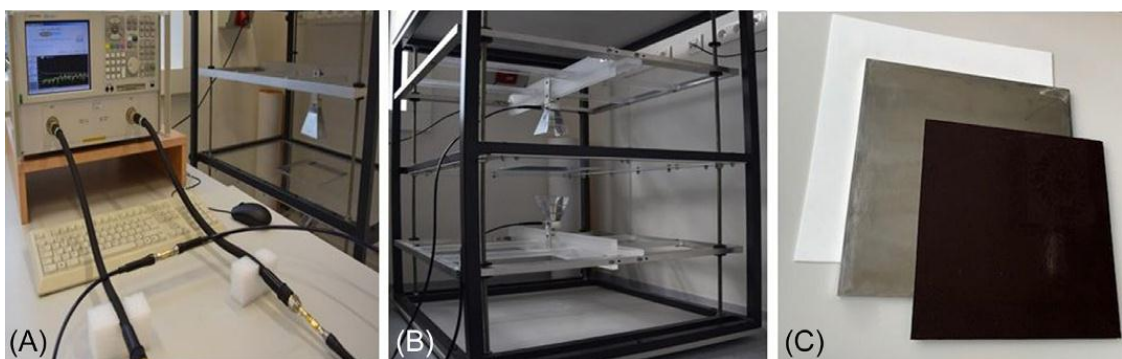

Figure 11: Free-space measurement method a) A two-port (A) PNA-L network analyser (N5230A) b) antennas c) calibration plates

Waveguides

Above 2 GHz, the wavelength is short enough to allow practical, efficient energy transfer by different means. A waveguide is a conducting tube through which energy is transmitted in the form of electromagnetic waves, as shown in Fig. 12. The tube acts as a boundary that confines the waves in the enclosed space. The Faraday cage phenomenon prevents electromagnetic effects from being evident outside the guide. The electromagnetic fields are propagated through the waveguide by means of reflections against its inner walls, which are considered perfect conductors.
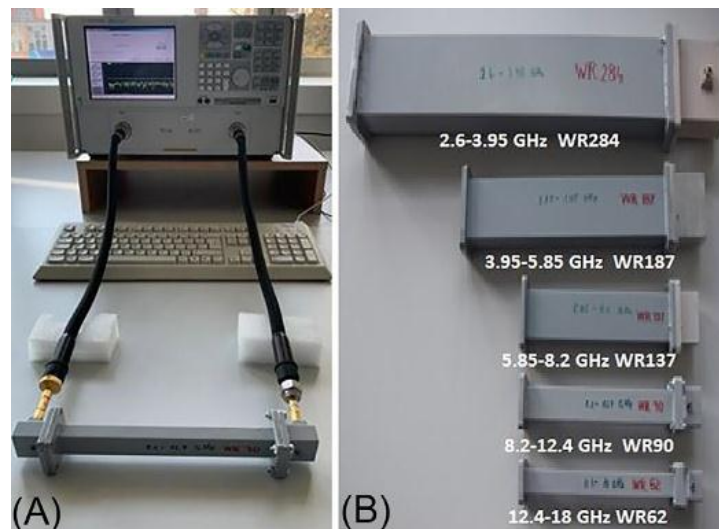
Figure 12: A two-port (A) PNA-L network analyser (N5230A) with (B) waveguide section WR 284, WR 187, WR 137, WR90, and WR 62

2. AIMS OF THE THESIS

The main aim of this work was the development of magnetic type polymer composites for EMI applications as radio absorbers (RAs) and the optimization of their mechanical properties.

To accomplish the aim, the following task was outlined:

a) Application of magnetically soft MnZn, CI, and conductive CB and CNT fillers in ER/PDMS and NBR and TPE rubber matrices with the aim of preparing composite materials with absorption shielding effects of electromagnetic waves.

b) Research on shielding efficiency against an electromagnetic field depending on composite parameters (matrix type, filler type, filler particle size, filler concentration, absorber thickness and operating frequency bandwidth).

c) Study of mechanical properties of polymeric composite materials with an epoxy or elastomeric matrix and electromagnetic filler (MnZn, CI, CB, CNT).

d) The calculations of reflection loss RL (dB) of single-layer RAs were carried out on the basis of the electromagnetic properties of the composites in the RF band using the impedance method (1 MHz − 3 GHz for ER/PDMS and NBR composites and 1 MHz − 18 GHz for TPE composites).

3. EXPERIMENTAL SECTION

3.1 Materials

Sintered MnZn ferrite is a commercially available sintered ferrite produced by Ferropribor, Russian Federation) with high initial permeability ($\mu_i = 3000 - 5000$), a maximum magnetic permeability of μ_{max} ~ 3700-5200, a conductivity of $\sigma_f = 2x10^{-2}$ S/m, and a density of $\rho_f = 4.8$ g/cm^3 [13, 14, 15]. Carbonyl irons (CI) are highly pure spherical iron particles (±98% Fe). CI used in this work was soft grade SL from company BASF with a diameter d50 = 5 μm. Soft grades are annealed in hydrogen atmosphere after thermal decomposition. This process leads to higher particle purity. The epoxy resin used was a bisphenol A diglycidyl ether (DGEBA, D-3415, epoxide equivalent weight = 172 – 176 g, liquid, Sigma Aldrich, USA). The curing agent was an aliphatic amine, diethylenetriamine (DETA-D93856, Sigma Aldrich, USA). Dicumyl peroxide (DCP, Sigma Aldrich, USA) was used as a free radical initiator. Vinyl terminated polydimethylsiloxane (PDMS-VT) (Sigma Aldrich, USA) was supplied in the liquid form. Propylene-based thermoplastic elastomer (TPE), trade name Vistamaxx™ 6202 (ExxonMobil, USA) is primarily composed of isotactic propylene (85 wt. %) repeat units with random ethylene (15 wt. %) distribution produced using metallocene catalyst technology (melt flow index of 7.4 g/10 min, with a density of 0.861 g/cm^3, 190 °C). The main characteristics of the fillers and matrix are presented in Tab. 2 and 3. Acrylonitrile-butadiene rubber (NBR), type SKN 3345, acrylonitrile content 31-33%, ρ = 0.94 g/cm^3 was supplied from Sibur, Russia Federation. Multi-walled CNT (type NC7000, content of carbon 90%, length of tubes is 1.5 μm, diameter of tubes 9.5 nm, specific surface area 250 – 300 m^2/g) was provided from Nanocyl SA, Sambreville, Belgium. CB (type Vulcan XC72, with moderate electrical conductivity, low sulphur and impurity level) was compounded in Vipo, a.s. Partizánske, Slovakia. A standard sulphur-based curing system consisting of activators zinc oxide and stearic acid (Slovlak, Košeca, Slovakia), accelerator N-cyclohexyl-2-benzothiazole sulfenamide (Duslo, Šaľa, Slovakia) and sulphur (Siarkopol, Tarnobrzeg, Poland) was used for cross-linking of composites.

Table 2: Physical-mechanical properties of selected matrix

Type of matrix	Vinyl-terminated polydimethylsiloxane	TPE
Tensile strength, MPa	0.4	5.5
Elongation at break, %	98	2000
Working temperature, °C	-50/153	-30/130
Specific gravity, g/cm^3	0.965	0.862
Viscosity at 25°C, mPa·s	850 - 1150	1137

Table 3: Basic properties of fillers

Filler	Diameter of particles	Purity	Density
	μm	%	g/cm^3
MnZn	45 – 50	99.5	4.8
CI	5	99.5	7.9
CB	0.05	99.5	1.8
CNT	0.03	99.5	1.74

According to the SEM image (Fig. 13a); polycrystalline particles of MnZn ferrite consist of separate grains in the form of polyhedrons with clear-cut boundaries. The CI particles are spherical and varying in size within a few microns in diameter; herewith, a significant part of the particles form irregularly-shaped aggregates (Fig. 13b).
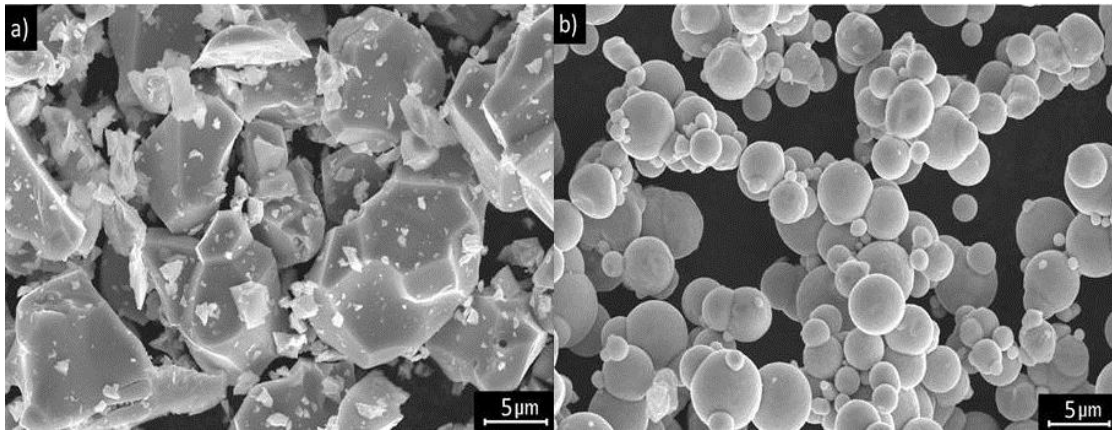
Figure 13: The SEM micrographs of the magnetic filler: a) MnZn ferrite b) CI

3.2 Sample preparation

3.2.1 Polymer blend preparation

An immiscible polymer blend of DGEBA, PDMS (10-30 wt.%) and DCP (0.5 wt.%) was prepared under mechanical stirring (MM-1000, Biosan, Germany) at 300 rpm under a nitrogen atmosphere for 2 hours at 130° C. This mixing procedure resulted in an improvement of the interphase between PDMS and the ER phase, leading to spherical particles and the cross-linking of PDMS.

3.2.2 Fabrication of the ER/PDMS/MnZn and ER/PDMS/CI blends

The obtained blend was loaded with magnetic filler (CI or MnZn ferrite) and stirred at 80 °C for 30 minutes. The concentration of the filler in the blend varied from 50 wt. % up to 80 wt. %. The equimolar amount of the DETA curing agent was added to the mixture after 10 minutes before casting the composition onto a preheated to 70 °C mold. The silicone mould created two types of samples: tablets and sticks. The curing process was performed at 100 °C for 30 minutes and 1 hour at 140 °C. A relaxation process was carried out for 6 h at 60 °C.

3.2.3 Preparation and vulcanization of the NBR/MnZn, NBR/CB and NBR/CNT elastomer composites

The amounts of curing additives were kept constant in all rubber compounds, and there was a change only in the type and amount of the filler. Recalculated values of phr are shown in Tab. 8 – 10. MnZn ferrite in a concentration scale ranging from 100 (48 wt. %) to 500 phr (82 wt. %) was used as filler in the first type of composites (NBR/MnZn). CB was incorporated in the second type (NBR/CB) of composites in the amount ranging from 2.5 phr (2.3 wt. %) to 25 phr (19 wt. %). The usual amount of CB in generally used rubber articles ranges from 10 to 30 phr, and therefore, the choice of CB concentration scale was adopted to this range. In the third composite types, the content of CB and CNT were kept at constant levels 20 phr and 5 phr, and the amount of MnZn ferrite was changed from 100 to 500 phr (44 wt.% – 80 wt.%). The detailed compositions of rubber composites are summarized in Tab. 4 – 7.

Table 4: Composition of composites filled with MnZn

Component	NBR	ZnO	Stearic Acid	CBS	Sulphur	MnZn
content (phr)	100	3	2	1.5	1.5	0-500

Table 5: Composition of composites filled with CB

Component	NBR	ZnO	Stearic Acid	CBS	Sulphur	CB
content (phr)	100	3	2	1.5	1.5	0-25

Table 6: Composition of composites filled with CB and MnZn

Component	NBR	ZnO	Stearic Acid	CBS	Sulfur	CB	MnZn
content (phr)	100	3	2	1.5	1.5	0-25	0-500

Table 7: Composition of composites filled with CNT and MnZn

Component	NBR	ZnO	Stearic Acid	CBS	Sulfur	CNT	MnZn
content (phr)	100	3	2	1.5	1.5	0-25	0-500

The compounding of additives was carried out in two steps using an industrial kneading machine Buzuluk (Buzuluk Inc., Komárov, Czech Republic) and laboratory kneading equipment Brabender (Brabender GmbH & Co. KG, Duisburg, Germany). The speed of the rotor was set up to 50 rpm, and the kneading chamber was heated to 90 °C [84].

In the case of composites filled with ferrite, NBR was first plasticised for 2.5 min. Subsequently, activators were added, and after the next two 2 minutes, filler was applied. The total time of the first step, mixing, was 9 min at 90 °C and 50 rpm. In the second step (4 min, 90 °C, 50 rpm), the accelerator N-cyclohexyl-22benzothiazole sulfenamide (CBS) and sulphur were introduced. Finally, the composites were homogenized in a two-roll calander.

The preparation procedure of composites filled with CB and magnetic filler proceeded in the same way as in the previous case, but the NBR/CB batch was first compounded with pure NBR to reduce the amount of CB to 20 phr (16 wt.%). Then, the compounding procedure followed in the same conditions. The curing process of composites was performed at 160 °C for the optimum curing time under a pressure of 15 MPa by using a hydraulic press Fontijne (Fontijne, Vlaardingen, Holland). Finally, thin sheets (width 15 x 15 cm, thickness 2 mm) of cured rubber compounds were obtained [84].

Table 8. Recalculation from phr of NBR/MnZn and NBR/CB composites to wt. %

NBR/MnZn	phr	wt. %
	100	48
	200	65
	300	73
	400	79
	500	82
NBR/CB		
	2.5	2.3
	5	4.4
	10	8.5
	15	12
	20	16
	25	19

Table 9. Recalculation from phr of NBR/CB20-MnZn hybrid composite to wt. %

NBR/CB20-MnZn	phr CB	phr MnZn	CB wt. %	MnZn wt. %
	20	100	8.7	44
	20	200	6	61
	20	300	4.7	70
	20	400	3.8	76
	20	500	3.2	80

Table 10. Recalculation from phr of NBR/CNT5-MnZn hybrid composite to wt. %

NBR/CNT5-MnZn	phr CNT	phr MnZn	CNT wt. %	MnZn wt. %
	5	100	2.3	45
	5	200	1.6	64
	5	300	1.2	73
	5	400	1	78
	5	500	0.8	81

3.2.4 Preparation of the TPE/MnZn and TPE/CI composites

The homogeneous TPE polymer composites filled with MnZn and CI particles were prepared by mixing both components. The compound was mixed using a micro-compounder (MC5, Xplore Instruments BV, Sittard, The Netherlands) with a capacity of 5 cm^3, consisting of twin screws. The melt mixing conditions were 190 °C for 7 minutes at 150 rpm. Before melt mixing, TPE and fillers were dried in a vacuum oven at 90 °C for 12 h. Further, the prepared TPE-based composites were placed into a silicon mold. The pellets and tablets were created with dimensions of 60 mm × 10 mm × 4 mm and a diameter of 8 mm. The TPE-based composites containing (50 wt. %, 70 wt. %, 80 wt. %) MnZn and CI fillers were studied.

3.3 Characterization techniques

Scanning electron microscopy

To investigate the phase morphology of the epoxy-polydimethylsiloxane/magnetic composites, a VEGA//LMU Tescan scanning electron microscopy (SEM) was used. The SEM images were obtained under conventional secondary electron imaging conditions with an acceleration voltage of 25 kV and a resolution of 3 nm at 30 kV.

X-ray photoelectron spectroscopy (XPS)

The X-ray photoelectron spectroscopy (XPS) signals were recorded using a Thermo Scientific K-AlphaXPS system (Thermo Fisher Scientific, UK) equipped with a micro-focused monochromatic Al Kα X-ray source (1486.68 eV). An X-ray beam of 400 μm in size was used at 6 mA and 12 kV. The spectra were

acquired in the constant analyser energy mode with pass energy of 200 eV for the survey. The narrow regions were collected with pass energy of 50 eV. The charge compensation was achieved with the system flood gun. Version 5.9199 (Thermo Fisher Scientific) was used for digital acquisition and data processing. The spectral calibration was determined using the automated calibration routine and the internal Au, Ag and Cu standards supplied with the K-Alpha system.

DC conductivity

The DC conductivity was measured by a four-point van der Pauw method (Keithley 6517A, USA) with a current meter and a Multimeter (Keithley 2410, USA) as a source.

Magnetic and dielectric spectra

The electromagnetic properties of the composites ($\varepsilon*$ and $\mu*$) in an RF range from 1 MHz to 3 GHz were measured by the impedance method using (Impedance/Material Analyser E4991A, Agilent Technologies USA). The dielectric spectra were measured on the circular samples with a diameter of 15 mm, and the magnetic spectra were measured on the toroidal samples with an outer diameter of 8 mm and an inner diameter of 3.1 mm and 2 mm thickness.

Dynamical mechanical analysis

The dynamical mechanical analysis (DMA) were carried out under dual cantilever geometry in dynamic (frequency/strain experiments) on a Mettler Toledo DMA1 dynamic mechanical thermal analyser (DMTA) equipped with a liquid-nitrogen apparatus operating in a three-point bending mode. The tested samples had a dimension of 35×10×3 mm. The dynamic analysis was carried out from -120 °C to 180 °C at a heating rate of 3 °C/min, with a fixed frequency of 1 Hz and an amplitude of 20 μm.

Charpy impact tests

The Charpy impact tests were performed in accordance with ISO 179 on unnotched izod specimens using an impact tester (Zwick/Roell, Germany). The dimensions of the samples were 35×10×3 mm. The fracture mechanism of the polymer systems was studied on the surface of the fractured area via SEM. The mean values over five specimens are presented.

Tensile tests

The tensile properties of composites were evaluated by using a Zwick Roell/Z 2.5 appliance (Zwick Roell Group, Ulm, Germany). The cross-head speed of the measuring device was set up to 500 mm/min., and the tests were carried out in compliance with the valid technical standards. Dumbbell-shaped test specimens (thickness 2 mm, length 80 mm, width 6.4 mm) were used for measurements.

4. RESULTS AND DISCUSSION

4.1 Morphology

4.1.1 The ER/PDMS/MnZn and ER/PDMS/CI composites

The SEM images of the polymer matrixes and the magnetic composites on their base are shown in Fig. 14. The neat ER shows a smooth fracture surface at the brittle failure (Fig. 14a). The epoxy resin modified by PDMS (10 – 30 wt. %) exhibits a two-phase microstructure consisting of spherical elastomeric particles (15-90 μm) uniformly distributed in the bulk of the ER (Fig. 14c, 3d). In the ER-PDMS SEM images, the presence of plastic shear deformation in composites is also visible, which can be identified by the presence of cracks propagating from the elastomer inclusions as stress concentrators. An increase in the filler content to 70 – 80 wt. % leads to the formation of particle clusters both in the bulk of the composite and at the ER-PDMS-interface (Fig. 14c, d).
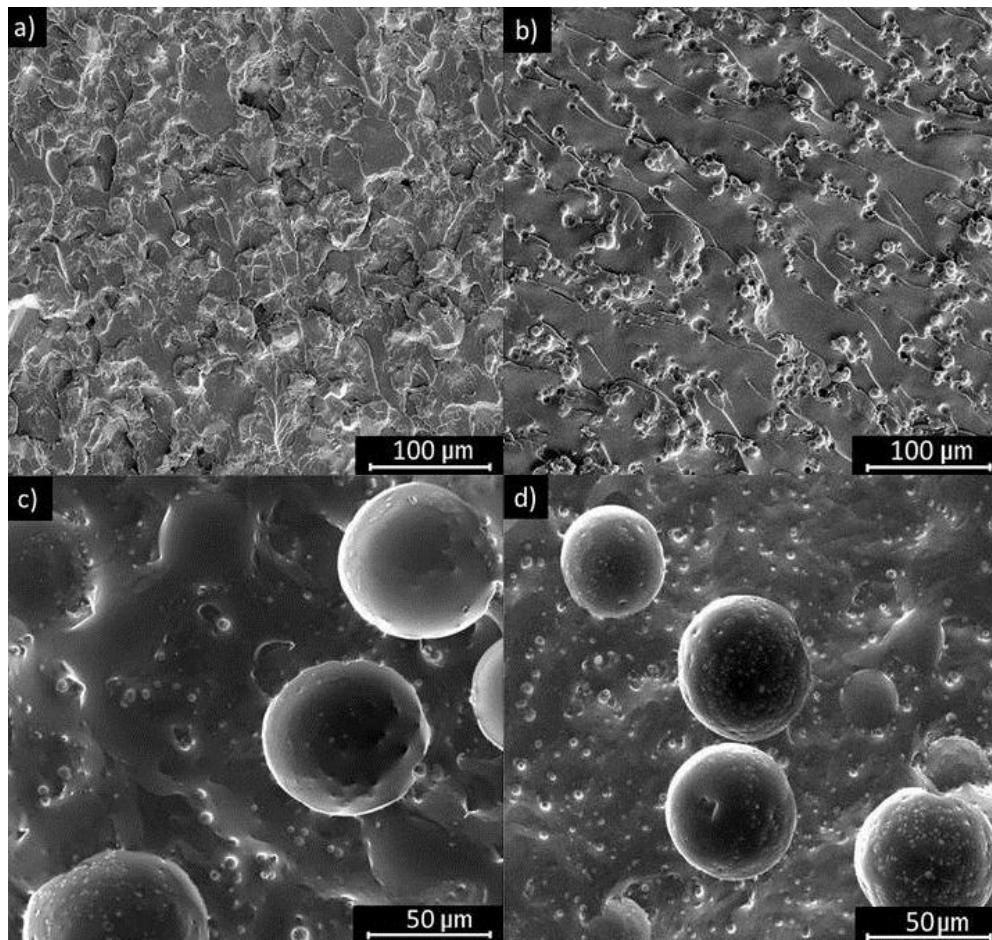
Figure 14: The SEM micrographs of the composites: a) ER/MnZn50 b) ER/CI50 c) ER/PDMS10/CI70 d) ER/PDMS10/CI80

4.1.2 The NBR/MnZn composites

Selected microscopic images of composite materials with quantities of 300 and 500 phr (73 wt. % and 82 wt. %) of the filler MnZn are given in Tab. 4. In Figs. 15 a, b, 16 a, b, SEM images with a magnification of 100x show the distribution of the filler in the used matrix, and at a magnification of 1000x, it is possible to see a more detailed view of the ferrite particles or even agglomerates of filler particles, while the individual phases of composites can be clearly identified. In addition, it is possible to notice defects that are probably caused by freezing the samples below the glass transition temperature and then breaking them in order to obtain fracture surfaces for microscopic analysis. These defects indicate poor adhesion between the filler and the rubber. With SEM images, it is possible to observe the formation of aggregates or agglomerates of magnetic filler particles that are not homogeneously dispersed in the rubber matrix.

The best distribution and dispersion of the filler could be observed in the case of NBR-based composites with 82 wt. % MnZn, precisely because of the high viscosity of the given rubber mixture. In addition, in terms of chemical structure, MnZn ferrite belongs among polar materials, therefore the assumption of mutual adhesion and compatibility with the partially polar rubber matrix (NBR) [84, 85].
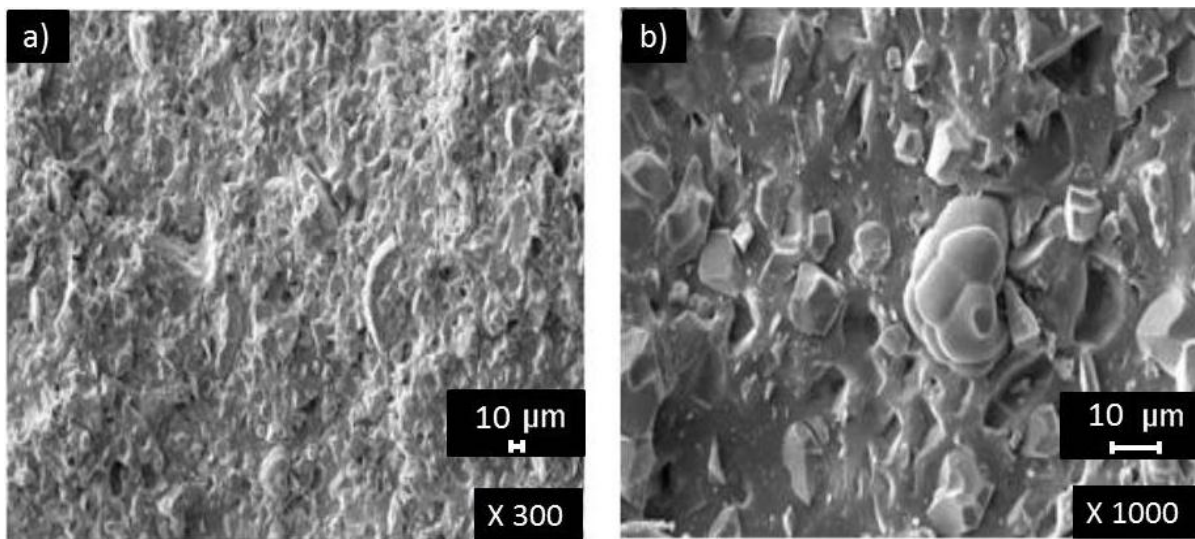
Figure 15: SEM images of NBR composite filled with 300 phr of MnZn
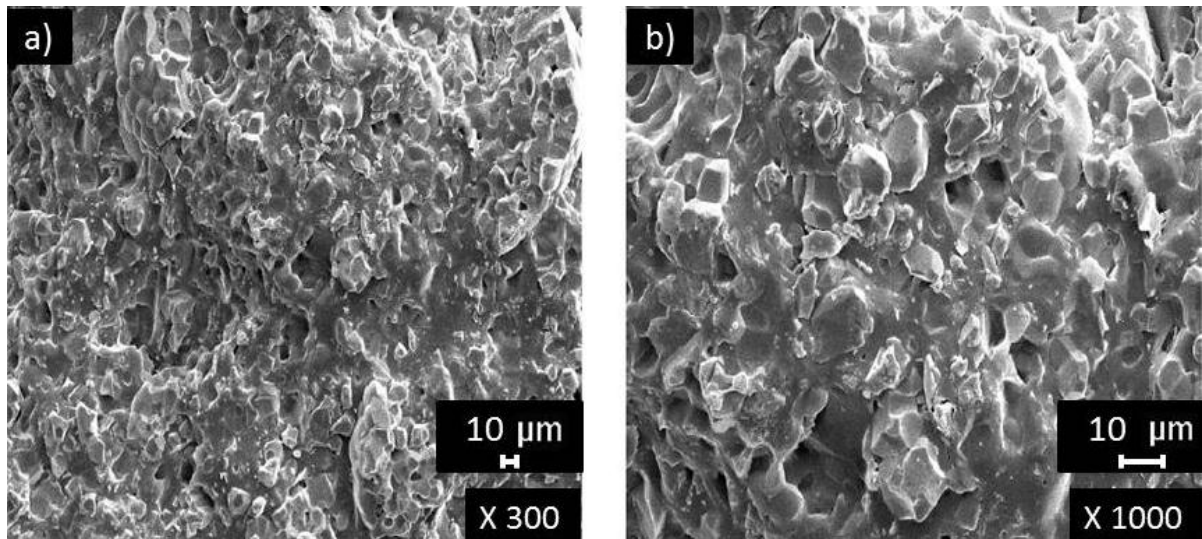
Figure 16: SEM images of NBR composite filled with 500 phr of MnZn

4.1.3 The NBR/CB and NBR/CNT composites

A SEM analysis of the fracture surfaces of the composites (Figs. 17, 18) confirmed that better dispersion, homogeneity and mutual adhesion between the carbon-based fillers and the elastomeric matrix were achieved for composites filled with CNT (Fig. 18a, b). The reason for the better adhesion between the CNT particles and the rubber matrix can be attributed to the larger specific surface area of the CNT and the strong physical or physicochemical interactions between the two components. On the contrary, it is possible to observe the formation of aggregates or agglomerates of CB particles on the fracture surfaces of composites filled with CB, which is obviously related to the very nature of CB, which tends to merge into higher structural units during production [33].
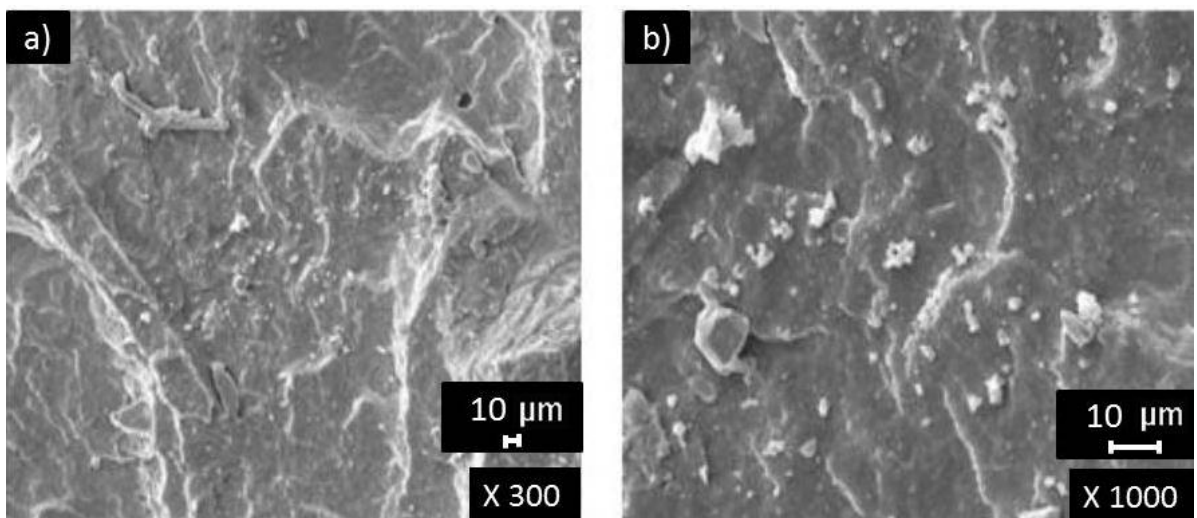
Figure 17: SEM images of fracture surfaces of NBR composites based on 20 phr CB

43
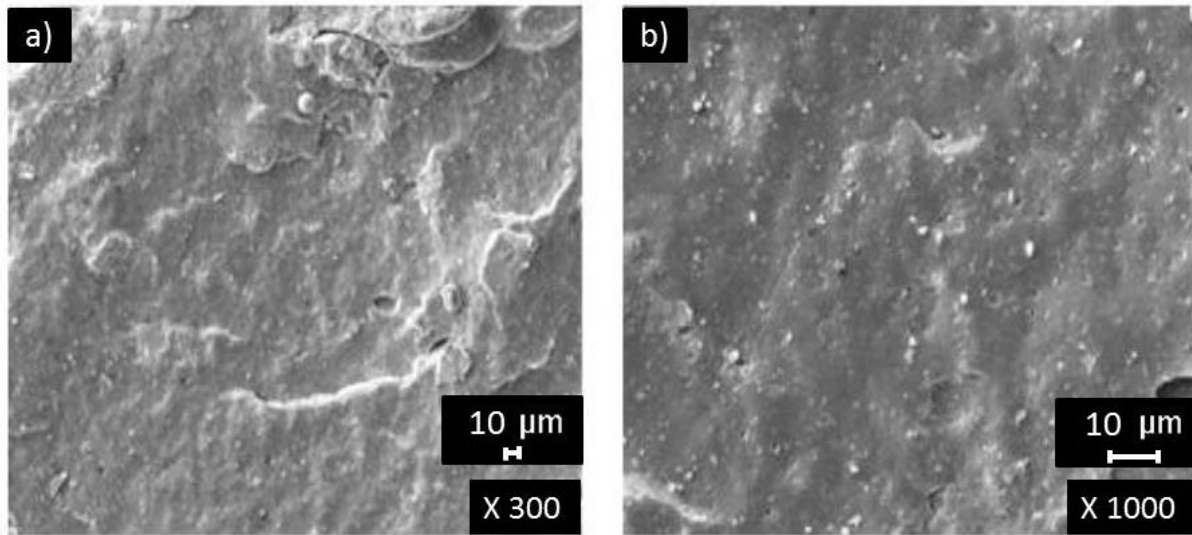
Figure 18: SEM images of fracture surfaces of NBR composites based on 5 phr CNT

4.1.4 The NBR/CB/MnZn and NBR/CNT/MnZn hybrid composites

The morphology of the fracture surfaces of composites filled with a combination of carbon fillers and MnZn is shown in the SEM images in Figs. 19a, b, and 20a, b. The MnZn particles are much larger (900x) compared to the carbon filler particles. In general, the larger the particles, the smaller their specific surface area and the lower the effective reactive sites for interactions with rubber chains. MnZn particles with a small specific surface area can act as steric hindrance against the formation of chemical cross-links between the segments of the elastomeric chains. Lower adhesion and weaker interactions between the MnZn and the rubber matrix caused the mechanical properties of the hybrid composites to deteriorate with increasing amounts of MnZn.
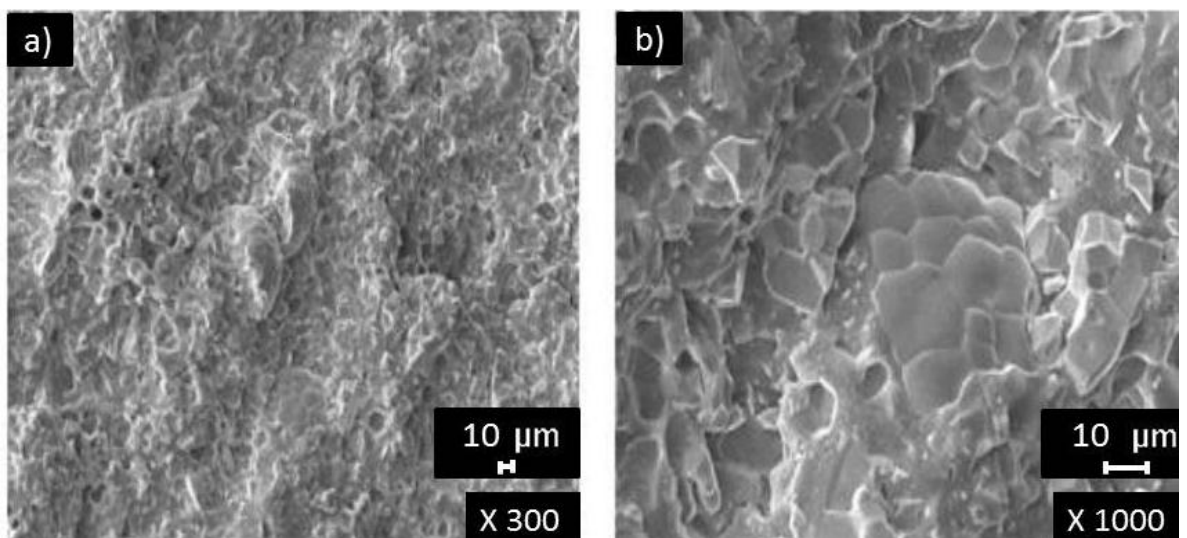
Figure 19: SEM images of fracture surfaces of NBR composites based on 20 phr CB and 300 phr MnZn

44
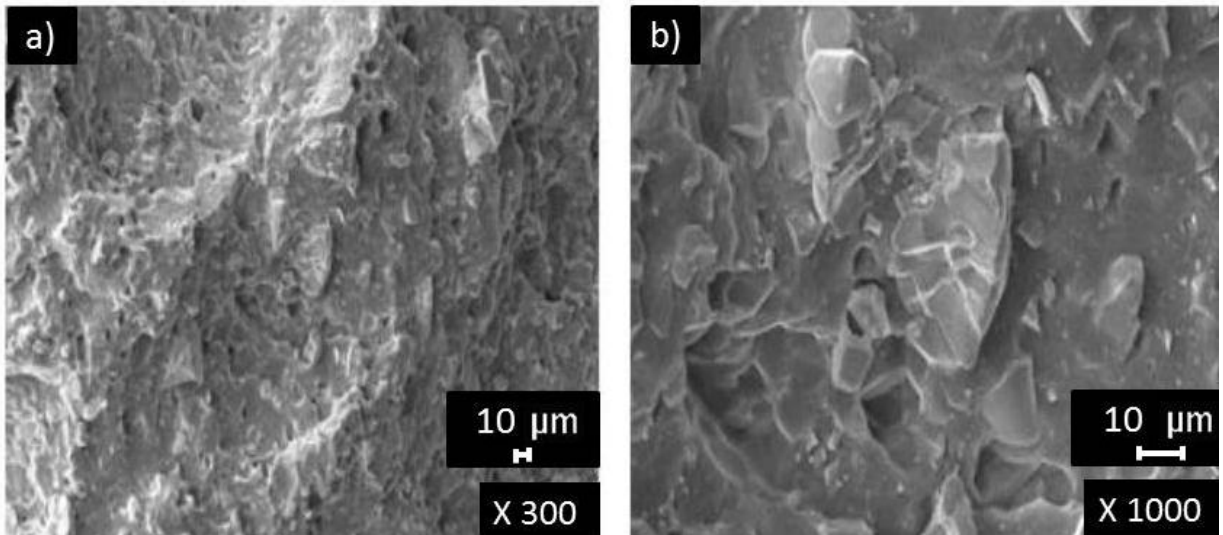
Figure 20: SEM images of fracture surfaces of NBR composites based on 5 phr CNT and 100 phr MnZn

4.1.5 The TPE/MnZn and TPE/CI composites

SEM images in Fig. 21a, b with a magnification of 100x show the distribution of the magnetic filler MnZn and CI in the used matrix. In addition, it is also possible to notice small defects, which were probably created by freezing the samples below the glass transition temperature and their subsequent breaking in order to obtain fracture surfaces for microscopic analysis. On the other hand, the distribution and dispersion of the MnZn and CI magnetic filler is better, which can be attributed to the higher viscosity of the TPE-based mixtures.
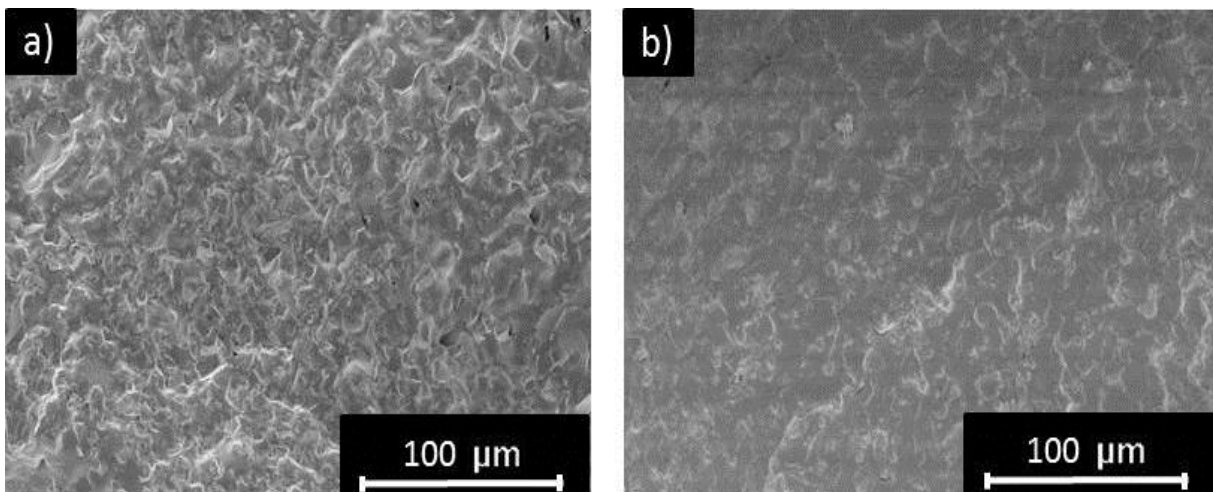
Figure 21: SEM images of fracture surfaces of TPE composites based on 70 wt. % of MnZn and CI

45

4.2 Dielectric and magnetic properties

4.2.1 The complex permittivity of ER/PDMS composites

The composites with MnZn ferrite show a frequency dispersion of $\varepsilon*$ in the entire investigated frequency range, and it is more pronounced for the highly-filled composites. The ε' and ε'' values gradually increase with the filler content (Fig. 22). The effect of the polymer matrix composition on the complex permittivity appeared for the composites with $70 - 80$ wt. % of filler. Thus, the ER/PDMS-MnZn composites show higher values of ε' and ε'' compared with the ER composites with the same filler concentration. As to the composites with CI, the frequency dispersion of the complex permittivity is less pronounced compared to the composites with MnZn, but ε' and ε'' are increasing with the filler concentration to approximately the same level as in the composites with MnZn ferrite. The polymer matrix composition affects ε' in the low RF region for the highly-filled CI-based composites, but it does not affect their dielectric losses. It seems that the permittivity spectra of the composites is caused by the electrical polarization induced in the filler particles and the particle clusters [91].
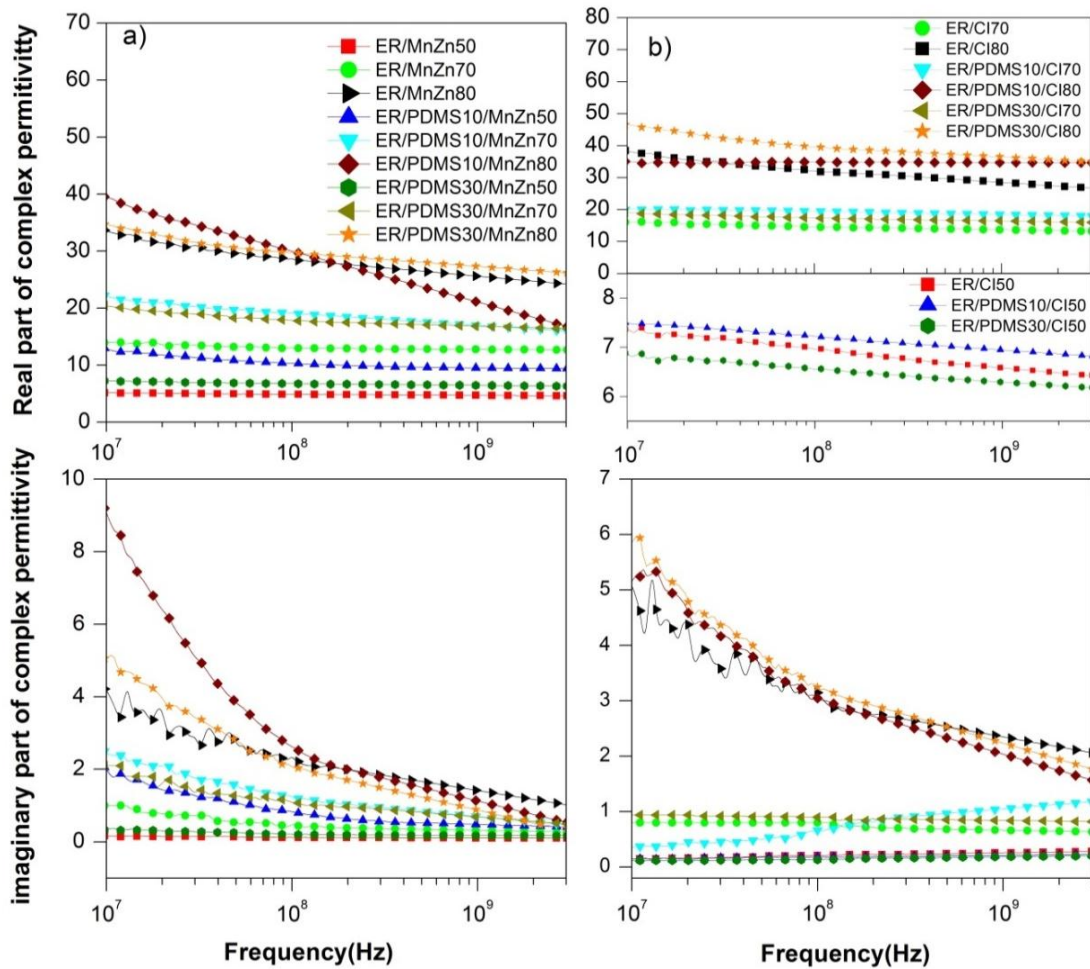
Figure 22: The frequency dependences of the complex permittivity of the polymer composites filled with a) MnZn and b) CI (wt. %)

46

4.2.2 The complex permittivity of NBR/MnZn composites

The frequency dependencies of real ε' and imaginary ε'' parts of complex (relative) permittivity $\varepsilon = \varepsilon' - j\,\varepsilon''$ for the composite materials are graphically illustrated in Fig. 23. It becomes obvious that the real part ε' steeply decreases at frequencies up to about 10 MHz, and then settles on a constant value. It can also be seen that with increasing content of MnZn in composites, the real permittivity shifts to higher values. When the amount of magnetic filler increased from 100 to 500 phr (48 – 82 wt. %), the real permittivity increased from 18.2 to 73.8. With increasing frequency of electromagnetic radiation, the differences in real permittivity became less visible. From frequency dependences of imaginary permittivity, it is possible to observe the similar decreasing trend of ε''. The real permittivity of composites provides higher values when compared to equivalent imaginary permittivity, and the differences in ε'' values became negligible at frequencies above 1 GHz. The achieved changes in frequency dependencies of complex permittivity may be attributed to various types of polarization mechanisms originating in the filler as well as the rubber matrix owing to their dielectric character (mainly the interfacial polarization caused by space charges, which accumulate at boundaries of the filler-rubber interface) [84].
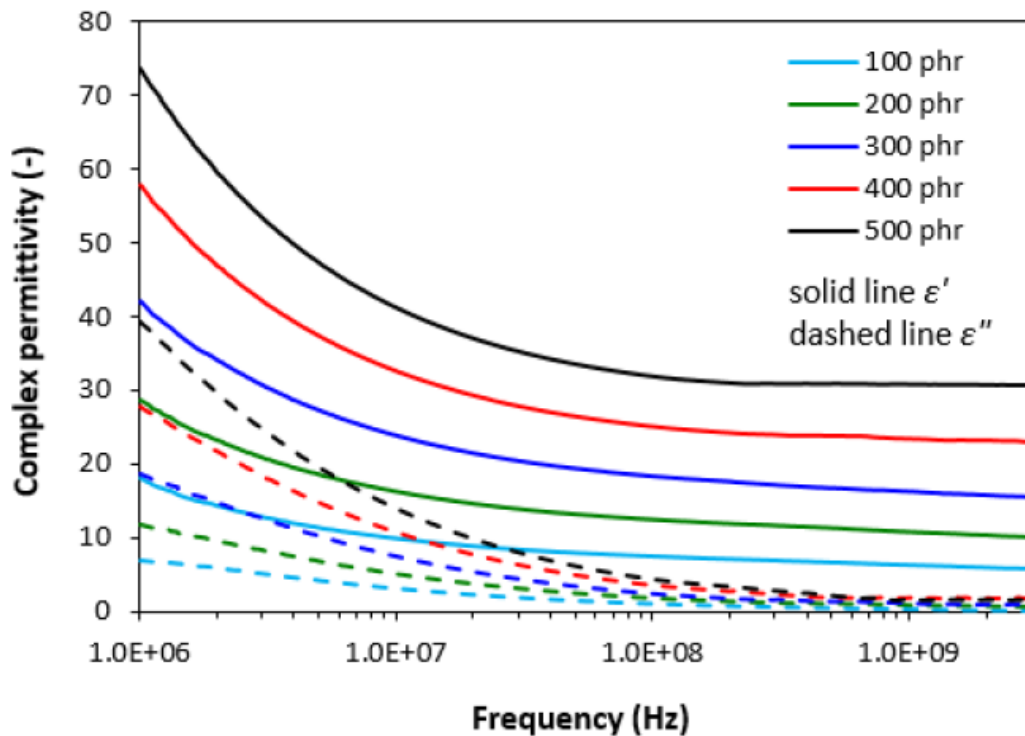
Figure 23: Frequency dependences of real ε' and imaginary ε'' parts of complex permittivity for NBR composites filled with ferrite MnZn [84]

4.2.3 The complex permittivity of NBR/CB composites

From frequency dependences of complex permittivity for CB-filled composites, it can be seen that both the real ε' and imaginary ε'' parts decreased with an increase in frequency (Fig. 24). It also becomes evident that both parts were dependent on the content of CB (2.3 – 19 wt. %), mainly at low frequencies. With the increasing frequency of electromagnetic radiation, the differences in permittivity became smaller. The frequency dependences of permittivity are not only influenced by polarization mechanisms (mainly interfacial polarization) but also by the resistivity of electrically conductive CB [84].
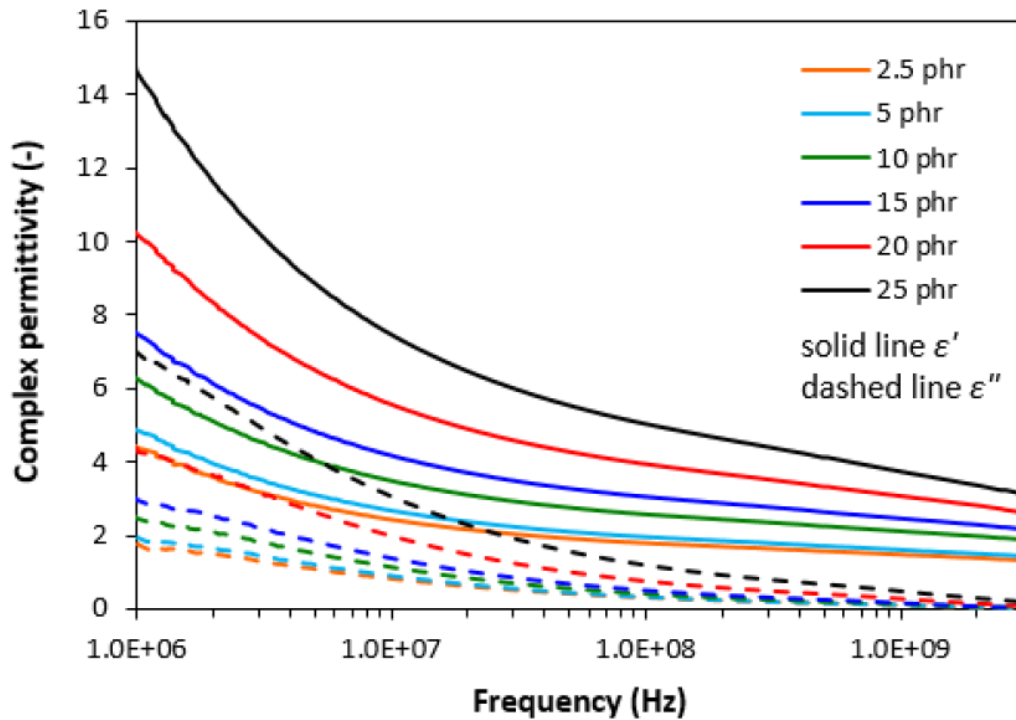
Figure 24: Frequency dependences of real ε' and imaginary ε'' parts of complex permittivity for NBR composites filled with CB [84]

4.2.4 The complex permittivity of hybrid NBR/CB/MnZn composites

As demonstrated in Fig. 25, after a sharp decrease of ε' at frequencies up to about 10 MHz, it fluctuates in a low range of experimental values. The lowest ε' was found to have the composite filled with 20 phr (16 wt. %) of CB ($\varepsilon' = 30$ at 1 MHz). By increasing the frequency up to 3 GHz, it decreased to 7. The real permittivity of the hybrid composite filled with 20 phr (8.7 wt.%) of CB and 100 phr (44 wt.%) of MnZn decreased from 47 down to 12 when the electromagnetic radiation frequency increased from 1 MHz to 3 GHz. The increase in magnetic filler content to 500 phr (80 wt. %) resulted in the increase of real permittivity up to almost 132 at 1 MHz. Then, it dropped down to 48 at the maximum tested

48

frequency. A similar trend can be also observed in frequency dependencies of imaginary permittivity. The initial decrease of real permittivity with frequency may be attributed to the semiconductive character of MnZn ferrite and the conductive character of CB. The increasing amount of filler loading results in the increase of both real and imaginary permittivity. The real permittivity is related to the electrical charge storage and mainly associated with the amount of polarization in the material, whereas the imaginary part is related to the loss in energy (dielectric loss). Polarization of the filler, the rubber matrix, as well as interfacial polarization can occur in dependence on frequency range [86, 87]. The dielectric loss can be attributed to interfacial polarization, dipole and electronic polarization, natural resonance, and relaxation phenomena [88, 89]. The presence of a high amount of interfaces in the composites paves the way for interfacial polarization, which occurs on the CB particles with relatively high conductivity. This leads to the accumulation of charges at the interfaces and the generation of dipoles on semiconductive MnZn particles. Thus, the interfacial polarization and associated space charge relaxation processes contribute to the EMI shielding performance [84, 90].
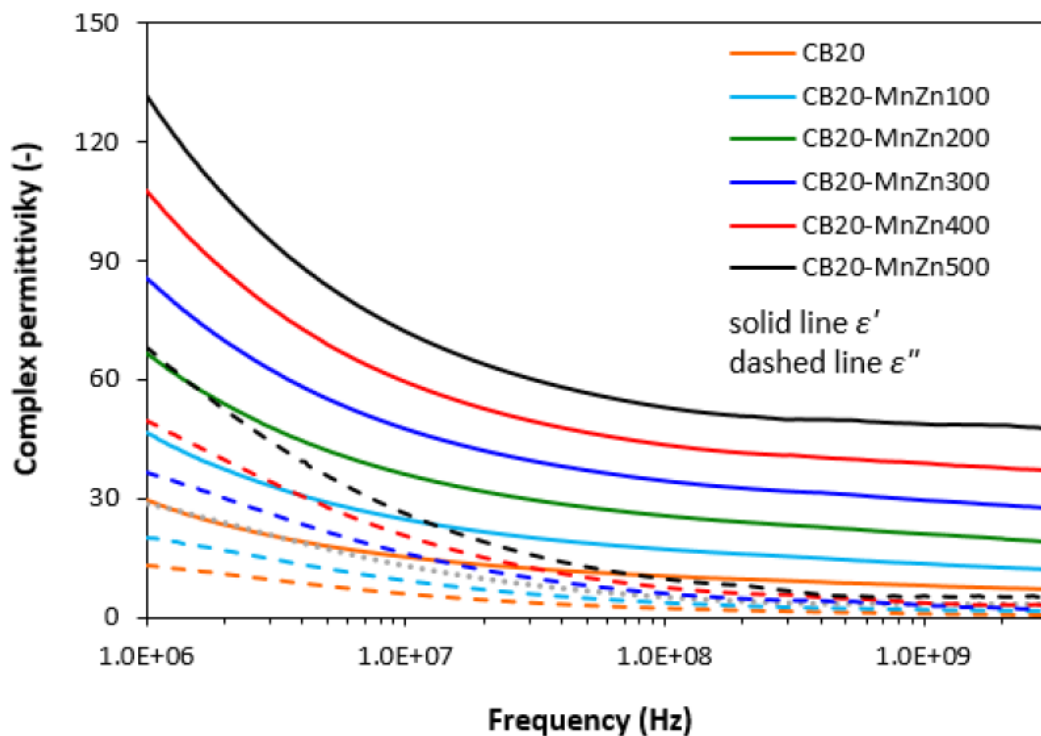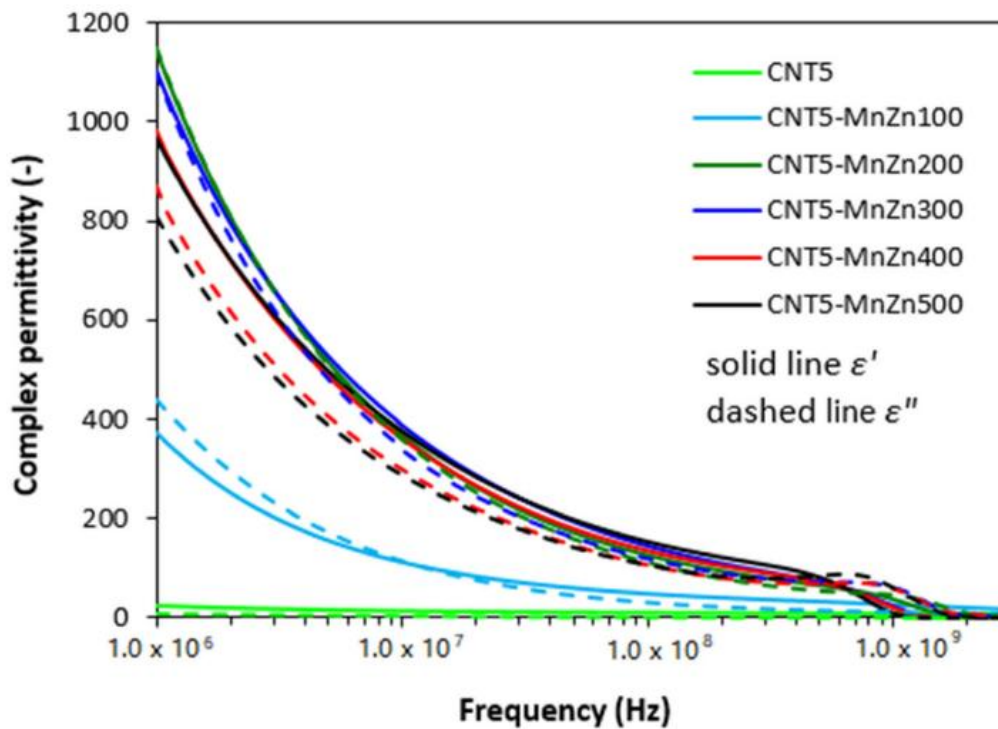

Figure 25: Frequency dependences of real ε′ and imaginary ε′′ parts of complex permittivity for hybrid NBR/CB/MnZn composites [84]

4.2.5 The complex permittivity of hybrid NBR/CNT/MnZn composites

As shown in Fig. 26, the real ε′ and imaginary ε′′ parts of complex permittivity for hybrid CNT/MnZn composites showed a significant decreasing trend with an increase in radiation frequency. In comparison with the composite filled only with

49

5 phr (2.3 wt. %) of CNT, the application of 100 phr (45 wt. %) of MnZn resulted in the increase of ε' from 23 up to 371 at 1 MHz. The increasing loading of MnZn in hybrid composites led to the increase of real permittivity up to 200 phr (64 wt. %) at 1 MHz ($\varepsilon' = 1147$ for the composite filled with 200 phr of MnZn and 5 phr of CNT). Subsequently, the real permittivity slightly decreased with the next increasing content of magnetic filler at 1 MHz ($\varepsilon' = 966$ for the composite filled 500 phr (81 wt. %) of MnZn and 5 phr (0.8 wt. %) of CNT). It also becomes obvious from Fig. 26 that the values of imaginary permittivity are quite similar with real part ε' of equivalent composites in the whole tested frequency range [4]. When comparing the complex permittivity of composites filled only with MnZn ferrite (Fig. 20), hybrid CB/MnZn filled composites (Fig. 23), and hybrid CNT/MnZn filled composites (Fig. 25), it becomes apparent that both the real and imaginary permittivity increase in the following order: MnZn composites < CB/MnZn composites < CNT/ MnZn composites.

Figure 26: Frequency dependences of real ε' and imaginary ε'' parts of complex permittivity for hybrid NBR/CNT/MnZn composites [4]

4.2.6 The complex permeability of ER/PDMS composites

The frequency dependence of the $\mu*$ of the MnZn and CI-based composites is determined first of all by the type of magnetic filler and its concentration. The permeability dispersion region for the MnZn-based composites occupy a frequency range from 10^6 Hz up to 10^9 Hz, with a maximum value of $\mu'=10$ and $\mu''=3$ for 80 wt.% of filler (Fig. 27).

The CI-based composites demonstrate a similar behaviour of magnetic spectra

with the difference being that the ferromagnetic resonance linewidth is broader, $10^6 - 10^{10}$ Hz. However, the absolute value of the $\mu*$ is lower compared to the composites filled with MnZn ferrite due to the skin effect, which masks the magnetization processes in the conductive CI particles (Fig. 28). Besides, there are two peaks on $\mu''(f)$ for the composites with 50−80 wt. % of CI at about 10^8 Hz (domain-wall resonance) and 4×10^9 Hz (spin resonance), which can be explained by the complex micro-magnetic structure of the SL type CI, exhibited polycrystalline structure [91].
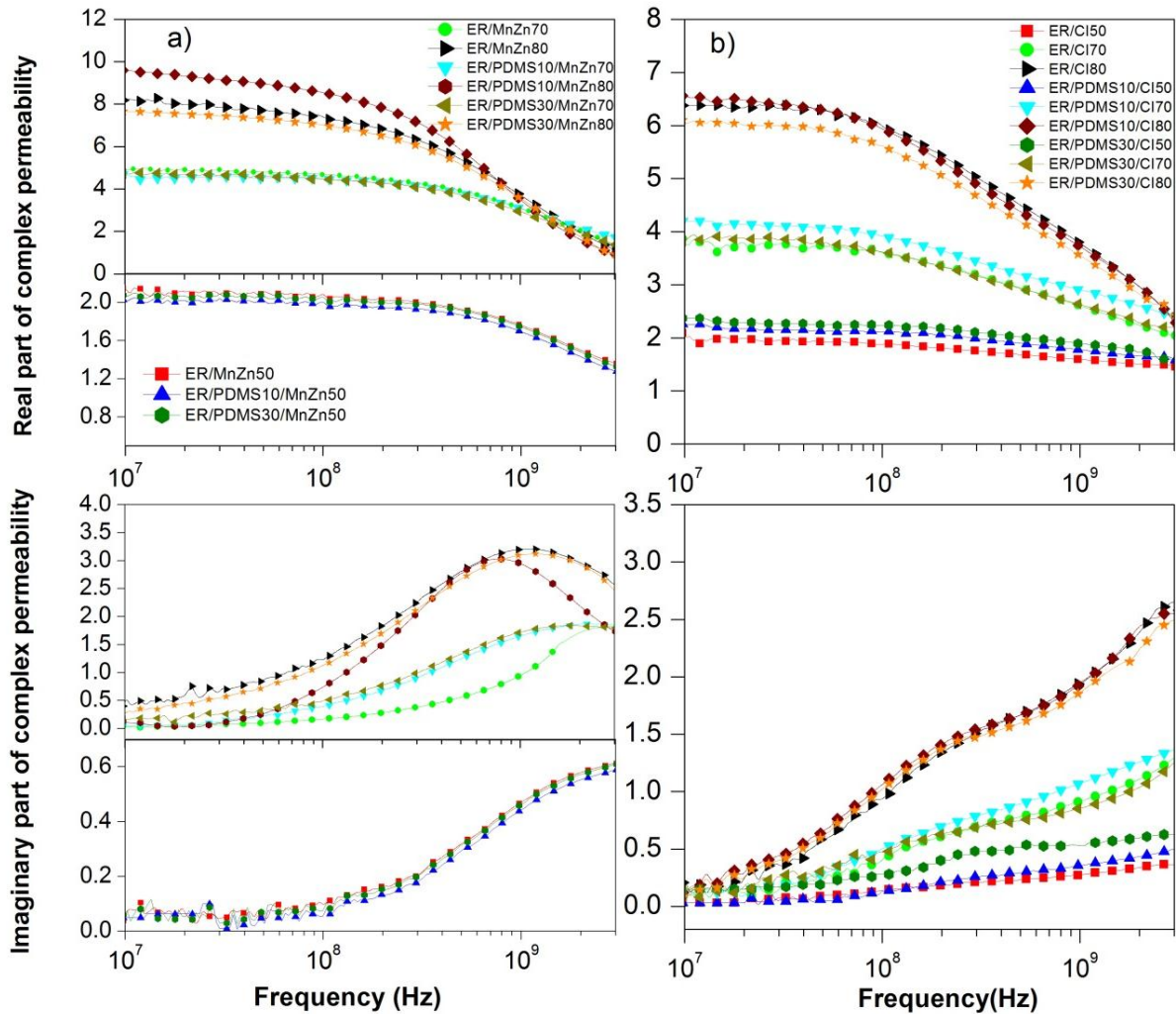
Figure 27: The frequency dependence of the complex magnetic permeability of the polymer composites filled with a) MnZn and b) CI (wt. %)

The real and imaginary part of the $\mu*$ in the composites increases with the concentration of the filler, regardless of the polymer matrix type. At the same time, there is a sharp increase in both components of $\mu*$ with a filler concentration, which indicates a gradual decrease in the internal demagnetizing field. The value of the demagnetizing field depends on the intrinsic properties of the filler, the shape and size of the magnetic particles, the particle volume fraction as well as on the interparticle interactions leading to the growth of clusters [92]. To quantify the intensity of the interparticle interactions in the composites, the reciprocity

factor was introduced by J.L. Mattei and M-Le Floc'h [93]. It was found theoretically and experimentally that at a filler concentration exceeding 35 vol. % reciprocity, the factor is close to the maximum value, while the demagnetizing field approaches its minimum [94].
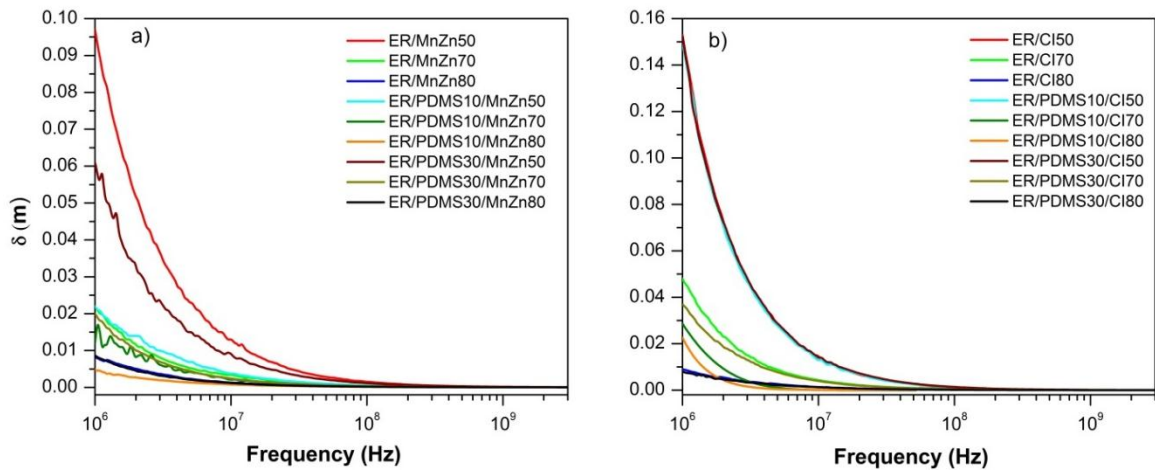
Figure 28: The skin depth of the composites as a function of frequency a) MnZn-based composites b) CI-based composites

According to the magnetic spectra, the demagnetizing field in the composites with all types of the matrix approaches a minimum at 80 wt. % (45 vol. %) of MnZn and CI. The SEM images of the highly-filled composites indicate the formation of particle clusters as in the volume of the composite as on the ER/PDMS interface (Fig. 14c, d). As the particles make a chain, demagnetization decreases due to a decrease in the magnetic poles number and the formation of the continuities magnetization flux lines (Fig. 29).
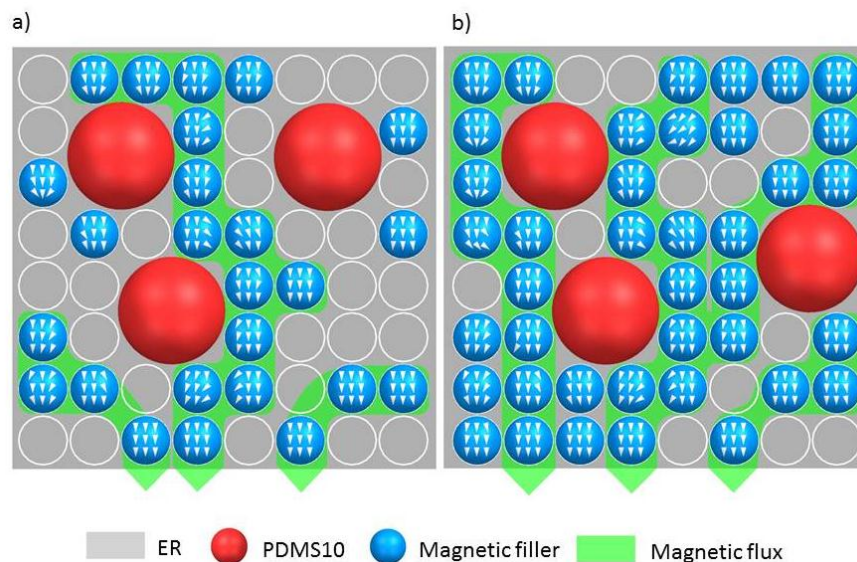
Figure 29: The effect of the filler concentration on the field internal demagnetizing in the magnetic composites: a) 50 wt. % magnetic filler b) 70 wt. % magnetic filler

4.2.7 The complex permeability of NBR/MnZn composites

Electromagnetic characteristics and the absorption shielding effectiveness of composites were investigated through determinations of complex permittivity, complex permeability and return loss in a frequency range from 1 MHz – 3 GHz. As mentioned, generally-used electronic equipment emit electromagnetic radiation within low frequency ranges, usually below 3 GHz. Therefore, an investigation of electromagnetic and shielding characteristics within this frequency range is of strong interest [4]. The frequency dependencies of real and imaginary parts of complex permeability ($\mu = \mu' - j\mu''$) for rubber magnetic composites are presented in Fig. 30. As shown, there is only small change of the real part μ' with the change in frequency up to about 200 MHz, and then it decreases close to one. The imaginary permeability μ'' can be neglected up to about 100 MHz, then increases and after reaching a maximum at a resonance frequency fr, it drops down to a low value. The maximum in frequency dependences of imaginary permeability corresponds to the maximal permeability loss, i.e., magnetic loss. It also becomes apparent from Fig. 30 that the real permeability of composites at low frequencies increases with an increasing content of magnetic soft filler, from 3.3 for the composite filled 100 phr (48 wt. %) of MnZn ferrite, to 7.5 for the maximally filled composite at 1 MHz. Then, the differences in μ' in dependence on MnZn content become smaller over 1 GHz. On the other hand, the differences in imaginary permeability of MnZn filled composites are insignificant at low frequencies. Then, the values of μ'' increases proportionally to the content of magnetic filler. Simultaneously, the resonance frequency fr decreases with MnZn content increasing, from about 3000 MHz for the composite filled with 100 phr (48 wt. %) of MnZn, to around 1356 MHz for the composite with maximum MnZn ferrite content [4].
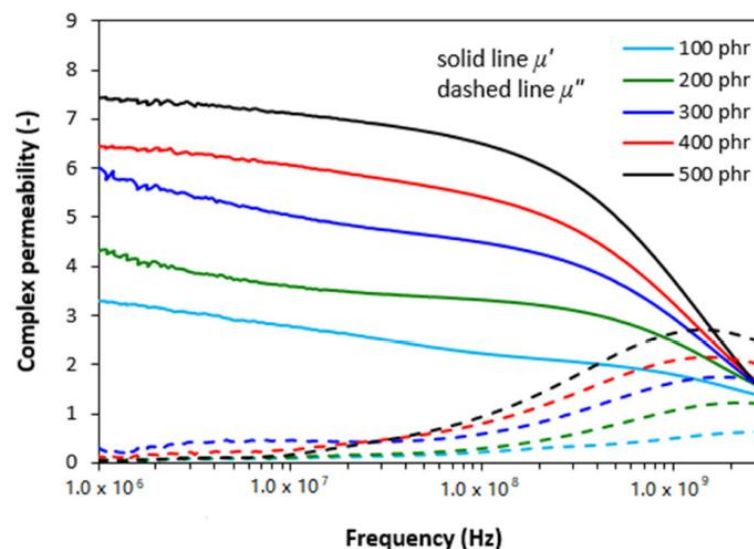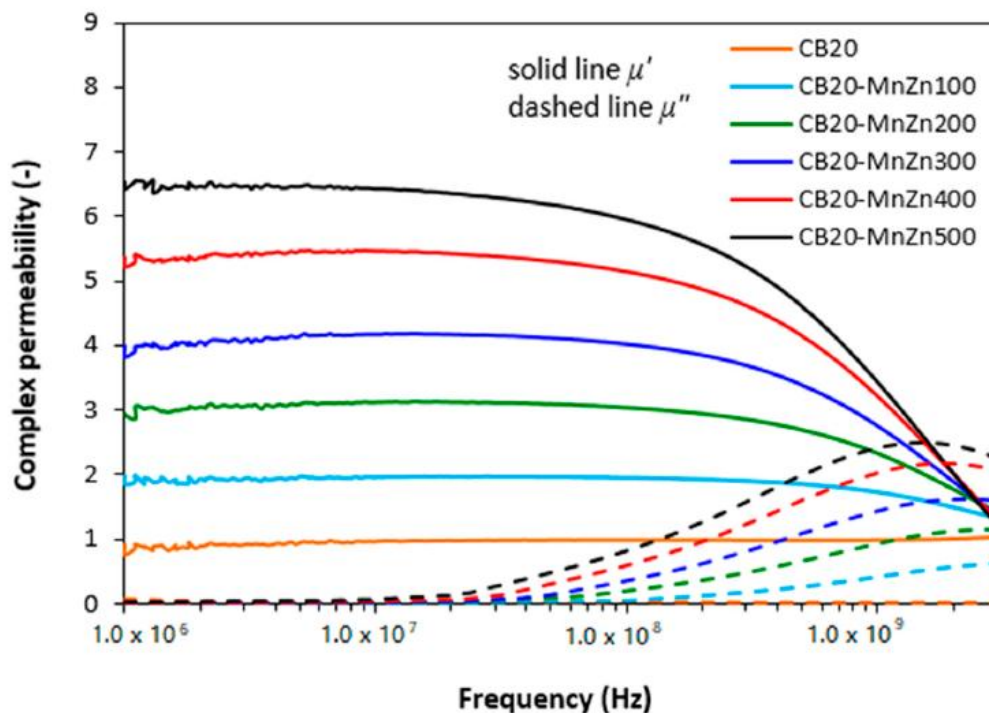
Figure 30: Frequency dependences of real μ' and imaginary μ'' parts of complex permeability for MnZn filled NBR composites [4]

4.2.8 The complex permeability of hybrid NBR/CB/MnZn composites

As demonstrated in Fig. 31, the lowest real and imaginary permeability was found to be the composite filled only with CB, and these values seem also to be independent on frequency. The increasing amount of magnetic filler in hybrid composites results in the increase of real permeability, mainly at lower frequencies, and imaginary permeability at higher frequencies. Looking at Fig. 30 and 31, one can see that both the real and imaginary parts for hybrid CB/MnZN composites are slightly lower in comparison with equivalent composites filled only with magnetic filler, mainly at low frequencies. This means that the addition of CB increases the demagnetization field, which leads to a reduction in the permeability value of the complex [4].

Figure 31: Frequency dependences of real μ′ and imaginary μ′′ parts of complex permeability for CB20/MnZn filled NBR composites [4]

4.2.9 The complex permeability of hybrid NBR/CNT/MnZn composites

The results obtained from the determination of complex permeability (Fig. 32) reveal that the lowest values of real and imaginary permeability are exhibited by the composite filled only with CNT, with almost no dependence of both parts on radiation frequency. The increasing degree of MnZn ferrite loading results in the increase of real permeability mainly at low frequencies and the imaginary part at higher frequencies. When comparing the frequency dependences of complex permeability for composites filled only with magnetic filler (Fig. 30) and hybrid

54

composites filled with MnZn and carbon-based fillers (Fig. 31), it becomes apparent that the differences are quite small, and generally it can be stated that no significant changes in the complex permeability of composites can be observed in dependence on the filler's composition [96]. In general, fillers with a carbon structure that are non-magnetic increase the demagnetization field in the composite and thus reduce the value of complex permeability.
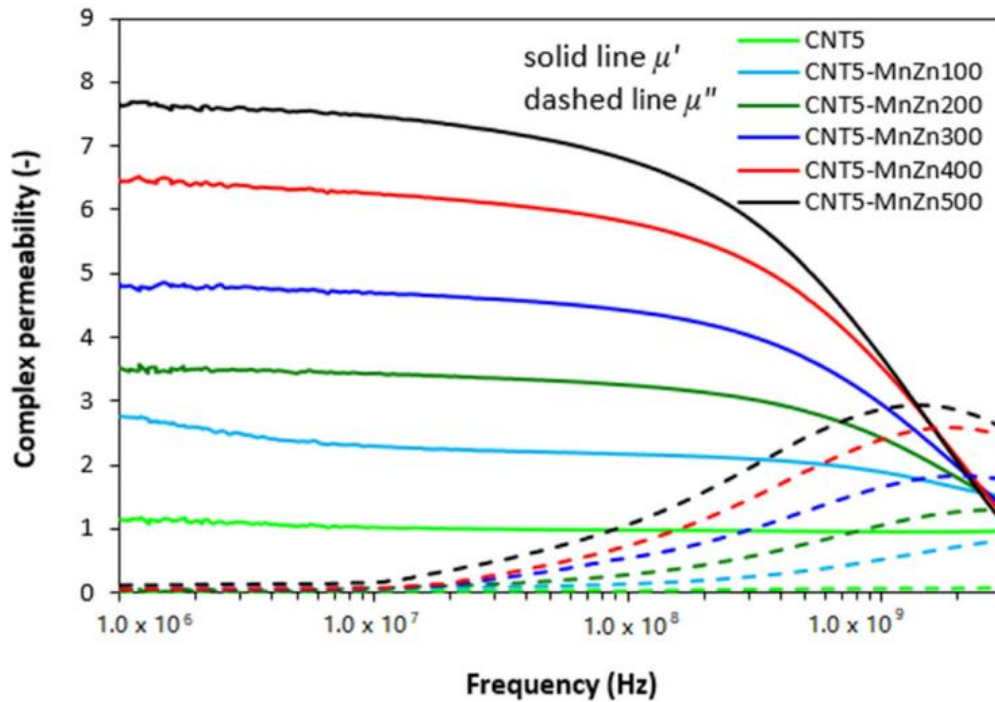

Figure 32: Frequency dependences of real μ´ and imaginary μ´´ parts of complex permeability for hybrid CNT/MnZn NBR composites [4]

4.3 Electromagnetic shielding characteristics of composites

4.3.1 RL of the ER/PDMS/MnZn and ER/PDMS/CI composites

The shielding characteristics of composite materials were evaluated in the form of RL (return loss) in decibels. The reflection losses (RL) express how much electromagnetic energy interfered with on the surface of the shielding material is shielded by the absorption (absorption) of this energy. From the results published so far in the field of measuring electromagnetic interference, it has been found that reflection losses at the level of -10 dB represent the absorption and shielding of more than 95% of interfering radiation. Materials achieving reflection losses of -20 dB are able to absorb 99% of electromagnetic radiation [95, 96]. Because most commonly used electronic and electrical devices, such as computers, laptops, cell phones, televisions, and others, emit EM radiation in the 0.6 – 3 GHz frequency range, shielding in this area is important for most commercial electronic devices. Based on these findings, the effective absorption range is taken to be the

frequency range corresponding to reflection losses of -10 dB and less. Thus, composite materials must achieve reflection losses of at least -10 dB to be sufficiently effective as EMI absorbers. Of course, it is also necessary for them to cover the widest possible shielding frequency band in the event of these reflection losses. The frequency dependences of the reflection losses of composite materials based on two types of polymer matrices and two types of fillers (MnZn and CI) are graphically shown in Figs. 33 – 34, while selected electromagnetic absorption parameters for prepared composites are given in Tab. 11, these being matching thickness d (mm) of the absorbers, RL_{min} (minimum value of reflection losses at frequency f_o, or maximum absorption shielding efficiency of composite material), f_o (frequency at minimum value of reflection losses, or at maximum absorption shielding efficiency composite material) and Δf (width of the frequency band of the absorption shielding of the composite material at reflection losses of -10 dB).

TABLE 11: Electrodynamic characteristics of RL_{min}

Composite	d_0	f_{min}	f_o	f_{max}	RL	f_{max}/f_{min}
	[cm]	[MHz]	[MHz]	[MHz]	[dB]	
ER/MnZn50	0,91	2731	-	-	-	-
ER/MnZn70	0,675	1760	2180	2710	-36.5	1.54
ER/MnZn80	0,868	521	688	915	-49.8	1.75
ER/PDMS10/MnZn50	0,593	1495	1758	2056	-16.1	1.37
ER/PDMS10/MnZn70	0,425	988	1291	1717	-56.3	1,73
ER/PDMS10/MnZn80	0.748	488	682	1036	-59,8	2,12
ER/PDMS30/MnZn50	0,841	-	-	-	-	-
ER/PDMS30/MnZn70	0.864	873	1147	1509	-46	1.72
ER/PDMS30/MnZn80	0.89	510	652	841	-47.9	1.65
ER/CI50	1,2	-	-	-	-	-
ER/CI70	0,478	2092	2637	-	-47	-
ER/CI80	0,757	684	873	1079	-49	1.57
ER/PDMS10/CI50	0,948	2260	2350	2440	-13,2	1,08
ER/PDMS10/CI70	0,147	1825	2260	2769	-50,5	1,51
ER/PDMS10/CI80	0,449	688,5	833,8	1000	-72,2	1,45
ER/PDMS30/CI50	0,451	2931	-	-	-	-
ER/PDMS30/CI70	0,717	2162	2658	-	-61.5	-
ER/PDMS30/CI80	0,32	2027	2360	2776	-49	1.37

For all types of composite materials, the statement can be made that with an increasing amount of filler, there is a shift of absorption maxima and effective absorption efficiency towards lower frequencies of electromagnetic radiation. From Fig. 33, it is evident that in the operating frequency range of 1 MHz - 3 GHz, the ER/PDMS30-based composite with an amount of 50 wt. % MnZn does not show a sufficient component of the shielding absorption efficiency, since it did not achieve reflection losses of -10 dB. As the amount of MnZn filler in the

composites increases, the absorption maxima and overall absorption efficiency shift toward lower frequency ranges. The ER/MnZn70 and ER/PDMS10/MnZn70 composites showed reflection losses of -10 dB in the widest frequency band, from 1.6 GHz to 2.6 GHz and 1.2 GHz to 2 GHz respectively at -10 dB. This composite showed a minimum value of reflection losses (RL_{min}), resp. maximum absorption shielding efficiency at -38 dB and -58 dB. We can see the content of PDMS in the matrix shifts the RL to lower frequencies. The relatively wide frequency band of absorption shielding at reflection losses at -10 dB was also shown by the composite ER/PDSM10 filled with MnZn at 80 wt.% (from 423 MHz to 936 MHz at -10 dB). This composite showed a lower absorption maximum (RL_{min} = -50 dB) at a lower frequency (f_m = 693 MHz).
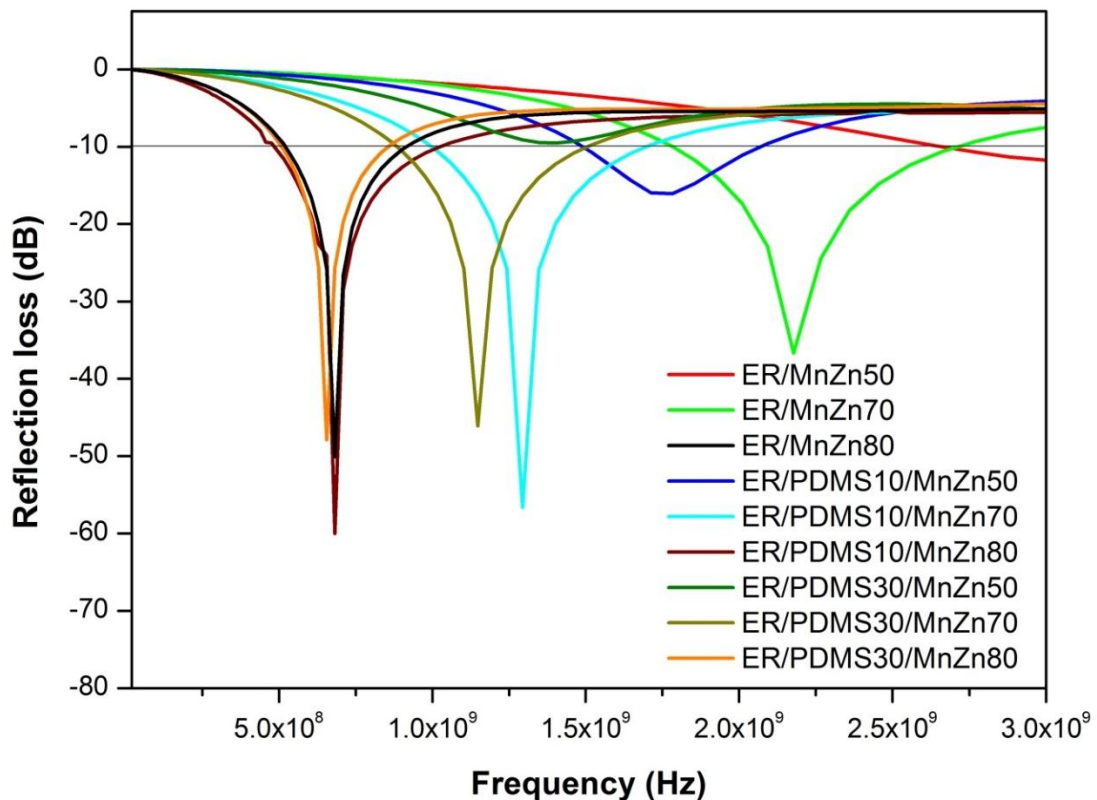
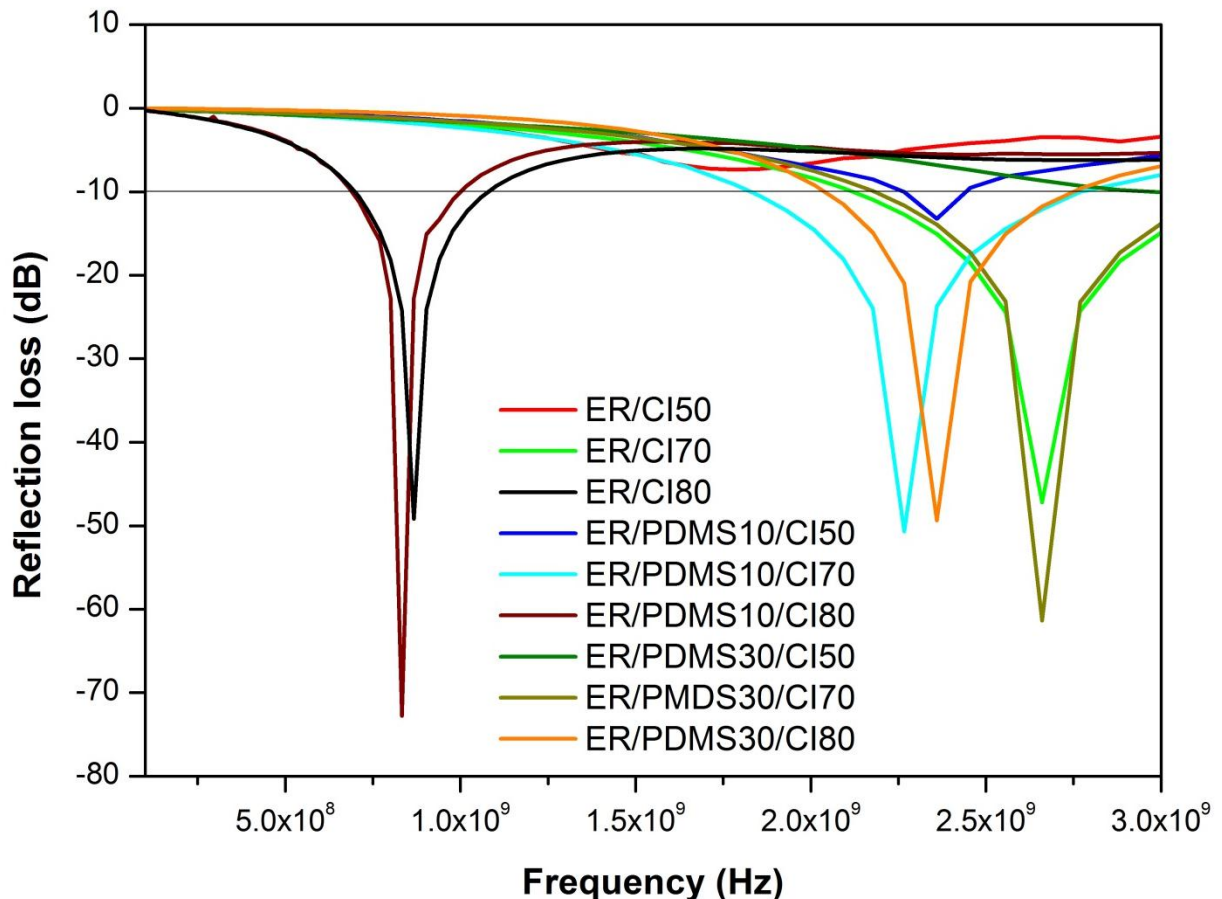*Figure 33: The frequency dependence of the reflection loss of the composites filled with MnZn based on: a) ER b) ER/PDMS10 and c) ER/PDMS30*

The type of filler as well as its concentration, size and shape will depend on the microwave absorption properties. Research studies conducted on MnZn and CI of composites are showcased in Tab. 12. Typically presented absorbers in these published studies operate in the microwave region, while our absorbers operate in the radio frequency band.

Table 12: Comparison of absorbing and mechanical properties of the various reported materials

Filler	Concentration (%)	Matrix	Operating Frequency range (GHz)	Thickness (mm)	$\Delta\lambda/d$	RL_{min} (dB)	Storage Modulus (MPa)	Impact strength (kJ/m^2)	Ref.
CI/CB	55 wt. %/20 wt.%	Epoxy	3.3 – 6.7	2	23.07	-8	-	-	[97]
CI	50 vol%	EPDM 4042	2.5 – 4.2	3.6	13.49	-11	-	-	[98]
CI/MWCNT	50 vol%/0.5 vol%	Epoxy/silicone	3.2 - 12	1.5	45.8	-10 (-15)	-	-	[99]
nano Fe$_3$O$_4$	40 vol%	Epoxy	2.5 – 2.8	5.5	2.34	-28	-	-	[100]
MnZn	40 vol%	PDMS	0.3 – 0.49	16.2	23.94	-67	-	-	[17]
CI (spherical SL)	50 vol%	PU	0.9 – 1.42	5.13	23.20	-62	-	-	[17]
Ni	8 vol%	Epoxy	-	-	-	-	-	11	[101]
Ni	4 vol%	Epoxy/PDMS30	-	-	-	-	-	16	[101]
CI (flake)	75 wt.%	Epoxy/silicone	2 - 4	2	37.5	-25	-	46.5	[102]
CI	80 wt.%	Polychloroprene	8 – 11.5	1.5	7.6	-40	-	-	[103]
MnZn	50 wt.%	Epoxy	-	-	-	-10	-	21	[91]
MnZn	50 wt.%	Epoxy/PDMS10	2.1 – 3	8	5.81	-23	3821	16	[91]
MnZn	50 wt.%	Epoxy/PDMS30	2.2 – 3	9	4.46	-15	3900	15	[91]
MnZn	70 wt.%	Epoxy	1.6 – 2.7	7	8.3	-20	-	12	[91]
CI (spherical SL)	70 wt.%	Epoxy	1.1 - 1.7	7	9.67	-22	-	20	[91]
MnZn	70 wt.%	Epoxy/PDMS10	1.6 – 2.7	7	16.33	-19	2134	9	[91]
CI (spherical SL)	70 wt.%	Epoxy/PDMS10	0.9 – 1.1	7	11.01	-26	3205	12.5	[91]
MnZn	70 wt.%	Epoxy/PDMS30	1.3 – 2.2	6	16.9	-19	2419	11.5	[91]
CI (spherical SL)	70 wt.%	Epoxy/PDMS30	1.4 – 1.6	5	8.97	-16	3649	13	[91]

The 70 wt. % CI-filled composite ER/PDMS30 (Fig. 34) showed reflection losses in the widest frequency band, from 2.1 GHz to 3 GHz at -10 dB. However, it should be emphasized that the shielding band of this composite at - 10 dB exceeded 3 GHz. However, it could not be measured in terms of available instrumentation. It is therefore highly likely that the frequency band of the absorption shield would be even wider. This composite showed a minimum value of reflection losses (RL_{min}), resp. maximum absorption shielding efficiency at - 48 dB but at a relatively high frequency $f_m = 2.83$ GHz.
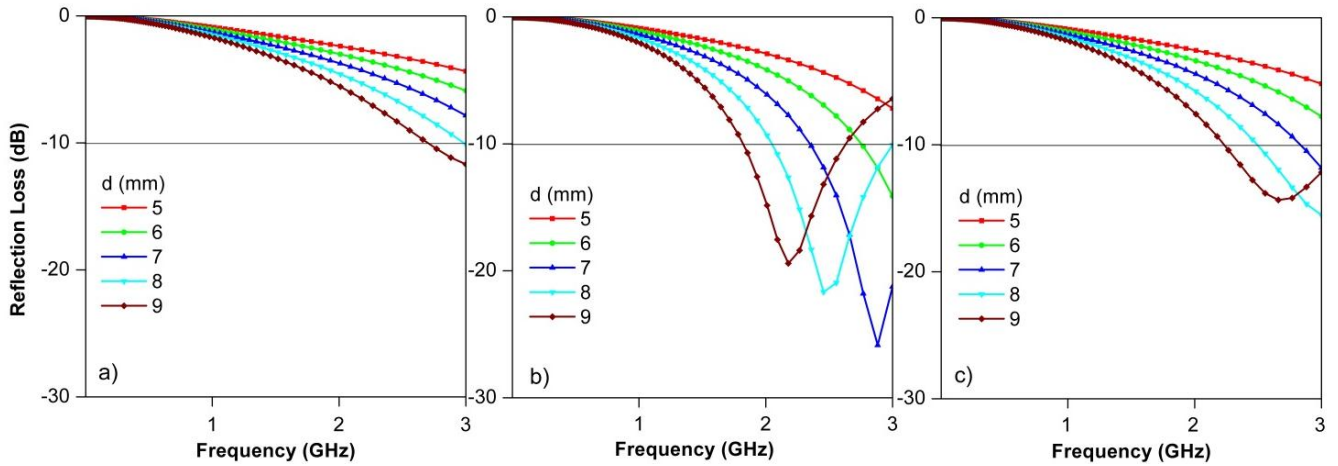

Figure 34: The frequency dependence of the reflection loss of the composites filled with CI based on: a) ER b) ER/PDMS10 and c) ER/PDMS30

In order to characterize the electromagnetic wave absorption properties of the composites obtained, the reflection minima of single-layer absorbers was calculated within the layer thickness (eq. 3). The results obtained are shown in Figs. 35 and 36. After that, the operating absorption bandwidth at the -10 dB level of RL was evaluated (eq. 9) and shown in Tab. 13.

The composites with MnZn ferrite demonstrate a larger bandwidth to thickness ratio in comparison with the CI-filled composites due to a proper ratio between $\varepsilon*$ and $\mu*$, which leads to the impedance matching conditions between the RAs

and the free space. It is also necessary to emphasize the effect of the polymer matrix on the radio-absorber performance of the magnetic composites. In general, it can be found that the magnetic composites based on the ER/ PDMS10 matrix achieved higher RL bandwidths than the ER and the ER/ PDMS30 composites with the same magnetic filler content.

Figure 35 depicts the RL of the composites based on the ER and the ER blends with 10 and 30 wt. % of PDMS and 50 wt. % of CI. Such a high concentration of CI in the polymer matrix leads to the RL varying from -5 dB to -10 dB, which is due to the low skin depth, which masks the magnetization processes in the conductive CI particles as discussed previously. However, there is a tendency that, in increasing the PDMS concentration to 30 wt. %, the value of the RL increases and the RL minimum shifts to a higher frequency range, which is more probably related to clustering and the localization of the conductive CI particles at the ER-PDMS interface as discussed in a study on percolation threshold [101].
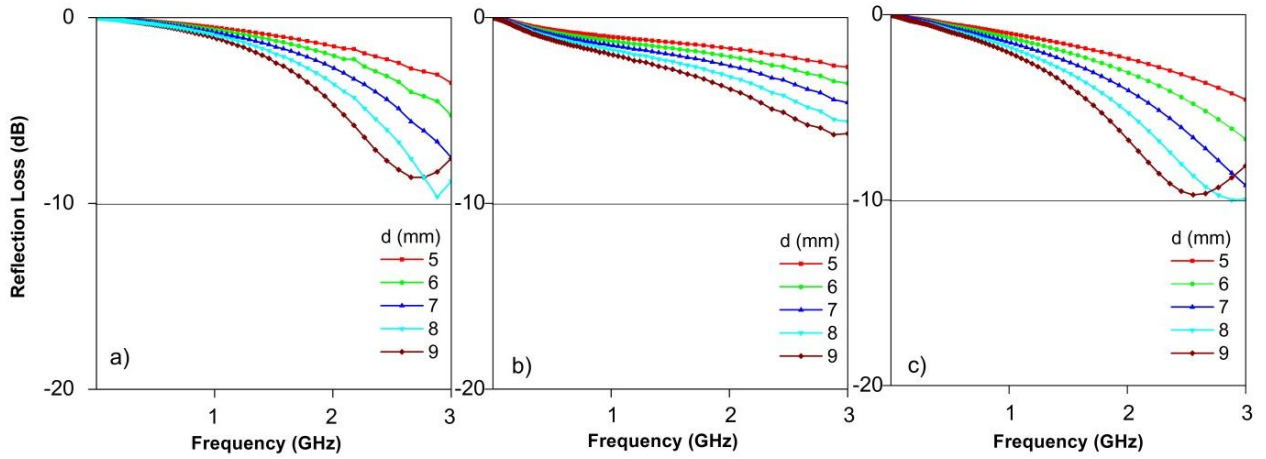
Figure 35: The frequency dependence of the reflection loss of the composites filled with 50 wt. % CI based on: a) ER b) ER/PDMS10 and c) ER/PDMS30 [91]

Figure 36 shows the calculated RL dependence for the composites with 50 wt. % of MnZn ferrite in the ER matrix and blends with different PDMS contents. The composite ER/MnZn50 demonstrates an RL of about 10 dB within a bandwidth ($\Delta\lambda/d = 2.21$) for 11 mm RA thickness and ($\Delta\lambda/d = 1.35$) for 12 mm RA thickness. The addition of 10 wt. % of PDMS to the ER (ER/PDMS10/MnZn50) results in a higher absorption (-25 dB) within a broader bandwidth ($\Delta\lambda/d = 6.28$) for an RA with a thickness of about 7 mm. However, an increase in the PDMS up to 30 wt. % leads to a lower RL (-18.5 dB) and a narrow bandwidth ($\Delta\lambda/d = 5.35$).

An increase in the filler concentration up to 70 wt. % (36 vol. %) provides 99% of the electromagnetic energy absorption (Fig. 37). Besides that, the magnetic composites with a different PDMS content in the ER matrix exhibit a different operating frequency range: for the MnZn-filled composites $\Delta f = 1.6 - 3$ GHz,

60

while for the CI-filled composites $\Delta f = 0.7 - 1.7$ GHz. According to the results obtained, the presence of 10 wt. % PDMS in both types of composites is sufficient to reduce the demagnetization effect and to obtain broadband RAs with a thickness of 5-7 mm.

Figure 36: The frequency dependence of the reflection loss of the composites filled with 50 wt. % MnZn based on: a) ER b) ER/PDMS10 and c) ER/PDMS30 [91]
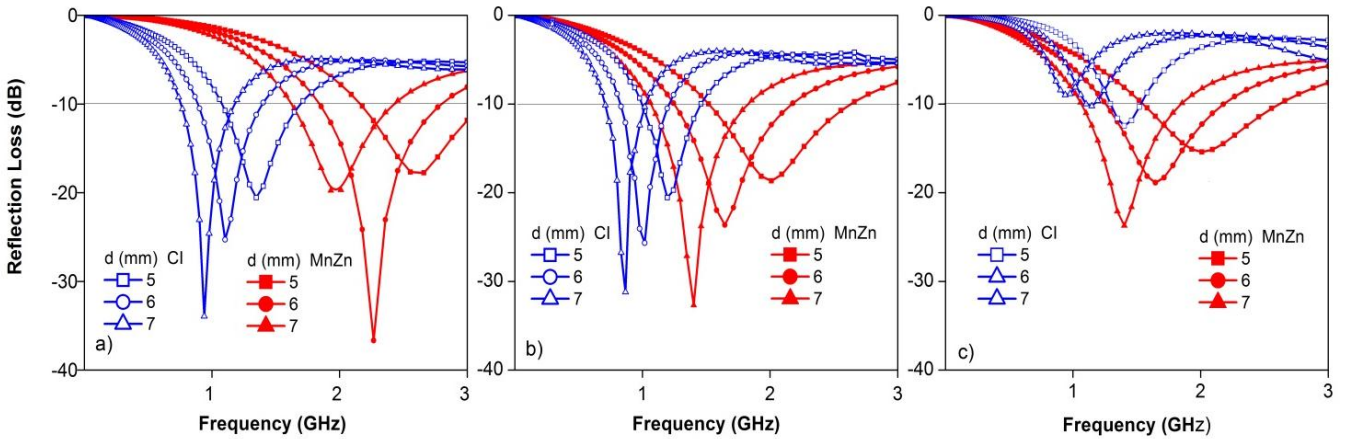
Figure 37: The frequency dependences of the reflection loss of the composites filled with MnZn (36 vol. % = 70 wt. %) and CI (36 vol. % = 80 wt. %) based on: a) ER b) ER/PDMS10 and c) ER/PDMS30 [91]

Table 13: The operating absorption bandwidth at -10 dB level of RL for the absorbers based on different composites

Composites	Δλ/d (at the level of -10 dB) d (mm)					
	5	6	7	8	9	10
ER/MnZn50	-	-	-	-	-	-
ER/MnZn70	7.60	9.15	8.30	7.48	3.68	-
ER/MnZn80	28.50	29.67	28.27	29.69	28.40	26.8
ER/PDMS10/MnZn50	6.6	6.3	6.28	5.81	5.64	5.24
ER/PDMS10/MnZn70	15.84	16.38	16.33	16.19	14.96	13.46
ER/PDMS10/MnZn80	35.88	38.23	38.10	38.35	42.48	35.21
ER/PDMS30/MnZn50	6.48	5.88	5.35	5.37	4.46	4.14
ER/PDMS30/MnZn70	15.44	16.60	16.90	16.68	16.06	15.03
ER/PDMS30/MnZn80	25.18	27.93	26.59	28.29	24.87	23.89
ER/CI50	0.92	0.78	0.94	-	-	-
ER/CI70	9.40	10.03	9.67	9.31	8.37	8.02
ER/CI80	19.94	19.78	19.94	20.15	19.47	18.83
ER/PDMS10/CI50	0.96	0.98	0.9	-	-	-
ER/PDMS10/CI70	12.16	11.82	11.01	11.29	9.47	9.44
ER/PDMS10/CI80	17.56	18.78	18.70	18.23	19.50	17.15
ER/PDMS30/CI50	0.54	0.86	0.9	0.61	-	-
ER/PDMS30/CI70	9.52	9.57	8.97	9.14	8.21	7.84
ER/PDMS30/CI80	6.80	2.68	-	-	-	-

4.3.2 RL of the NBR/MnZn composites

Figure 38 depicts the reflection loss of composites with different contents of MnZn ferrite in the operating frequency range. It is shown that all composites containing 200 phr (65 wt. %) of filler and more provide satisfactory absorption shielding efficiency. It also becomes apparent that with increasing content of magnetic filler, the absorption maxima and absorption shielding efficiency of composites shift to lower frequencies of electromagnetic radiation. The composite containing 200 phr (65 wt.%) of MnZn exhibited reflection loss at level -10 dB and -20 dB in the widest frequency range, i.e., from 1.5 GHz to 2.7 GHz at -10 dB and from 1.85 GHz to 2.2 GHz at -20 dB. This composite can be considered to be the best absorption shielding material. The absorption maximum of this composite shield is at -48 dB at a frequency of 2 GHz of the incident electromagnetic radiation. The composite filled with 400 phr (79 wt.%) of MnZn showed a lower absorption maximum (-60 dB), but also a lower frequency range, in which it is able to effectively absorb EMI (return loss at -10 dB in the frequency range 0.6 – 0.98 GHz and return loss at -20 dB in the frequency range only 0.72

– 0.83 GHz). The composite containing 500 phr (82 wt. %) of MnZn ferrite was found to have the highest absorption maximum and the lowest effective absorption frequency range [84]. From Fig. 38 and tab. 14 it is also clear that the composites with high amounts of filler (400 and 500 dsk) (79 wt. % and 82 wt. %), show much narrower effective absorption shielding frequency bands.
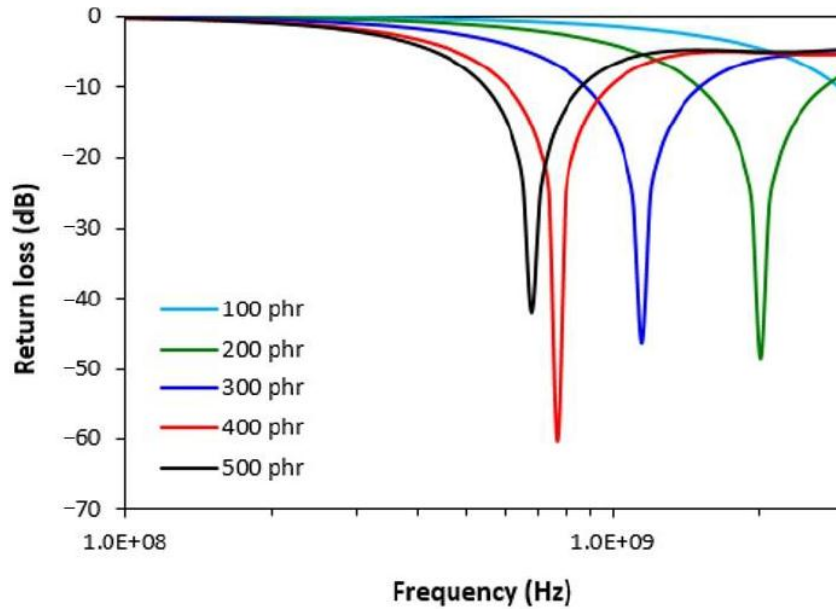
Figure 38: Frequency dependences of RL for NBR composites filled with MnZn [84]

Table 14: Electromagnetic absorption characteristics of hybrid NBR/MnZn filled composites

MnZn (phr)	RL_{min} (dB)	f_m (MHz)	Δf (MHz) for -10 dB
100	-	-	
200	-48	2010	1220
300	-46	1148	630
400	-60	769	380
500	-42	682	310

4.3.3 RL of the NBR/CB composites

The absorption shielding efficiency of composites NBR/CB slightly increases with increasing content of CB (Fig. 39). The lowest value of RL is achieved by the composite filled with 25 phr (19 wt. %) of CB. However, the absorption maximum is at only -2 dB, which is insufficient to reach satisfactory absorption shielding efficiency. Those composites are not able to absorb EMI in the tested

frequency range. The main reason can be attributed to the high electrical conductivity of CB, which is an important criterion for reflection shielding [84].
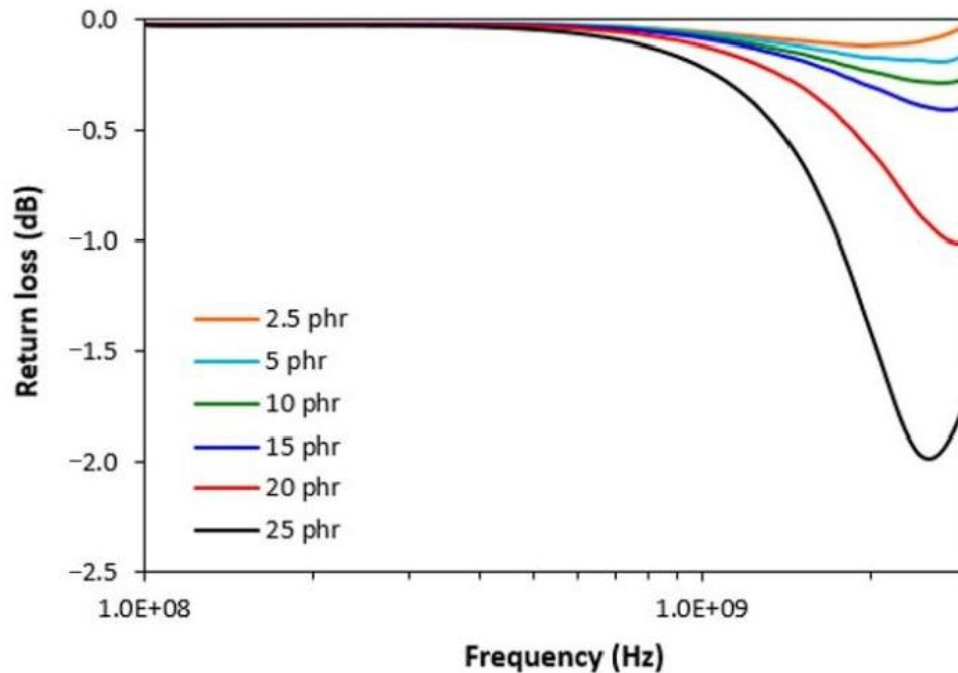
Figure 39: Frequency dependences of RL for NBR composites filled with CB [84]

4.3.4 RL of the NBR/CB/MnZn hybrid composites

From frequency dependences of reflection loss for hybrid CB/MnZn filled composites (Fig. 40), it becomes apparent that the composite filled only with CB does not provide any absorption shielding effectiveness, because it did not reach the return loss at at least -10 dB. With exclusion of the CB-filled composite, all hybrid composites exhibited EMI absorption shielding performance. The best absorption shield can be considered the composite filled with 100 phr (44 wt. %) of MnZn, as this shield exhibited a return loss at -10 dB in the widest frequency bandwidth, i.e., from 1.6 to 2.35 GHz. The absorption maximum was detected at -48 dB at a frequency of 1.9 GHz of electromagnetic radiation. The lowest reflection loss was demonstrated by the maximally filled composite (-60 dB). However, this composite also showed the lowest efficient absorption frequency range at -10 and -20 dB, as also seen in Tab. 15. It becomes obvious that increasing content of MnZn resulted in lower absorption maxima, and the total absorption shielding effectiveness of hybrid composites moved to lower frequencies. In addition, with the increase in MnZn ferrite content, the effective absorption bandwidth of composites became narrower. When comparing composites filled only with magnetic filler (Fig. 38) and hybrid CB/MnZn composites (Fig. 40, Tab. 15) it can be observed that composites filled with a combination of MnZn and CB show lower absorption maxima, but also lower

64

matching frequencies and narrower frequency ranges for RL at -10 dB and -20 dB. It can be stated that the combination of MnZn and CB caused the shifting of effective absorption shielding ability to lower frequencies of EMI.
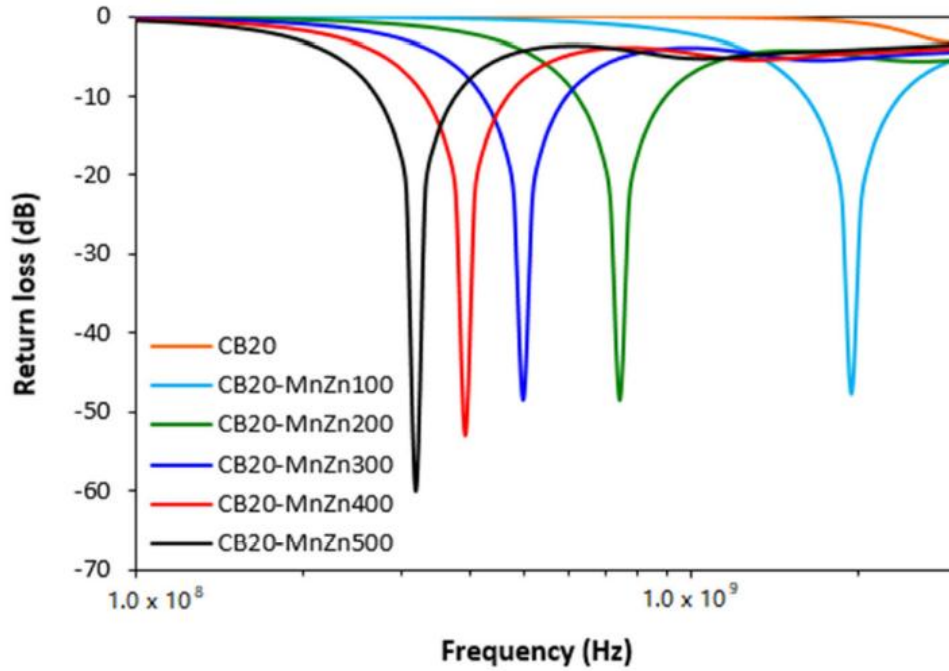
Figure 40: Frequency dependences of return loss for hybrid CB/MnZn NBR composites [4]

Table 15: Electromagnetic absorption characteristics of hybrid CB/MnZn-filled composites

MnZn (phr)	RL_{min} (dB)	f_m (MHz)	Δf (MHz) for -10 dB
100	-48	1931	750
200	-49	739	270
300	-49	495	170
400	-53	390	140
500	-60	319	110

4.3.5 RL of the hybrid NBR/CNT/MnZn composites

From the presented graph of frequency dependences of return loss for hybrid CNT/MnZn composites (Fig. 41), we can see that the composite filled only with CNT and hybrid composites containing 5 phr (1.6 wt.%) of CNT and 200 – 500 phr (64 – 81 wt. %) of MnZn do not provide any absorption shielding performance, because they did not reach reflection loss at at least -10 dB. Only the composite filled with 5 phr (2.3 wt. %) of CNT and 100 phr (45 wt. %) of MnZn was found to have a slight absorption shielding ability. However, the

effective absorption frequency bandwidth of this composite at -10 dB was narrow and ranged only from 1.14 to 1.39 GHz. The absorption maximum was at - 11.2 dB at frequency 1.24 GHz of EMI [4].
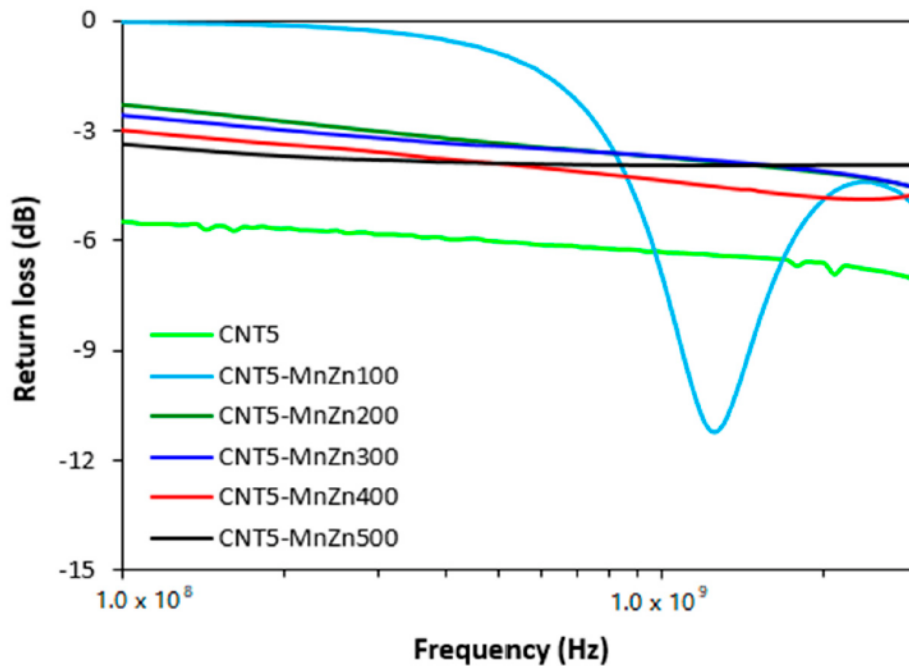
Figure 41: Frequency dependences of return loss for hybrid CNT5/MnZn NBR composites [4]

4.3.6 RL of the TPE/MnZn and TPE/CI composites

In the case of propylene-based thermoplastic elastomer (TPE) composites (Fig. 42), which were measured in the frequency range of 1 MHz – 18 GHz, it is also clear that all composites containing 70 wt. % of MnZn filler and more show sufficient absorption shielding efficiency at -10 dB, which means absorption of almost 95% of incident radiation. Even in this case, it is possible to consider as the best absorbent materials those composites filled with MnZn at the level of 70 and 80 wt. %, which have the widest frequency bands of the absorption shield. The effective absorption band of a composite with 70 wt.% of filler at -10 dB ranges from 2.79 to 6.22 GHz, while Δf at -10 dB of a composite with 80 wt.% of MnZn ranges from 670 MHz to 1.28 GHz. The peaks of the absorption maxima of these composites are at the level of -62 dB at the frequency of 4.3 GHz for the composite with 70 wt. % of filler, resp. -50 dB at 911 MHz for a composite with 80 wt. % of filler. From Fig. 42 and tab. 16, it is also apparent that increasing the amounts of filler shifts RL peaks to lower frequencies similar to ER/PDMS and NBR composites.
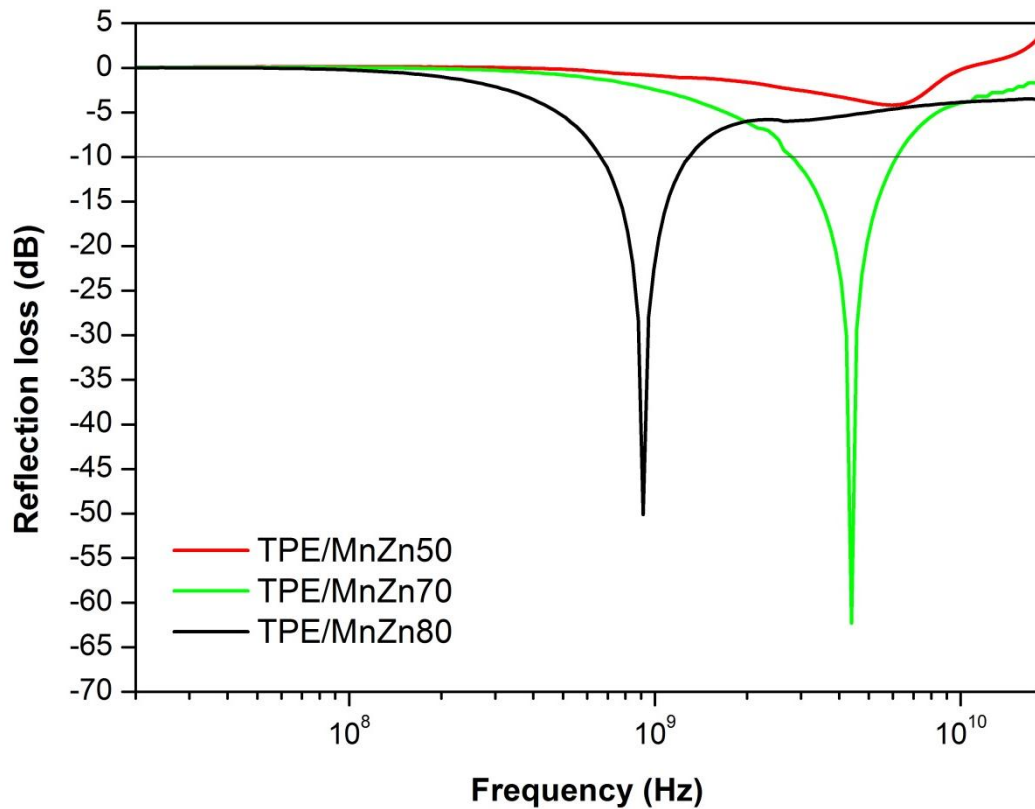
Figure 42: The frequency dependence of the reflection loss of the composites filled with MnZn based on TPE

From the frequency dependences of the reflection losses and absorption parameters of the TPE-based composites (Fig. 43), it can also be stated that these composites containing 80 wt. % CI provide sufficient absorption shielding efficiency in the operating frequency range. In this case, a composite containing 70 wt. % of CI can be considered the most effective absorbent shielding material because it showed reflection losses at -10 dB in the widest frequency range, from 11.6 GHz to 18 GHz at -10 dB. The absorption maximum of this composite material is at the level of -47 dB at a frequency of 17.2 GHz of incident electromagnetic radiation. The composite filled with 80 wt. % of CI showed the same absorption maximum (-47 dB), in a frequency range with effective EMI absorption (reflection losses at -10 dB in the frequency range 1.4 GHz – 2.4 GHz).
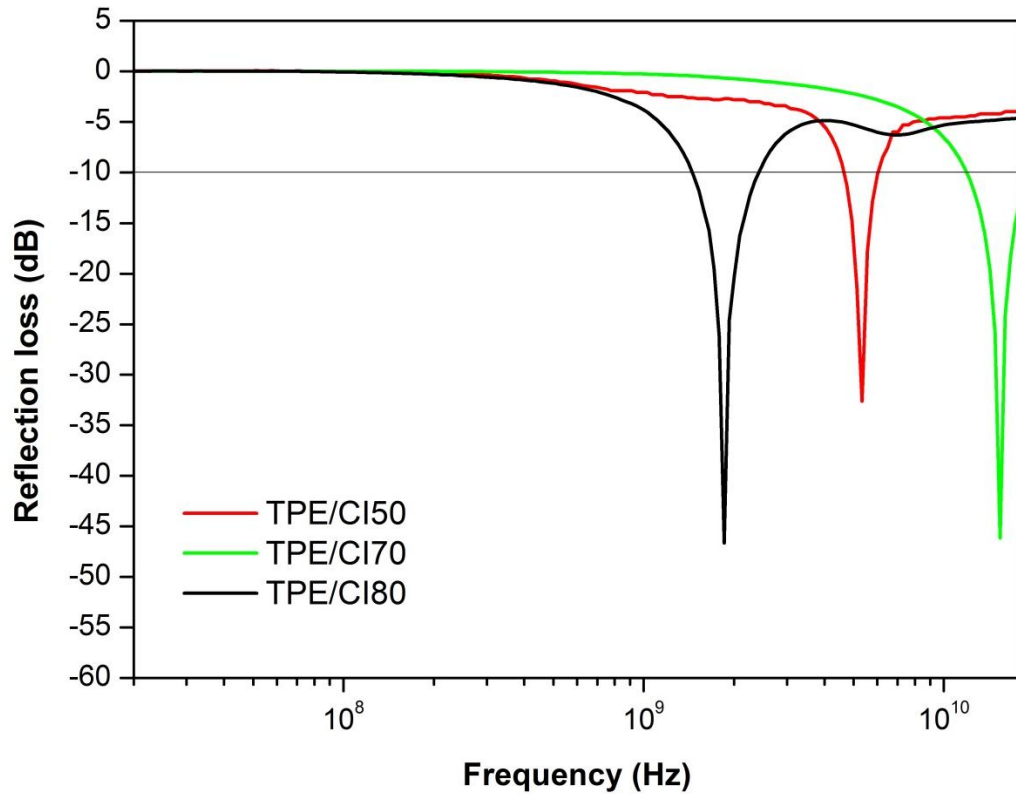
Figure 43: The frequency dependence of the reflection loss of the composites filled with CI based on TPE

Table 16: Electromagnetic absorption characteristics of TPE/MnZn-filled composites

Composites	RL_{min} (dB)	f_m (MHz)	Δf (MHz) for -10 dB
TPE/MnZn50	-	-	-
TPE /MnZn70	-62	4333	3378
TPE /MnZn80	-50	907	642
TPE /CI50	-32	5347	1391
TPE /CI70	-46	15423	-
TPE /CI80	-47	1854	958

4.4 Mechanical properties

4.4.1 Charpy impact of the ER/PDMS/MnZn and ER/PDMS/CI composites

The variation of the impact strength with MnZn and CI content for the composite is shown in Fig. 44. Incorporating a magnetic filler and PDMS into the epoxy resin enhances the composite's toughness. The addition of 50 wt. % of MnZn or CI has a similar effect on the impact strength as the addition of 10 – 30 wt. % of PDMS, which is about 17 KJ/m^2 [104]. A further increase in the filler or the PDMS content leads to a gradual decrease in the impact strength. The values of the impact strength for the composites with 50 wt. % of magnetic filler with 10 or 30 wt. % of PDMS are about 15 KJ/m^2. The polymer composites with a high filler concentration increase the likelihood of particle agglomeration generating defects, which initiates failure. High filler content can also contribute to debonding at the elastomer-matrix interface, which can lead to crack propagation across the elastomer interface. The samples with the highest values of impact strength contained 50 – 70 wt. % of filler. There are no significant differences among the composites with different PDMS contents, i.e. 10 or 30 wt. %. Generally, the size and the shape of the filler play an important role in the impact strength of composites. Composites with rough and larger MnZn particles are more brittle than composites with smaller spherical CI particles due to crack formation during loading.
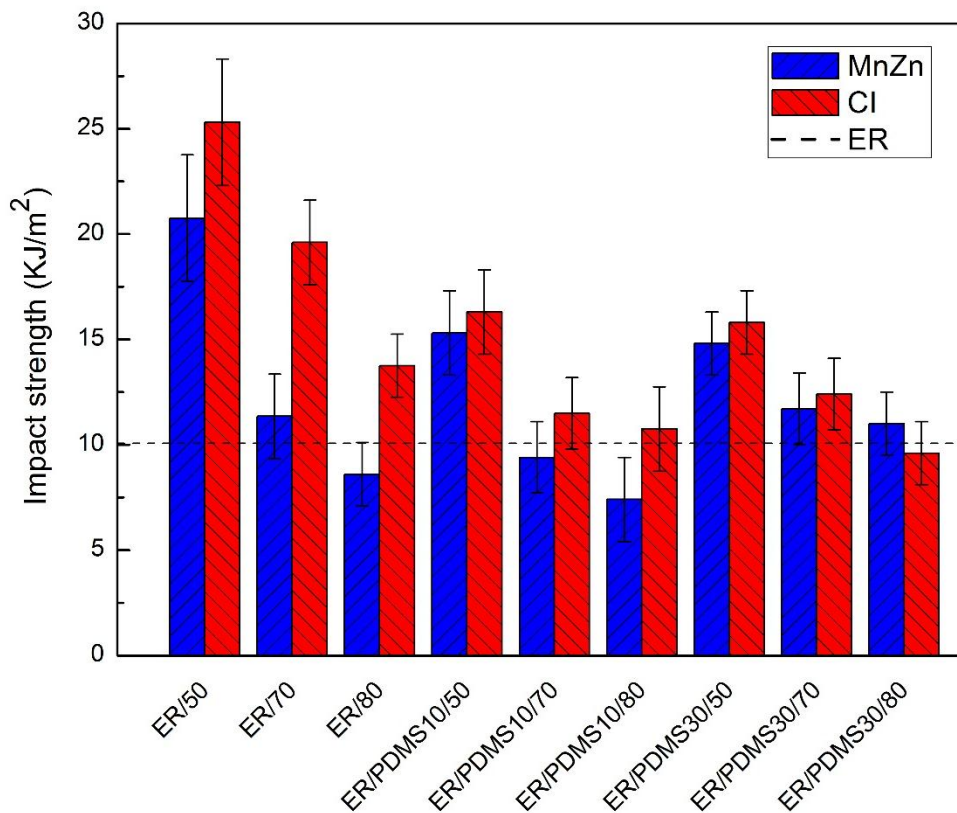
Figure 44: The Impact strength of the magnetic composites filled by MnZn and CI [91]

4.4.2 DMA of the ER/PDMS/MnZn and ER/PDMS/CI composites

The polymer blend of neat epoxy resin (ER) and PDMS was studied in [54]. Figures 45 and 46 show the result of a dynamical mechanical analysis (DMA) of the magnetic composites filled with MnZn and CI. The storage modulus (E´) of the composites increases with increases in the filler concentration from 50 up to 70 wt.% due to the high Young´s modulus of filler (MnZn ~ 124 GPa; CI ~ 207 GPa) (Tab. 17 a, b). However, Young´s modulus of composites decreased at 80 wt. % of the filler, which attributed to the lowering of the cross-linking density due to high-particle content in the polymer matrix (Fig. 45a, 46a).

The effect of interfacial interactions on the dynamic mechanical properties of the filled polymers depends on several factors. These factors include the physical properties of the fillers (particle size, surface area, particle size distribution, geometry of the particles, etc.), the quality of the filler dispersion in the matrix, and the concentration of the filler in the composite.

Most of the studies [8, 11] suggested that, in the event of a strong interfacial interaction between the matrix and the filler, the peak value of tan δ reduces, whereas Tg of the composite increases. In our study, we did not find a visible change in Tg for the composites filled with MnZn ferrite, but for a composite with CI, Tg decreases due to the filler oxidation processes, which was confirmed by the results of the XPS (Fig. 46c).
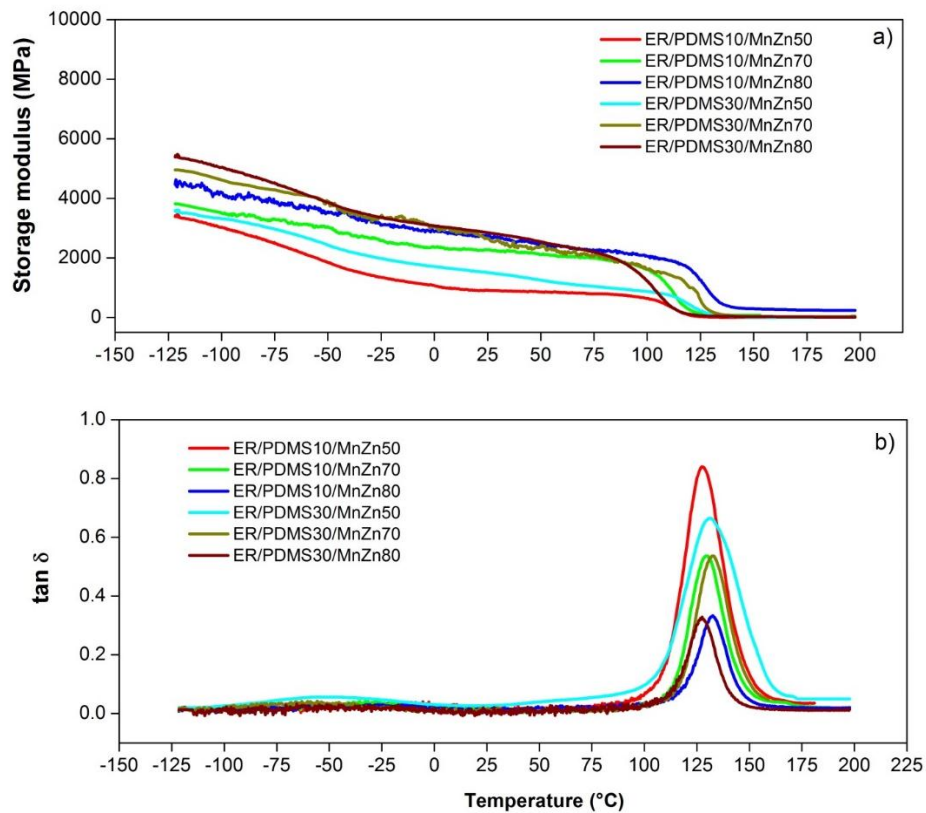
Figure 45: The temperature dependences of a) the storage modulus E´ and b) tan δ of composite filled by MnZn [91]
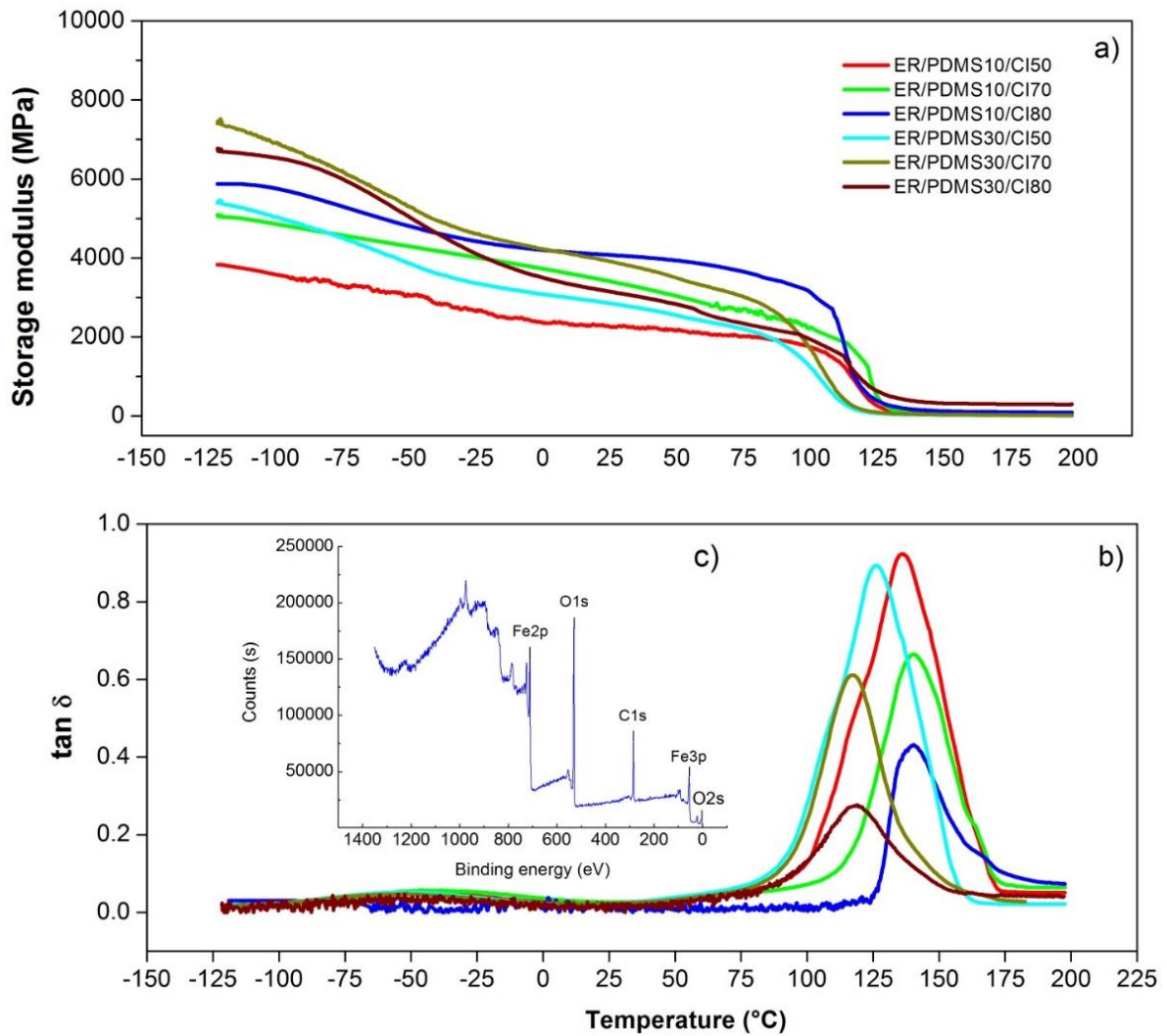
*Figure 46: The temperature dependences of a) the storage modulus E´
b) tan δ of the composite filled by CI and c) XPS of the ER/PDMS10/CI80* [91]

Table 17 a) The values of E´ and T_g of the composites as a function of the temperature

Composites	E´ (MPa) - 80 °C	E´ (MPa) 40 °C	Tan δ	T_g (°C)
ER	4005	1677	0.53	146
ER/PDMS10	3688	1571	0.56	139
ER/PDMS30	3880	1508	0.63	130
ER/PDMS10/MnZn50	2646	888	0.84	127
ER/PDMS10/MnZn70	3300	2134	0.54	130
ER/PDMS10/MnZn80	3950	2588	0.33	132

Table 17 b) The values of E´ and T_g of the composites as a function of the temperature

Composites	E´ (MPa) - 80 °C	E´ (MPa) 40 °C	Tan δ	T_g (°C)
ER/PDMS30/MnZn50	2988	1342	0.65	130
ER/PDMS30/MnZn70	4319	2419	0.54	132
ER/PDMS30/MnZn80	4634	2673	0.33	127
ER/PDMS10/CI50	3354	2225	0.92	135
ER/PDMS10/CI70	4631	3205	0.65	140
ER/PDMS10/CI80	5461	4005	0.42	139
ER/PDMS30/CI50	4631	2640	0.88	130
ER/PDMS30/CI70	6411	3649	0.61	118
ER/PDMS30/CI80	6174	2819	0.27	118

4.4.3 DMA of the NBR/CB and CNT composites

The peak maximum corresponds to the glass transition temperature Tg, and it becomes evident that there was almost no change in Tg of the CB/MnZn composites in dependence on magnetic filler content (Fig. 47, Tab. 18). On the other hand, as seen in Fig. 48 and Tab. 19, the Tg of the CNT/MnZn composites shifted to higher temperatures with an increase in filler loading. However, it should be noted that the differences in Tg of the composites were not substantial, and generally it can be stated that glass transition temperature is not significantly influenced by the composition of composites. It becomes evident that both tan δ and loss modulus increase with the increasing content of magnetic filler in the composite materials. This suggests that higher dynamic strain applied on composites causes a higher transformation of dynamic-mechanical forces into heat [105].
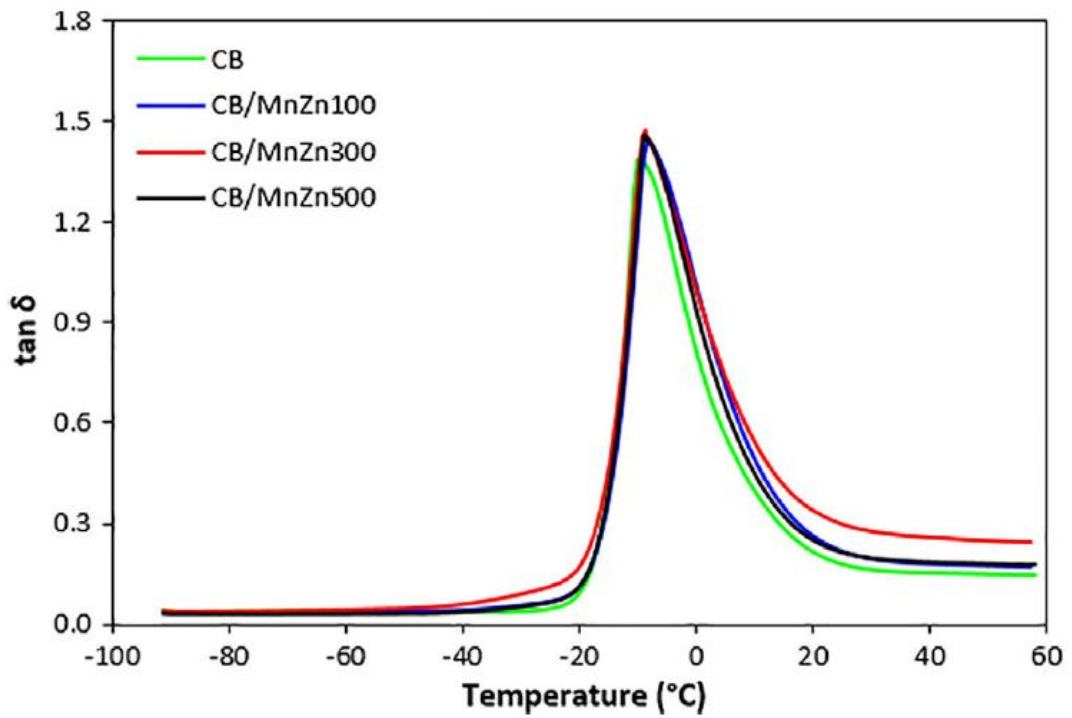
Figure 47: Temperature dependences of tan δ for CB/MnZn NBR composites [105]
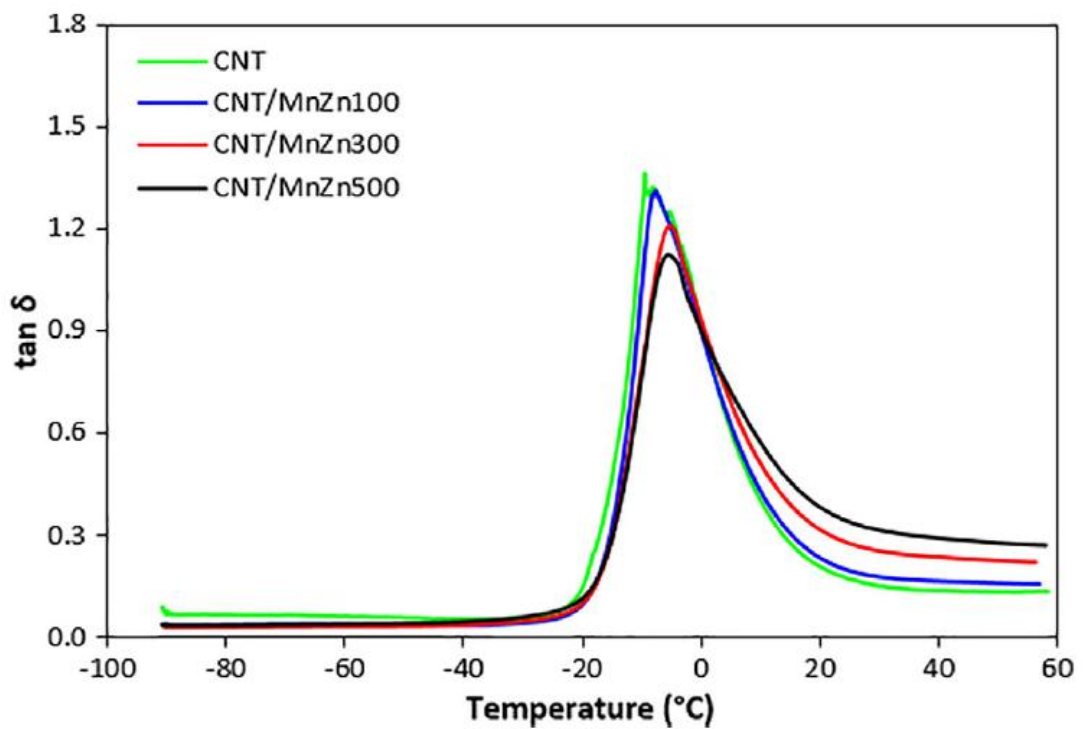
Figure 48: Temperature dependences of tan δ for CNT/MnZn NBR composites [105]

.

Table 18: Dynamic-mechanical characteristics for CB/MnZn composites

Content of MnZn (phr)	T_g (0 °C)	tanδ (0 °C)	tanδ (20 °C)	E´´ (Mpa) (0 °C)	E´´(Mpa) (20 °C)
0	-9.7	0.81	0.21	11.49	1.43
100	-8.3	1	0.26	24.83	2.91
300	-8.6	1.01	0.34	31.35	5.51
500	-9	0.94	0.25	21.58	2.74

Table 19: Dynamic-mechanical characteristics for CNT/MnZn composites

Content of MnZn (phr)	T_g (0 °C)	tanδ (0 °C)	tanδ (20 °C)	E´´ (Mpa) (0 °C)	E´´(Mpa) (20 °C)
0	-9.5	0.92	0.21	16.05	1.33
100	-7.6	0.9	0.23	28.22	3.09
300	-5.1	0.93	0.32	59.62	8.59
500	-5.4	0.9	0.38	63.83	12.8

4.4.4 Tensile properties of the NBR and TPE composites

The physical-mechanical properties of composites filled with a combination of CB and MnZn are, in the presented graphs, compared with the characteristics of equivalent composites filled only with magnetic filler. As shown in Fig. 49, the tensile strength of M300 (modulus at 300 % elongation) of hybrid CB/MnZn composites was higher in comparison with the corresponding composites filled with magnetic filler. The application of CB leads to the reinforcement of the rubber matrix and thus to the increase of tensile strength. The greatest difference in tensile strength was possible to see in the case of reference samples and composites with lower MnZn ferrite content. With an increasing amount of magnetic filler, the difference in tensile strength of the tested composites became less visible, but the tensile strength of hybrid CB/MnZn composites was still higher compared to those filled with magnetic soft ferrite. A SEM analysis of hybrid composites (Fig. 19) demonstrated that the dispersion of fillers, mainly MnZn in hybrid composites, was higher when compared to ferrite-filled composites (Fig. 15). This can be attributed to the higher viscosity of the rubber matrix due to the presence of CB and, thus, higher shear stress during compounding, which facilitates the dispersion and distribution of MnZn ferrite particles within the rubber matrix. The higher dispersion state of MnZn in the rubber matrix might also contribute to better physical-mechanical properties of hybrid composites [84].
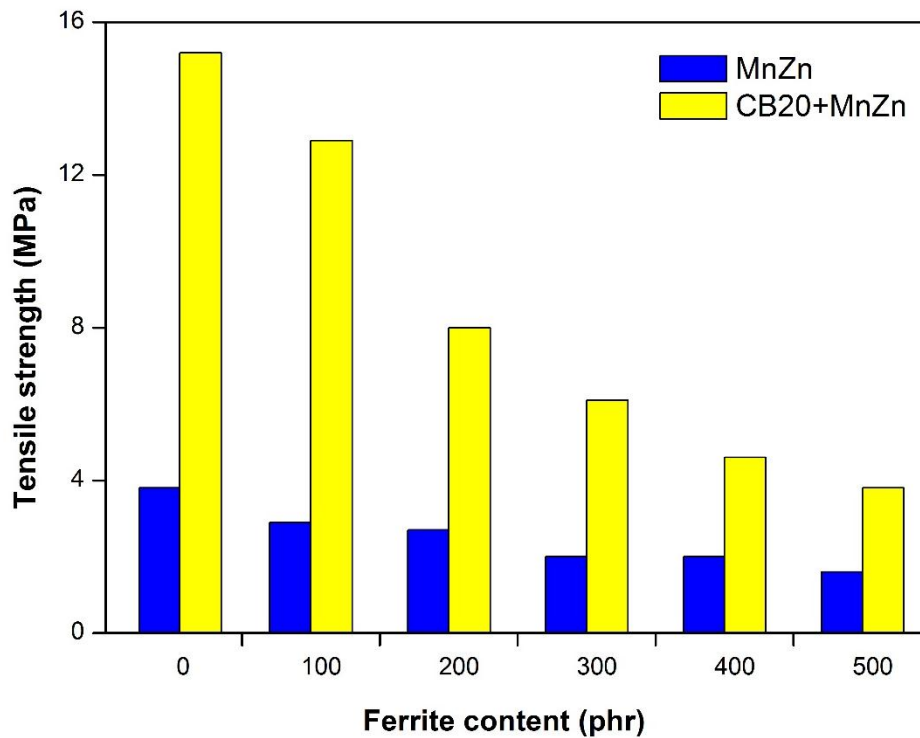
Figure 49: Tensile strength of NBR/MnZn and CB20-MnZn hybrid composites
[84]

The mechanical properties of composites filled only with MnZn and hybrid composites are graphically illustrated in Fig. 50. From the graphs, it becomes apparent that the lowest tensile strength was exhibited by composites filled only with magnetic filler. In addition, the higher the amount of magnetic filler in the composites, the lower the tensile strength. The application of CB and CNT resulted in an increase in tensile strength. The biggest difference in tensile strength among all types of composites was recorded for the reference samples and composites with lower ferrite content. As seen in Fig. 50, the highest tensile strengths were demonstrated by the composite filled with 20 phr (8.7 wt. %) of CB and the composite filled with a combination of CB and 100 phr (44 wt. %) of MnZn. The tensile strength of the hybrid CNT/MnZn composite with 100 phr (45 wt. %) of MnZn ferrite first increased in almost 3 MPa when compared to the reference CNT-filled composite (from 4.3 MPa for the composite filled with 5 phr (44 wt.%) of CNT to nearly 7.5 MPa for the composite filled with CNT and 100 phr (45 wt. %) of MnZn). Then, the tensile strength of hybrid CNT/MnZn composites was found to decrease with the next increasing content of magnetic filler. The initial enhancement of tensile strength for hybrid CNT/MnZn composites can be ascribed to some synergistic effect of both the CNT and MnZn. It also becomes obvious that the higher the content of MnZn in all types of composites, the lower the difference in tensile strength, but the tensile strength of

75

composites filled with a combination of carbon-based fillers and MnZn was higher in all MnZn ferrite concentration scales when compared to the corresponding composites filled only with MnZn filler [4].
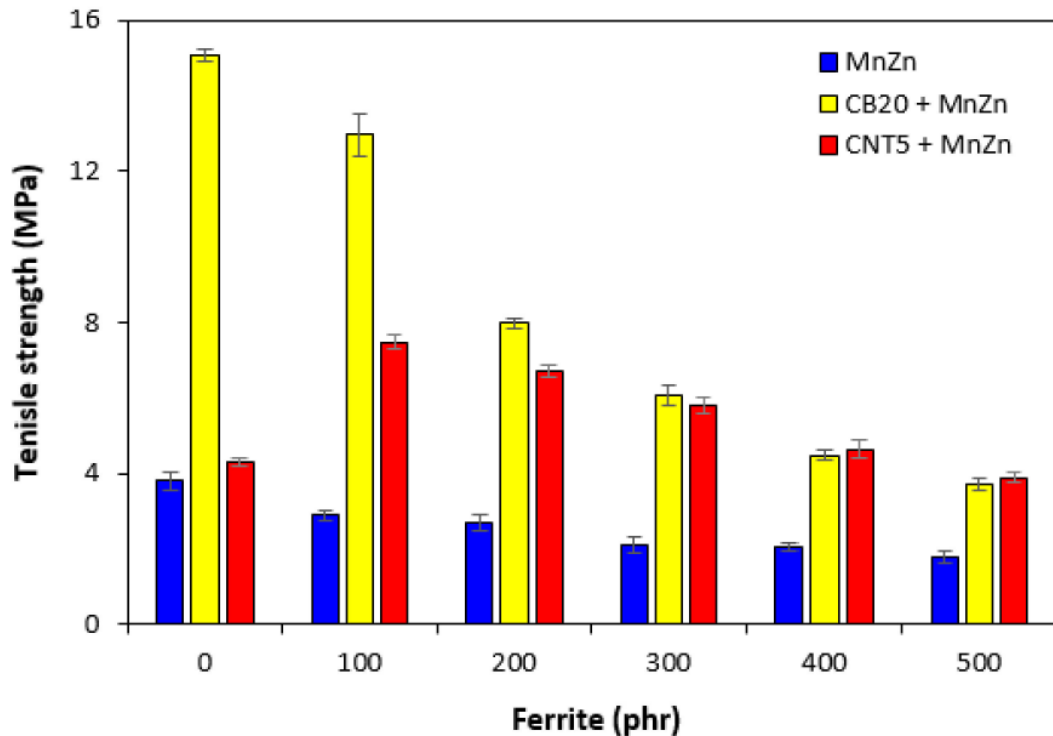
Figure 50: Tensile strength of hybrid NCB20/MnZn and CNT/MnZn NBR composites [4]

Dependence of the tensile strength of the TPE/MnZn and TPE/CI composites on the concentration of the magnetic fillers (Fig. 51) shows that the highest tensile strength at break was shown by the TPE composite filled with the lowest filler content of 50 wt.% MnZn and CI as well. It is also evident that the composites filled with MnZn in the amount of 50 wt. % and 70 wt. % showed higher values of strength characteristics compared to the equivalent composites filled with CI. The difference between the tensile strength of the composites filled with MnZn and CI can be explained by the interface between the matrix and the filler and by the influence of the size and shape of the filler particles. With a further increase in the concentration of the magnetic filler in the TPE/MnZn composites, the tensile strength shows a decreasing course of dependence. From Fig. 51 it is also apparent that the tensile strength of the maximally filled MnZn and CI composites also settled at almost the same values. It is obvious that the higher the content of fillers in both types of composites, the smaller the difference in tensile strength values at break. Composites based on TPE/MnZn/CI show a similar behaviour as hybrid NCB20/MnZn and CNT/MnZn NBR composites.
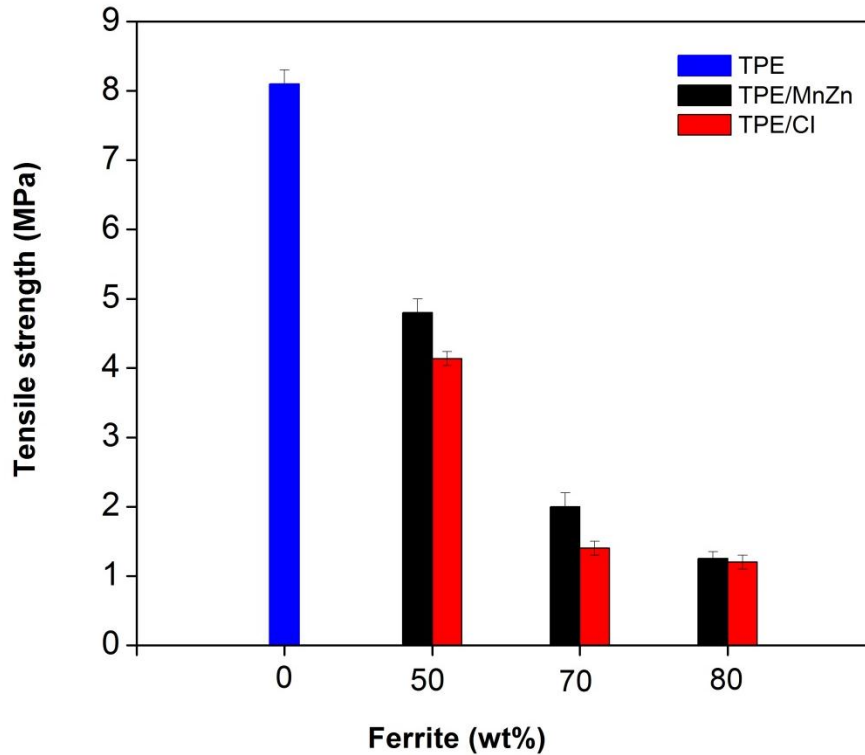
Figure 51: Tensile strength of TPE/MnZn and TPE/CI composites

4.4.5 DC electrical conductivity of the ER/PDMS, NBR and TPE composites

The electrical conductivity of the pure matrix is around 10^{-10} S/m. The MnZn conductivity $\sigma_f = 2$ S/m was determined by four-point method using a silver paste for contacts. In the case of composites (matrix+filler), their electrical conductivity exhibits an increase (Fig. 52). Electrical conductivity is an important material parameter that defines the ability of a material to conduct electrical current. Compared to composites with 50 wt. % of MnZn, the electrical conductivity of maximally filled composites has approximately 1 order of magnitude higher value than composites with 50 wt. % of magnetic filler. Differences in the electrical conductivity of the measured composites could be related to the different distribution and dispersion of the MnZn filler in the polymer matrix. The conductivity increases slightly and almost linearly with a low filler content. With an increase in MnZn content from 70 to 80 wt.%, there was an increase in conductivity by 2 times (from $1.15.10^{-6}$ S/m for a composite filled with 70 wt.% of MnZn to $2.7.10^{-6}$ S/m for a maximum filled composite). No abrupt changes in the electrical conductivity of the composites based on the MnZn combination were observed and the conductivity showed a linearly increasing trend with the increasing amount of MnZn ferrite. Percolation was not clearly achieved, as composites were prepared only with a high concentration (50 - 80 wt. %) where the conductivity of the MnZn filler reached the value ($2x10^{-2}$ S/m) [13].
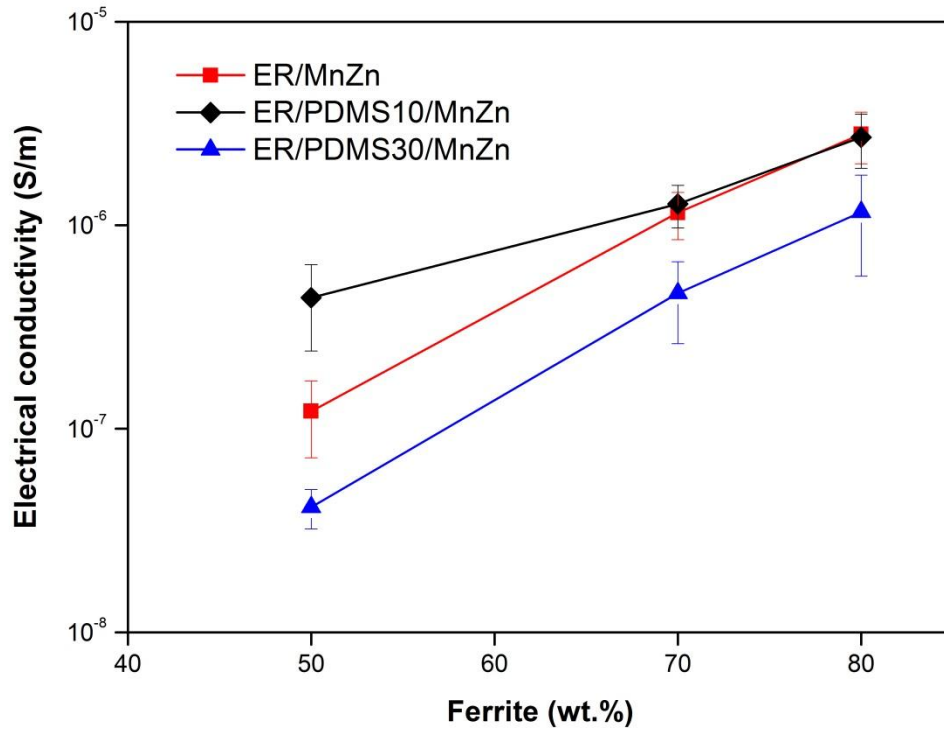
Figure 52: The concentration dependence of DC electrical conductivity on ER/MnZn and ER/PDMS/MnZn composites

In the case of composites filled with CI (Fig. 53), the DC electrical conductivity at the low filler content changed only slightly, but then with an increase in the CI content from 70 to 80 wt. %, there was a sharp increase in conductivity (from 5×10^{-7} S/m for a composite ER/CI (50 wt. %) to 2.7×10^{-6} S/m for a maximum filled composite. The nature of the dependence of conductivity may be related to the type and amount of filler and aspect ratio (L/d) of the studied fillers. As mentioned, the CI particles have a spherical shape, and already during their production the primary particles are combined into larger or smaller structural aggregates. The electrical conductivity of CI is affected by oxidation processes on the surface of the filler.
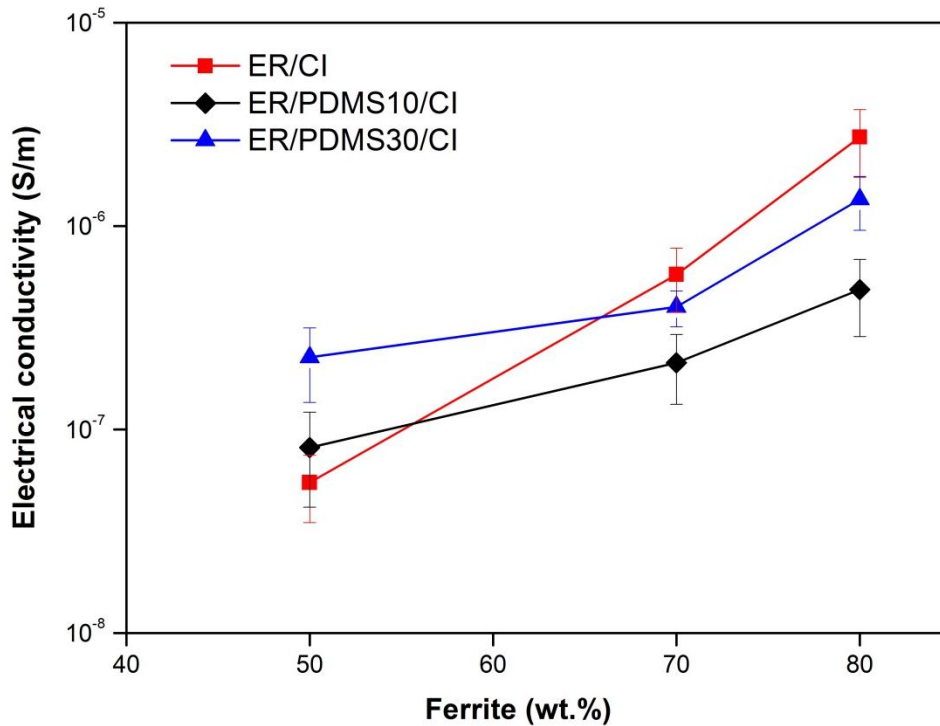
Figure 53: The concentration dependence of DC electrical conductivity on ER/CI and ER/PDMS/CI composites

The electrical conductivity of composites filled with MnZn ferrite and hybrid composites is depicted in Fig. 54. As shown, the lowest electrical conductivity was exhibited by composites filled only with MnZn ferrite. It also becomes obvious that the increasing content of MnZn results in the increase of electrical conductivity of composites, despite the fact that MnZn ranks among dielectric materials. Composites filled with a combination of MnZn and carbon-based fillers exhibit higher electrical conductivity compared to equivalent composites filled only with MnZn ferrite. As also seen in Fig. 54, the electrical conductivity of composites filled only with 20 phr (16 wt. %) of CB or 5 phr (2.3 wt. %) of CNT is almost the same. The incorporation of 100 phr (45 wt. %) magnetic filler results in a significant increase of electrical conductivity of hybrid CNT/MnZn composites. Based upon the achieved results it might be stated that by a combination of CNT and a magnetic filler, the percolation threshold and formation of conductive filler paths are reached even at low magnetic filler content, resulting in outstanding increase of electrical conductivity. When comparing graphical illustrations of permittivity of composites filled only with MnZn (Fig. 23), hybrid CB/MnZn composites (Fig. 31) and CNT/MnZn composites (Fig. 32) and their electrical conductivity, one can see that the higher the electrical conductivity, the higher the imaginary permittivity, and consequently, the higher the complex permittivity of composites, mainly at low frequencies [4].
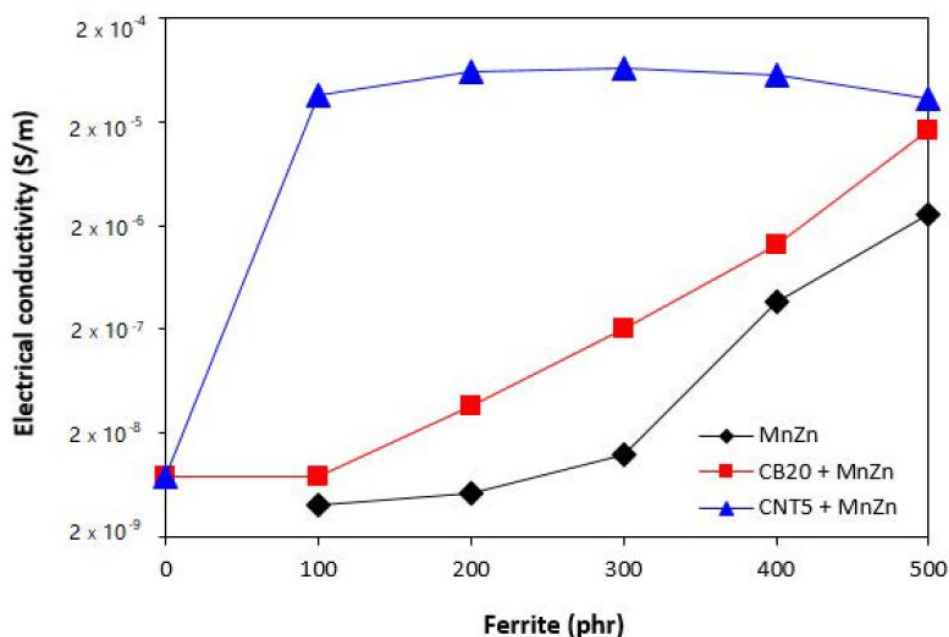
Figure 54: The concentration dependence of DC electrical conductivity on NBR/MnZn and hybrid NBR/CB20/MnZn, NMR/CNT5/MnZn composites [4]

In the case of a TPE composite (Fig. 55), we can observe that the conductivity for concentrations of 70 wt. % increases by 1 order for TPE/CI and by 3 orders for TPE/MnZn. As the concentration increases up to 80 wt. %, the conductivity increases by 1 order for both types of fillers. Low conductivity values at concentrations of 50 wt. % and 70 wt. % are probably due to the formation of aggregates that do not allow efficient formation of conductive pathways. The concentrations 70 wt. % and 80 wt. % are already high enough to exceed the percolation threshold.

The results revealed that composites with MnZn and CI in the ER/PDMS matrix can be used in absorption shielding applications. They are equivalent with fillers (CNT/MnZn) and (CB/MnZn) and in NBR systems are much less effective than EMI absorbers. To explain the different shielding behaviour of the two types of composite materials, their electrical conductivity was also investigated. As shown in Fig. 54, composites filled with 20 phr (16 wt. %) of CB or 5 phr (2.3 wt. %) of CNT have almost identical electrical conductivity. The electrical conductivity of the hybrid composite CB/MnZn filled with 100 phr (44 wt. %) of magnetic filler was almost the same as the reference composite filled with CB only. On the other hand, there was a significant decrease in electrical conductivity of the ER/PDMS composite filled with MnZn and CI.
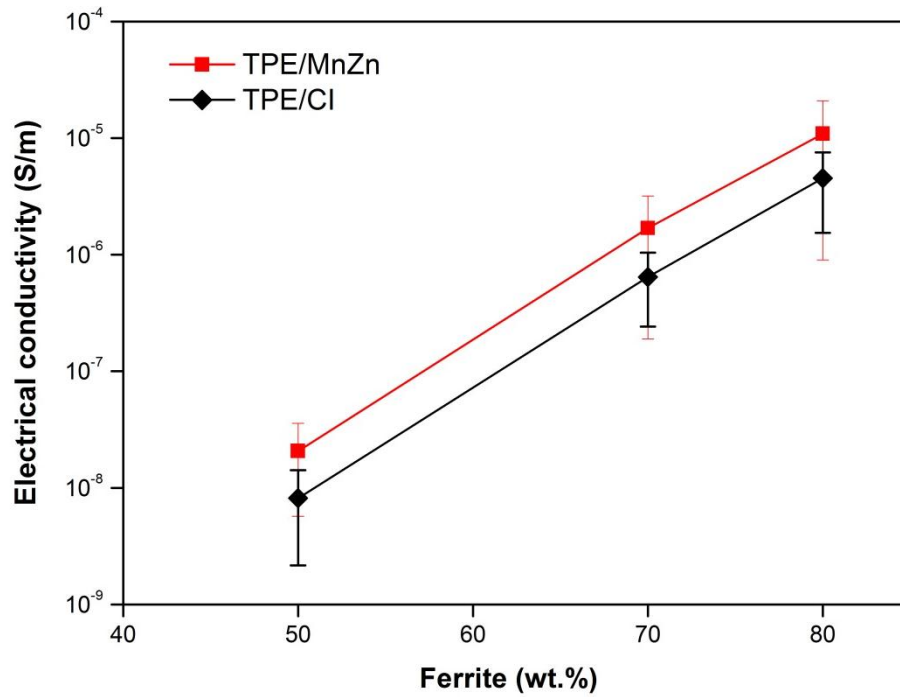
Figure 55: The concentration dependence of DC electrical conductivity of TPE/MnZn and TPE/CI composites

As shown in Fig. 54, apparently, the electrical conductivity of NBR/CB/MnZn composites is lower compared to equivalent NBR/CNT/MnZn composites over the entire MnZn ferrite concentration range. As no sudden changes in the electrical conductivity of the CB/MnZn combination hybrid composites were recorded and the conductivity showed a linearly increasing trend with increasing amount of filler, it can be deduced that the percolation threshold in the given composites was not reached even with a high MnZn ferrites content.

Based on these results, it can be stated that electrical conductivity is one of the key parameters that affects the shielding mechanisms of EMI materials at low frequencies. The higher the carbon filler (conductive) content of the NBR/CB/MnZn and NBR/CNT/MnZn hybrid composite materials, the higher the electrical conductivity and the lower the absorption shielding efficiency. On the other hand, a significant increase in the electrical conductivity (most likely due to reaching the percolation threshold) of NBR/CNT/MnZn composites prevents the use of these composites as effective EMI absorbers at low frequencies.

Based on the available literature sources and the mentioned facts, it can be stated that the main mechanism of the shielding of ER/PDMS and TPE composites with MnZn and CI filler is based on the absorption mechanism, whereas highly electrically conductive materials as well as NBR/CNT/MnZn and NBR/CB/MnZn composites are based on the reflection of electromagnetic radiation, especially at low frequencies.

5. SUMMARY OF THE RESULTS

A dual-phase polymer matrix (ER and PDMS) filled with MnZn-ferrite and CI was investigated with the aim of optimizing the electromagnetic properties of the composites in the RF range (1 MHz – 3 GHz), as well as their mechanical properties and price. To meet this goal, the concentration of PDMS was varied from 10 to 30 wt. %, which affects the distribution of the magnetic particles in the polymer matrix, leading to locally-increased filler concentration in the ER phase. The SEM results showed that the filler is localized inside the ER phase and at the ER-PDMS-interface with good homogeneity.

According to the dielectric and magnetic spectra, measured by the impedance method, the magnetic filler concentration and the polymer matrix composition affect the electromagnetic properties of composites, i.e., with increases in the filler and the PDMS content, both complex permittivity and complex permeability increase. Based on the obtained results, the reflection minima of single-layer absorbers was calculated within the layer thickness, and then the operating absorption bandwidth at -10 dB level of RL was evaluated. An analysis of the obtained results showed that the position of the RL minima moves to a lower frequency, and the loss factors of the composites increase along with increasing the filler concentration. It has been shown that, via a selection of the matrix (ER, ER/PDMS), it is possible to change the distribution of the filler, thereby significantly lowering the reflection loss.

Overall, the presence of 10 wt. % PDMS in both types of composites is sufficient to reduce the demagnetization effect and to obtain broadband RAs with a thickness of 5 – 7 mm.

Hybrid elastomeric (NBR) composites showed that the permeability of MnZn and its combination with carbon fillers (CB and CNT) was dependent only on the content of magnetic filler (from 48 – 82 wt. %), regardless of the type and concentration of carbon filler. The electrical conductivity and permittivity of the composites increased in the order: NBR/MnZn composites < NBR/CB/MnZn composites < NBR/CNT/ MnZn composites (σ=3x10^{-9} S/m, 3x10^{-8} S/m and 5x10^{-4} S/m; ε' = 74, 130 and 1008). On the other hand, it reduced the absorption shielding ability of the composites in the same order (RL = -60 dB, -53 dB, -3 dB, -2.3 dB). A clear correlation was established between the electrical conductivity, permittivity and absorptive shielding ability of the composites. This means that the higher the electrical conductivity, the higher the permittivity and the lower the absorption shielding efficiency of the composites.

During the experiments, it was also shown that MnZn acts as inactive filler and deteriorates the mechanical properties of the composites. Tensile strength decreases in the order: < CB/MnZn composites < CNT/MnZn composites < MnZn composites. At the same time, the tensile strength decreases with an increasing amount of MnZn filler. The most significant decrease is for CB/MnZn composites

(from 15 – 4.2 MPa). The application of carbon-based filler led to the strengthening of the rubber matrix, better dispersion and distribution of MnZn ferrite, and subsequently to the improvement of the mechanical properties of the composites. The tensile strength increased from 3.3 MPa for the NBR/MnZn composite to 13.5 MPa for the NBR/CB20/MnZn composite (MnZn 48% by weight). The conductive CB contributed to the charge storage, various polarization mechanisms, and related relaxation phenomena in the rubber composite, which was manifested by an increase in real and imaginary permittivity. This was subsequently reflected in the change of absorption peaks and the corresponding electromagnetic absorption parameters for the hybrid composites. The MnZn-filled composite containing 200 phr (65% by weight) of magnetic filler can be considered the best absorption shielding material among all tested composites, as it demonstrated the largest absorption frequency bandwidth ($\Delta f = 1220$ MHz) for reflection loss at -10 dB, which indicates absorption of 95% of EMI, respectively. The results also revealed an improvement in the mechanical properties of the hybrid NBR/CB/MnZn composites, where the tensile strength reached a value of 8.1 MPa.

TPE composites based on MnZn and CI fillers were investigated in the RF region (1 MHz – 18 GHz). The results show that the shielding ability of the TPE/MnZn composite occurs in the frequency band (907 MHz – 4.3 GHz) and shifts to lower frequencies with increasing concentration. The measured values show that the best absorption in the widest frequency range was achieved by the TPE/MnZn70 composite (RL = -62 dB and $\Delta f = 3.37$ GHz). The TPE/CI70 composite achieves absorption in a wider frequency band (from 15.4 GHz to 18 GHz and RL = -46 dB), while f_{max} is already outside the measuring range of the device. The tensile strength of both composites decreases with increasing amount (2.1 MPa and 1.6 MPa for 70 wt.%).

6. CONCLUSION

Based on the results obtained as part of the thesis, which was devoted to the preparation of ER/PDMS and elastomeric (NBR, TPE) composite materials filled with magnetically soft ferrite (MnZn and CI) and the combination of MnZn with carbon fillers with the effects of shielding against electromagnetic radiation, especially of absorption mechanisms, the following conclusions were reached:

- In the case of the ER/PDMS-based composite, the best result was achieved with the ER/PDMS10 matrix. It clearly follows from the calculated RL values that composites with this matrix achieve the best values in terms of RL_{min} in the widest frequency range. At the same time, they achieve the best absorption values for MnZn 70 wt.% and CI 70 wt.%. ER/PDMS30 composites also show good values of RL_{min} in a wide frequency range, however, these results are no longer significantly different from the values for ER/PDMS10 composites with 70 wt.% filler. From the point of view of optimizing weight and price, their use is not advantageous.

- For composites with elastomeric matrix (TPE), we can observe that the best values of R_{Lmin} in the widest frequency band at the -10 dB level are achieved by the MnZn 70 wt.%. The TPE composites with MnZn 80 wt.% achieve similar RL minimum values leading to higher weights of the final product. We observe a similar result for composites with CI. A composite with a higher filler content (70 wt.%) does not bring any significant improvement of RL_{min}. In the case of both types of fillers, it is therefore preferable to use a filler with 70 wt.%.

- Carbon-based fillers have a stiffening effect in rubber compounds, which is reflected in the good strength characteristics of composite materials. The electrical percolation threshold for composites with CB was found at 16 wt.%, which proves that it is a conductive composite, where the dominant shielding mechanism against electromagnetic waves is based on reflectivity. For this reason, it achieves exceedingly low absorption values (RL_{min} ~ -2 dB).

- The application of CB and CNT in an elastomeric (NBR) composite filled with a combination of these fillers and MnZn ferrite leads to an improvement in the physical-mechanical properties. Composites filled with a combination of MnZn and CB provide absorption shielding efficiency, with a shift of absorption maxima and overall absorption efficiency towards lower frequency regions (1.9 – 0.32 GHz) compared to composites filled only with MnZn ferrite, and at the same time the effective frequency band of absorption shielding narrows. On the other hand, composites filled with a combination of MnZn and CNT are not able to absorb electromagnetic radiation using absorption mechanisms because they do not show absorption maxima below -10 dB, mainly due to their electrical conductivity of CNT and high permittivity.

ACKNOWLEDGEMENTS

Here is my chance to express my appreciation to some of those who made this work possible. I am extremely grateful for the opportunity to participate in the Ph.D. programme at Tomas Bata University in Zlín. First and foremost, I would like to thank my supervisor, Prof. Ing. Jarmila Vilčáková, Ph.D., for her guidance, support and encouragement throughout my years of studying. I gratefully acknowledge the opportunity to present my work at international conferences during my studies. I am also deeply grateful to my consultant, Assoc. Prof. Natalia Kazantseva, who has greatly supported me and given me new ideas, and taught me practical and scientific matters about magnetic materials. I am grateful to all co-authors of my papers for sharing with me their experiences and professional advice. Particularly, I am grateful to Ing. Marek Jurča, who was always available for scientific discussions. Finally, I owe my gratitude to my family and my beloved mom, whom I will miss forever.

REFERENCES

[1] SEUNG, Han Ryu et al. Absorption-dominant, low reflection EMI shielding materials with integrated metal mesh/TPU/CIP composite. *Chemical Engineering Journal* [online]. 2022, **428**, 131167 [viewed 2022-07-06]. Available from: https://doi.org/10.1016/j.cej.2021.131167

[2] HIRATA, Akimasa. Estimation of Whole-Body Average SAR in Human Models Due to Plane-Wave Exposure at Resonance Frequency. *IEEE transactions on electromagnetic* [online]. 2010, **52**, 41-48 [viewed 2022-07-06]. Available from: http://dx.doi.org/10.1109/TEMC.2009.2035613

[3] CABANOVÁ, Z. Biologické účinky elektromagnetického poľa. In Advances in Electrical and Electronic Engineering. [online]. s. 24–29 [viewed 2022-07-06]. Available from: https://core.ac.uk/download/pdf/8986386.pdf

[4] KRUŽELÁK, Ján et al. Mechanical, Thermal, Electrical Characteristics and EMI Absorption Shielding Effectiveness of Rubber Composites Based on Ferrite and Carbon Fillers. *Polymers-Basel* [online]. 2021, **13**, 2937 [viewed 2022-07-06]. Available from: https://doi.org/10.3390/polym13172937

[5] ZHOU, Yanfen et al. Lightweight and highly conductive silver nanoparticles functionalized meta-aramid nonwoven fabric for enhanced electromagnetic interference shielding. *Journal of Materials Science* [online]. 2021, **56,** 6499–6513 [viewed 2022-07-06]. Available from: https://doi.org/10.1007/s10853-020-05600-8

[6] STERGIOU, Charalampos A. et al. Hybrid polymer composites for electromagnetic absorption in electronic industry. *Hybrid Polymer Composite Materials: Applications* [online]. 2017, 53-106 [viewed 2022-07-06]. Available from: https://doi.org/10.1016/B978-0-08-100785-3.00003-6

[7] NASEER, Anam et al. Reinforcement of Electromagnetic Wave Absorption Characteristics in PVDF-PMMA Nanocomposite by intercalation of Carbon Nanofibers. *Electronic Matterials Letters* [online]. 2019, **15**, 201-207 [viewed 2022-07-06]. Available from: https://doi.org/10.1007/s13391-018-00104-9

[8] ROZANOV, Konstantin N. Ultimate thickness to bandwidth ratio of radar absorbers. *IEEE Transactions on Antennas and Propagation*. [online].2000, **48** (8), 1230-1234 [viewed 2022-07-06]. Available from: http://doi:10.1109/8.884491

[9] Microwave absorbing materials. Laird technologies. [online]. [viewed 2022-07-06]. Available from: http://www.lairdtech.com

[10] Ferrite absorbers. TDK RF Solutions Inc. [online]. [viewed 2022-07-06]. Available from: http://www.tdkrfsolutions.com

[11] VOVCHENKO, L.L. et al. Microwave shielding and absorbing properties of single and multilayered structures based on two-phase filler/epoxy composites. *Applied Nanoscience* [online]. 2021 [viewed 2022-07-06]. Available from: https://doi.org/10.1007/s13204-021-01765-z

[12] PERIGO, E.A. et al. Past, Present, and future of soft magnetic composites. *Applied Physics Reviews* [online]. 2018, **5,** 031301 [viewed 2022-07-06]. Available from: https://doi.org/10.1063/1.5027045

[13] SISTA, Kameswara Srikar et al. Carbonyl iron powders as absorption material for microwave interference shielding: A review. *Journal of Alloys and Compounds* [online]. 2021, **853** [viewed 2022-07-06]. Available from: https://doi.org/10.1016/j.jallcom.2020.157251

[14] YADAV, Raghvendra Singh et al. Advanced Spinel Ferrite Nanocomposites for Electromagnetic Interference Shielding Applications. 2020, *Elsevier Inc. Netherlands* [online]. [viewed 2022-07-06]. Available from: https://www.elsevier.com/books-and-journals

[15] BATEL, Lotfi et al. Tunable Magneto-Dielectric Material for Electrically Small and Reconfigurable Antenna Systems at Vhf Band. *Ceramics* [online]. 2020, **3** (3), 276-286 [viewed 2022-07-06]. Available from: https://doi.org/10.3390/ceramics3030025

[16] CHEVALIER, A. et al. Dynamic permeability in soft magnetic composite materials. *Journal of Applied Physics* [online]. 2001, **90**, 3462-3465 [viewed 2022-07-06]. Available from: https://doi.org/10.1063/1.1389520

[17] LOPATIN, A.V. et al. The efficiency of application of magnetic polymer composites as radio-absorbing materials. *Journal of Communications Technology and Electronics* [online]. 2008, **53**, 487–496 [viewed 2022-07-06]. Available from: https://doi.org/10.1134/S106422690805001X

[18] BABAYAN, V. et al. Combined effect of demagnetizing field and induced magnetic anisotropy on the magnetic properties of MnZn ferrite composites. *Journal of Magnetism and Magnetic Materials* [online]. 2012, **324**, 161-172 [viewed 2022-07-06]. Available from: https://doi.org/10.1016/j.jmmm.2011.08.002

[19] SERRA, N. Epoxy–graphite resistive composites: formulation, characterization and applications. Doctoral Thesis. *Ecole Polytechnique Federale de Lausanne*. 2012.

[20] FORTUNATI, E. et al. Carbon nanotubes and silver nanoparticles for multifunctional conductive biopolymer composites. *Carbon* [online]. 2011, **49**(7), 2370–9 [viewed 2022-07-06]. Available from: https://doi.org/10.1016/j.carbon.2011.02.004

[21] CHEN, L.V. et al. Microwave electronics: measurement and materials characterization. *John Wiley & Sons* [online]. 2004 [viewed 2022-07-06]. Available from: https://doi.org/10.1002/0470020466

[22] AVILA, Antonio F. et al. A dual analysis for recycled particulate composites: linking micro-and macro-mechanics. *Materials characterization* [online]. 2003, **50**(4), 281-291 [viewed 2022-07-06]. Available from: https://doi.org/10.1016/S1044-5803(03)00124

[23] STRÜMPLER, R. and GLATZ-REICHENBACH, J. Conducting Polymer Composites. *Journal of Electroceramics* [online]. 1999, **3**(4): 329 [viewed 2022-07-06]. Available from: https://doi.org/10.1023/A:1009909812823

[24] NIE, Yan et al. Preparation, surface modification and microwave characterization of magnetic iron fibres. *Journal of Magnetism and Magnetic Materials* [online]. 2006, **306**, pp. 125-129 [viewed 2022-07-06]. Available from: https://doi.org/10.1016/j.jmmm.2006.02.233

[25] FENG, Y.B. et al. Absorbing properties and structural design of microwave absorbers based on carbonyl iron and barium ferrite. *Journal of Magnetism and Magnetic Materials* [online]. 2007, **318**, pp. 8-13 [viewed 2022-07-06]. Available from: https://doi.org/10.1016/j.jmmm.2007.04.012

[26] ZHANG, Baoshan et al. Microwave-absorbing properties of deaggregated flake-shaped carbonyl-iron particle composites at 2-18 GHz. *IEEE Transactions on Magnetics* [online]. 2007, **42**, pp. 1778-1781 [viewed 2022-07-06]. Available from: https://doi.org/10.1109/TMAG.2006.874188

[27] KAZANTSEVA, Natalia Magnetic Particle-Filled Polymer Microcomposites. In: SABU, Thomas et al. Polymer Composites, Vol. **1**: Macro- and Microcomposites. First Edition. *Wiley-VCH Verlag GmbH & Co. KgaA* [online]. 2012, 613-672 [viewed 2022-07-06]. Available from: ISBN: 978-3-527-32624-2

[28] DRÁPALA, J. – KURSA, M. Elektrotechnické materiály. 1. Vyd. Ostrava: VŠB – Technická univerzita Ostrava, 2012. 439 s. ISBN 978-80-248-2570-0 [viewed 2022-07-06]. Available from: http://www.person.vsb.cz/archivcd/FMMI/ETMAT/index.htm

[29] BHALLA, D. et al. 2012. Material Processing Technology for Soft Ferrites Manufacturing. *American Journal of Materials Science* [online]. 2012, vol. 2, no. 6, p. 165–170 [viewed 2022-07-06]. Available from: https://doi.org/10.5923/j.materials.20120206.01

[30] Soft Ferrites and Accessories. *Data Handbook. 2013. Ferroxcube*. [online]. 2013, p. 1098 [viewed 2022-07-06]. Available from: https://www.ferroxcube.com/en-global/download/download/11

[31] HESSIEN, M. M. et al. Synthesis of Nanocrystalline Magnesium Ferrites

Powder from Mill Scale. *International Journal of Material Science* [online]. 2011, vol.1, no.**1**, p. 30–34 [viewed 2022-07-06]. Available from: https://archive.org/details/IJMS10010/IJMS10010

[32] LEAL, E. et al. Structural, textural, morphological, magnetic and electromagnetic study of Cu-doped NiZn ferrite synthesized by pilot-scale combustion for RAM application. *Arabian Journal of Chemistry* [online]. 2020, vol. 13, no. 11, p. 8100–8118 [viewed 2022-07-06]. Available from: https://doi.org/10.1016/j.arabjc.2020.09.041

[33] KRUŽELÁK, J. et al. 2021. Progress in polymers and polymer composites used as efficient materials for EMI shielding. *In Nanoscale Adv*. [online]. 2021, vol. 3, p. 123–172 [viewed 2022-07-06].
Available from: https://doi.org/10.1039/D0NA00760A

[34] RICHES, E. E. Ferrites, A Review of Materials and Applications. Londýn: Mills & Boon Limited, 1972. 85 p. ISBN 0 263.05071.8

[35] Kapitola 13 - Magnetické materiály, skriptá FEI TUKE. [online]. [viewed 2022-07-06]. Available from:http://web.tuke.sk/feikte/slovak/subjects/ZIM/

[36] Magnetizmus, cievky, jadrá. [online]. 2019 [viewed 2022-07-06]. Available from: http://www.matfyz.estranky.sk/clanky/magnetizmus--cievky--jadra

[37] https://electronics.stackexchange.com [online], [viewed 2022-07-06]. Available from:
https://electronics.stackexchange.com/questions/177863/can-anyone-explain-why-a-b-h-curve-with-hysteresis-doesnt-result-in-a-highly-no

[38] BROŽ, J. 1962. Moderní problémy feromagnetismu. Praha: Nakladatelství Československé Akademie Věd, 1962. 192 s. ISSN 0528-7103

[39] MESHRAM, M. R. et al. Characterization of M-type barium hexagonal ferrite-based wide band microwave absorber. *J Magn Magn Mater* [online]. 2004, **271**: 207–214 [viewed 2022-07-06]. Available from: https://doi.org/10.1016/j.jmmm.2003.09.045

[40] IQBAL, M. J. et al. Physical, electrical and dielectric properties of Ca-substituted strontium hexaferrite ($SrFe_{12}O_{19}$) nanoparticles synthesized by co-precipitation method. *J Magn Magn Mater* [online]. 2010, **322**:1720–1726 [viewed 2022-07-06]. Available from: https://doi.org/10.1016/j.jmmm.2009.12.013

[41] HARRIS, V. G. et al. Recent advances in processing and applications of microwave ferrites. *J Magn Magn Mater* [online]. 2009;321:2035–2047 [viewed 2022-07-06]. Available from: https://doi.org/10.1016/j.jmmm.2009.01.004

[42] FOULGER, Stephen H. Electrical Properties of Composites in the Vicinity of the Percolation Threshold. *Journal of Applied Polymer Science* [online].

1999, **72**(12), 1573-82 [viewed 2022-07-06]. Available from: https://doi.org/10.1002/(SICI)1097-4628(19990620)72:12<1573::AID-APP10>3.0.CO;2-6

[43] FOULGER, Stephen H. Reduced percolation thresholds of immiscible conductive blends. *Journal of Polymer Science Part B: Polymer Physics* [online]. 1999, **37**(15), 1899-1910 [viewed 2022-07-06]. Available from: https://doi.org/10.1002/(SICI)1099-0488(19990801)37:15<1899::AID-POLB14>3.0.CO;2-0

[44] VILČÁKOVÁ, Jarmila et al. Effect of Surfactants and manufacturing methods on the electrical and thermal conductivity of carbon nanotube/silicone composites. *Molecules* [online]. 2012, **17**(11), 13157-74 [viewed 2022-07-06]. Available from: https://doi.org/10.3390/molecules171113157

[45] MOUČKA, R. et al. The influence of interfaces on the dielectric properties of MnZn-based hybrid polymer composites. *Journal of Applied Physics* [online]. 2008, **104**, 103718 [viewed 2022-07-06]. Available from: http://dx.doi.org/10.1063/1.3028272

[46] PARK, Jun Kue et al. Enhanced anomalous magnetization in carbonyl iron by Ni+ ion beam irradiation. *Scientific Reports* [online]. 2021, **11** [viewed 2022-07-06]. Available from: https://doi.org/10.1038/s41598-021-99673-3

[47] KONG, L. B. et al. Recent progress in some composite materials and structures for specific electromagnetic applications. *International Materials Reviews* [online]. 2013, **58**(4), 203-259 [viewed 2022-07-06]. Available from: https://doi.org/10.1179/1743280412Y.0000000011

[48] ABSHINOVA, Madina A. et al. Thermomagnetic stability and heat-resistance properties of carbonyl iron filled siloxanes. *Materials Chemistry and Physics* [online]. 2009, **114**, 78-89 [viewed 2022-07-06]. Available from: https://doi.org/10.1016/j.matchemphys.2008.08.091

[49] MIN, Dandan et al. Facile preparation and enhanced microwave absorption properties of flake carbonyl iron/Fe3O4 composite. *Journal of Magnetism and Magnetic Materials* [online]. 2017, **435**, 26-32 [viewed 2022-07-06]. Available from: https://doi.org/10.1016/j.jmmm.2017.03.065

[50] KUMAR, P. et al. 2019. Recent advances in polymer and polymer composites for electromagnetic interference shielding: review and future prospects. *Polym Rev.* [online]. 2019;59(4):687–738 [viewed 2022-07-06]. Available from: https://doi.org/10.1080/15583724.2019.1625058

[51] JIA, L. CH. et al. A Strong and tough polymer–carbon nanotube film for flexible and efficient electromagnetic interference shielding. *J Mater Chem C* [online]. 2017, **5**:8944–8951 [viewed 2022-07-06]. Available from: https://doi.org/10.1039/C7TC02259J

[52] DEVI, R., GILL, S.S. A squared bossed diaphragm piezoresistive pressure sensor based on CNTs for low pressure range with enhanced sensitivity. *Microsystem technologies* [online]. 2021 [viewed 2022-07-06]. Available from: https://doi.org/10.1007/s00542-020-05208-7

[53] DAI, K. et al. Electrically conductive carbon black (CB) filled in situ microfibrillar poly(ethylene terephthalate) (PET)/polyethylene (PE) composite with a selective CB distribution. *Polymer* [online]. 2007, **48**(3):849–859 [viewed 2022-07-06]. Available from: https://doi.org/10.1016/j.polymer.2006.12.026

[54] JANI, R. K. et al. Tuning of microwave absorption properties and electromagnetic interference (EMI) shielding effectiveness of nanosize conducting black-silicone rubber composites over 8–18 GHz. *Prog Electromang Res* [online]. 2017, **58**:193–204 [viewed 2022-07-06]. Available from: https://doi.org/10.2528/PIERM17022704

[55] LIM, K. M., et al. Complex Permeability and Electromagnetic Wave Absorption Properties of Amorphous Alloy-epoxy Composites. *Journal of Non-Crystalline Solids* [online]. 2005, **351**, 75–83 [viewed 2022-07-06]. Available from: https://doi.org/10.1016/j.jnoncrysol.2004.09.025

[56] YOSHIDA, T. et al. Evaluation of absorbing characteristics and thermal contact resistance of electromagnetic wave absorbing composite rubber. *IEEJ Transactions on Fundamentals and Materials* [online]. 2012, **132**, 180–186 [viewed 2022-07-06]. Available from: https://doi.org/10.1541/ieejfms.132.180

[57] https://hollandshielding.com [online] [viewed 2022-07-06]. Available from: https://hollandshielding.com/Nonflammable-high-power-handling-absorbers

[58] CHEN, Junfeng et al. High-impedance surface-based broadband absorbers with interference theory. *IEEE Transactions on Antennas and Propagation* [online] 2015, **63**, 4367–4374 [viewed 2022-07-06]. Available from: https://doi.org/10.1109/TAP.2015.2459138

[59] HE, Yun et al Design of an adjustable polarization-independent and wideband electromagnetic absorber. *Journal of Applied Physics* [online]. 2016, **119**, 105103 [viewed 2022-07-06]. Available from: https://doi.org/10.1063/1.4943593

[60] NAITO, Yoshiyuki and SUETAKE, Kunihiro Application of ferrite to electromagnetic wave absorber and its characteristics. *IEEE Transactions on Microwave Theory and Techniques* [online]. 1971, **19**, 65–72 [viewed 2022-07-06]. Available from: https://doi.org/10.1109/TMTT.1971.1127446

[61] HUANG, Xianjun et al. Experimental demonstration of printed graphene

nano flakes enabled flexible and conformable wideband radar absorbers. *Scientific Reports* [online]. 2016, **6**, 38197 [viewed 2022-07-06]. Available from: https://doi.org/10.1038/srep38197

[62] KUNDU, Debidas et al. A compact ultrathin broadband absorber by reducing cross-polarized reflection from metal- backed anisotropic array. *Microwave and Optical Technology Letters* [online] 2017, **59**, 970–976 [viewed 2022-07-06]. ISSN: 8952477. Available from: https://doi.org/10.1002/mop.30437

[63] AHMADIA, Farzad and IDAB, Nathan A broadband ultrathin metamaterial absorber using tilted parallel strips. *Proceedings SPIE* [online]. 2017, **10103**, 101031V–1 [viewed 2022-07-06]. Available from: https://doi.org/10.1117/12.2254479

[64] YOO, Young Joon et al. Metamaterial absorber for electromagnetic waves in periodic water droplets. *Scientific Reports* [online]. 2015, **5**, 14018 [viewed 2022-07-06]. Available from: https://doi.org/10.1038/srep14018

[65] MUNAGA, Praneeth et al. A fractal-based compact broadband polarization insensitive metamaterial absorber using lumped resistors. *Microwave and Optical Technology Letters* [online]. 2016, **58**, 343–347 [viewed 2022-07-06]. Available from: https://doi.org/10.1002/mop.29571

[66] WANG, Han et al. Broadband tunability of polarization-insensitive absorber based on fre- quency selective surface. *Scientific Reports* [online]. 2016, **6**, 23081 [viewed 2022-07-06]. Available from: https://doi.org/10.1038/srep23081

[67] LI, Zhenyu et al. Theoretical Study of Electromagnetic Interference Shielding of 2D MXenes Films. *Metals* [online]. 2018, **8**, 652 [viewed 2022-07-06]. Available from: https://doi.org/10.3390/met8080652

[68] GE, Yaqing et al. $ZnFe_2O_4$@PDA@Polypyrrole composites with efficient electromagnetic wave absorption properties in the 18–40 GHz region. *Journal of Materials Science* [online]. 2021, **56**, 10876–10891 [viewed 2022-07-06]. Available from: https://doi.org/10.1007/s10853-021-05968-1

[69] SANKARAN, Sowmya et al. Recent advances in electromagnetic interference shielding properties of metal and carbon filler reinforced flexible polymer composites: A review. *Composites Part A: Applied Science and Manufacturing* [online]. 2018, *S.* **114**, 49–71 [viewed 2022-07-06]. Available from: https://doi.org/10.1016/j.compositesa.2018.08.006

[70] JAROSZEWSKI, M. et al. Advanced Materials for Electromagnetic Shielding. Fundamentals, Properties and Applications. *John Wiley & Sons, Inc. 1st Ed*. [online]. 2019 [viewed 2022-07-06]. Available from: https://doi.org/10.1002/9781119128625

[71] www.mathworks.com [online]. [viewed 2022-07-06]. Available from: https://www.mathworks.com/help/rfpcb/gs/scatterring-parameters-or-s-parameters.html

[72] FISKE, T. J. et al. Percolation in magnetic composites. *Journal of Materials Science* [online]. 1997, **32**(20), 5551-60 [viewed 2022-07-06]. Available from: https://doi.org/10.1023/A:1018620407013

[73] wikimedia.org [online] [viewed 2022-07-06]. Available from: https://commons.wikimedia.org/wiki/File:Electromagnetic_spectrum_with_sources.svg

[74] MOUČKA, Robert et al. Enhancement of magnetic losses in hybrid polymer composites with MnZn-ferrite and conducting fillers. *Journal of Material Science* [online]. 2007, **42**, 9480-90 [viewed 2022-07-06]. Available from: https://doi.org/10.1007/s10853-007-2081-0

[75] LAGARKOV, Andrey N. et al. High-frequency behavior of magnetic composites. *Journal of Magnetism and Magnetic Materials* [online] 2009, **321**(14), 2082-92 [viewed 2022-07-06]. Available from: https://doi.org/10.1016/j.jmmm.2008.08.099

[76] SONG, W.L. et al. Highly ordered porous carbon/wax composites for effective electromagnetic attenuation and shielding, *Carbon* [online]. 2014, **77** (2014) 130–142 [viewed 2022-07-06]. Available from: https://doi.org/10.1016/j.carbon.2014.05.014

[77] QUAN, B. et al. Dielectric polarization in electromagnetic wave absorption: review and perspective, *J. Alloys Compd.* [online] (2017, **728**, 1065–1075 [viewed 2022-07-06]. Available from: https://doi.org/10.1016/j.jallcom.2017.09.082

[78] CHEN, Y. et al. A three-dimensional absorber hybrid with polar oxygen functional groups of MWNTs/graphene with enhanced microwave absorbing properties, *Compos. Part B* [online]. 2017, **108**, 386–392 [viewed 2022-07-06]. Available from: https://doi.org/10.1016/j.compositesb.2016.10.014

[79] ZHENG, Y. et al. Fabrication of porous graphene-Fe_3O_4 hybrid composites with outstanding microwave absorption performance, *Compos. Part A Appl. Sci. Manuf.* [online] 2017, **95** 237–247 [viewed 2022-07-06]. Available from: https://doi.org/10.1016/j.compositesa.2017.01.015

[80] JIAN, X. et al. Facile synthesis of Fe_3O_4/GCs composites and their enhanced microwave absorption properties, *ACS Appl. Mater. Interfaces* [online]. 2016, **8**, 6101–6109 [viewed 2022-07-06]. Available from: https://doi.org/10.1021/acsami.6b00388

[81] DORING, W. Über die Trägheit der Wände zwischen Weißschen Bezirken,

Z. Naturf. [online]. *3a* 1948 **373** [viewed 2022-07-06]. Available from: https://doi.org/10.1515/zna-1948-0701

[82] MILES, P.A. et al. Dielectric spectroscopy of ferromagnetic semiconductors, *Rev. Mod. Phys.* [online]. 1957, **29**, 279–307 [viewed 2022-07-06]. Available from: https://doi.org/10.1103/RevModPhys.29.279

[83] J.H.E. GRIFFITHS, J.H.E. Anomalous high-frequency resistance of ferromagnetic metals, *Nature* [online]. 1946, **158**, 670–671 [viewed 2022-07-06]. Available from: https://doi.org/10.1038/158670A0

[84] KRUŽELÁK, J. et al. Electromagnetic Interference Shielding and Physical-Mechanical Characteristics of Rubber Composites Filled with Manganese-Zinc Ferrite and Carbon Black. *Polymers* [online]. 2021, **13** (4), 616 [viewed 2022-07-06]. Available from: https://doi.org/10.3390/polym13040616

[85] www.jvmicronics.co [online]. [viewed 2022-07-06]. Available from: https://www.jvmicronics.co.in/rf-absorber.html

[86] AL-SALEH, M.H. et al. EMI shielding effectiveness of carbon based nanostructured polymeric materials: A comparative study. *Carbon* [online]. 2013, **60**, 146–156 [viewed 2022-07-06]. Available from: https://doi.org/10.1016/j.carbon.2013.04.008

[87] ZHU, J. et al. Carbon nanostructure-derived polyaniline metacomposites: Electrical, dielectric, and giant magnetoresistive properties. *Langmuir* [online] 2012, **28**, 10246–10255 [viewed 2022-07-06]. Available from: https://doi.org/10.1021/la302031f

[88] ZHU, Y. et al. Facile synthesis of $BaTiO_3$ nanotubes and their microwave absorption properties. *ACS Appl. Mater. Interfaces* [online]. 2012, **4**, 2101–2106 [viewed 2022-07-06]. Available from: https://doi.org/10.1021/am300069x

[89] GUPTA, T.K. et al. MnO_2 decorated graphene nanoribbons with superior permittivity and excellent microwave shielding properties. *J. Mater. Chem. A* [online]. 2014, **2**, 4256–4263 2106 [viewed 2022-07-06]. Available from: https://doi.org/10.1039/C3TA14854H

[90] YADAV, R.S. et al. $NiFe_2O_4$ nanoparticles synthesized by dextrin from corn-mediated sol-gel combustion method and its polypropylene nanocomposites engineered with reduced graphene oxide for the reduction of electromagnetic pollution. *ACS Omega* [online]. 2019, **4**, 22069–22081 2106 [viewed 2022-07-06]. Available from: https://doi.org/10.1021/acsomega.9b03191

[91] GOŘALÍK, M. et al. Engineering Magnetic Type Radio-Absorbers Based on Composites with a Dual-Phase Polymer Matrix. *Electronic Materials*

Letters [online]. 2022 [viewed 2022-07-06]. Available from: https://doi.org/10.1007/s13391-022-00351-x

[92] MOORE, R.L. Development and test of concentration scalled demagnetization in effective media theories of magnetic composites. *J. Appl. Phys.* [online]. 2019, **125**, 085101 [viewed 2022-07-06]. Available from: https://doi.org/10.1063/1.5053791

[93] MATTEI, J.L., LE FLOC'H, M. Effects of the magnetic dilution of the ferromagnetic resonance of disordered heterostructures. *J. Magn. Magn. Mater.* [online.]. 2003, **264**, 86-94 [viewed 2022-07-06]. Available from: https://doi.org/10.1016/S0304-8853(03)00143-4

[94] MATTEI, J.L., LE FLOC'H, M. Percolative behavior and demagnetizing effects in disordered heterostructures. *J. Magn. Magn. Mater.* [online]. 2003, **257**, 335-345 [viewed 2022-07-06]. Available from: https://doi.org/10.1016/S0304-8853(02)01232-5

[95] SHUKLA, V. Review of electromagnetic interference shielding materials fabricated by iron ingredients. *Nanoscale Adv.* [online]. 2019, **1**, 1640–1671 [viewed 2022-07-06]. Available from: https://doi.org/10.1039/C9NA00108E

[96] IDRIS, MF. et al. Recent developments of smart electromagnetic absorbers based polymer-composites at gigahertz frequencies. *J Magn Magn Mater.* [online]. 2016, **405**, 197–208 [viewed 2022-07-06]. Available from: https://doi.org/10.1016/j.jmmm.2015.12.070

[97] LIU, L. et al. Microwave absorption properties of a wave-absorbing coating employing carbonyl-iron powder and carbon black. *Appl. Surf. Sci.* [online]. 2010, **257**, 842-846 [viewed 2022-07-06]. Available from: https://doi.org/10.1016/j.apsusc.2010.07.078

[98] FENG, Y.B. et al. Absorbing properties and structural design of microwave absorbers based on carbonyl iron and barium ferrite. *J. Magn. Magn. Mater.* [online]. 2007, **318** (1–2) 8–13 [viewed 2022-07-06]. Available from: https://doi.org/10.1016/j.jmmm.2007.04.012

[99] QING, Y. et al. Epoxy-silicone filled with multi-walled carbon nanotubes and carbonyl iron particles as a microwave absorber. *Carbon* [online]. 2010, **48**, 4074–4080 [viewed 2022-07-06]. Available from: https://doi.org/10.1016/j.carbon.2010.07.014

[100] KONG, J. et al. Electromagnetic wave absorption properties of Fe_3O_4 octahedral nanocrystallines in gigahertz range. *Appl. Phys. A* [online]. 2011, **105**, 351–354 [viewed 2022-07-06]. Available from: https://doi.org/10.1007/s00339-011-6593-8

[101] JURČA, M. et al. Reduced percolation threshold of conductive adhesive

through nonuniform filler localization: Monte Carlo simulation and experimental study. *Composites science and technology* [online]. 2021, vol. **214**, 29 108964 [viewed 2022-07-06]. Available from: https://doi.org/10.1016/j.compscitech.2021.108964

[102] QING, Y. et al. Microwave-absorbing and mechanical properties of carbonyl-iron/epoxy- silicone resin coatings. *J. Magn. Magn. Mater.* [online]. 2009, **321**, 25-28 [viewed 2022-07-06]. Available from: https://doi.org/10.1016/j.jmmm.2008.07.011

[103] PINHO, M.S. et al. Performance of radar absorbing materials by waveguide measurements for X- and Ku-band frequencies. *Eur. Polym. J.* [online]. 2002, **38,** 2321e2327 [viewed 2022-07-06]. Available from: https://doi.org/10.1016/S0014-3057(02)00118-0

[104] VILČÁKOVÁ, Jarmila et al. Enhanced Charpy impact strength of epoxy resin modified with vinyl-terminated polydimethylsiloxane. *Journal of Applied Polymer Science* [online] 2018, **135**, 45720 [viewed 2022-07-06]. Available from: https://doi.org/10.1002/app.45720

[105] KRUŽELÁK, J. et al. Cross-linking, mechanical, dynamical, and EMI absorption shielding effectiveness of NBR based composites filled with combination on ferrite and carbon based fillers. *Polymers Advanced Technologies* [online]. 2021, 1-11 [viewed 2022-07-06]. Available from: https://doi.org/10.1002/pat.5305

[106] BARR, R. et al. ELF and VLF radio waves. *J. Atmospheric Sol.-Terr. Phys*. [online]. 2000, **62**, 1689-1718 [viewed 2022-07-06]. Available from: https://doi.org/10.1016/S1364-6826(00)00121-8

[107] LOPATIN, A.V. Polymer Magnetic Composites for Microwave Absorbers [online]. 9788073188443. Doctoral Thesis. Tomas Bata University, Faculty of Technology, Supervisor Prof. Ing. Petr Sáha, Ph.D. [viewed 2022-07-06]. Available from: https://vufind.katalog.k.utb.cz/Record/57651

[108] KOTSUKA, Y. Electromagnetic Wave Absorbers: Detailed Theories and Applications. *Wiley & Sons, Inc.* [online]. 2019 [viewed 2022-07-06]. Available from: https://lccn.loc.gov/2019003710

LIST OF FIGURES

LIST OF TABLES

LIST OF SYMBOLS AND ABBREVIATIONS

DGEBA	diglycidyl ether bisphenol A
PDMS	polydimethylsiloxane
DETA	diethylentriamine
DCP	dicumyl peroxide
MPS	multiphase polymer systems
DMA	dynamic mechanical analyze
MF	magnetic field
RF	radio frequency
σ	electrical conductivity
ε^*	complex permittivity
ε'	real part of complex permittivity
ε''	imaginary part of complex permittivity
μ^*	complex permeability
μ'	real part of complex permeability
μ''	imaginary part of complex permeability
H_i	magnetic field
B	magnetic induction
Bs	saturation magnetization
Br	remanence
Hc	coercivity
δ	skin depth
ER	epoxy resin
SBR	styrene-butadiene rubber
NBR	acrylonitrile-butadiene rubber
TPE	thermoplastic elastomer
iPP	isostatic propylene

CPC	conductive polymer composite
CB	carbon black
CNT	carbon nanotubes
PU	polyurethanes
SWNT	single-wall nanotubes
MWNT	multi-wall nanotubes
Tg	glass transition temperature
E´	dynamic storage modulus
T	temperature
RL	reflection loss
SE	shielding effectiveness
SE_R	shielding effectiveness reflection
SE_A	shielding effectiveness absorptin
λ	wave length
p	aspect ratios
MnZn	manganese-zinc
CI	carbonyl iron
CPC	conductive polymer composites
DC	direct current
AC	amplitude current
PC	percolation threshold
wt.%	weight concentration
vol.%	volume concentration
SEM	scanning electron microscopy
EMI	electromagnetic interference
EWA	electromagnetic wave absorbers
RCS	radar cross section
EPC	electromagnetic polymer composites

RA	radio absorber
RF	radio frequency
RAM	radio absorbing material
EMC	electromagnetic compatibility
MUT	material under test
SAR	specific absorption rate

CURRICULUM VITAE

Personal information

Name	Marek Gořalík
Address	Martinice 170, 769 01, Czech Republic
Telephone	+420 732 450 785
E-mail	goralik@ft.utb.cz, mgoralik@gmail.com
Nationality	Czech
Date of birth	12. 03. 1979

Education and training

Dates	2014 – present
Title of qualification awarded	Doctoral study – expected defence 2022
Principal branch	Technology of Macromolecular Substances
Organisation providing education	Centre of Polymer Systems – Tomas Bata University in Zlín

Dates	2001–2004
Title of qualification awarded	Ing.
Principal branch	Chemistry and Materials Technology
Organisation providing education	Faculty of Technology – Tomas Bata University in Zlín

Dates	1998-2001
Title of qualification awarded	Bc.
Principal branch	Chemistry and Materials Technology
Organisation providing education	Faculty of Technology – Tomas Bata University in Zlín

LIST OF PUBLICATIONS

1. **GOŘALÍK, M**., JURČA, M., BUBULINCA, C., BABAYAN, V.A., VILČÁKOVÁ, J., KAZANTSEVA, N.E., SÁHA, P. Engineering Magnetic Type Radio-Absorbers Based on Composites with a Dual-Phase Polymer Matrix. *Electronic Materials Letters*. 2022, **18**, p. 345–360. https://doi.org/10.1007/s13391-022-00351-x

2. YADAV, R.S., KUŘITKA, I., VILČÁKOVÁ, J., MACHOVSKÝ, M., ŠKODA, D., URBÁNEK, P., MASAŘ, M., **GOŘALÍK, M**., URBÁNEK M., KALINA, L., and HAVLICA, J. Polypropylene Nanocomposite Filled with Spinel Ferrite NiFe2O4 Nanoparticles and In-Situ Thermally-Reduced Graphene Oxide for Electromagnetic Interference Shielding Application. *Nanomaterials*. 2019, **9**(4), p. 621 -674. https://doi.org/10.3390/nano9040621

3. STEJSKAL, J., SAPURINA, I., VILČÁKOVÁ, J., PLACHÝ, T., SEDLAČÍK, M., BUBULINCA, C., **GOŘALÍK, M**., TRCHOVÁ, M., KOLSKÁ, Z., and PROKEŠ, J. Conducting and Magnetic Composites Polypyrrole Nanotubes/Magnetite Nanoparticles: Application in Magnetorheology. *Applied Nano Materials*.2021, **4**, 2247-2256. https://dx.doi.org/10.1021/acsanm.1c00063

4. KRUŽELÁK, J., MEDLENOVÁ, E., KVASNIČÁKOVÁ, A., DOSOUDIL R., HUDEC, I., and **GOŘALÍK, M**. Rubber Magnetic Composites Cross-Linked with Peroxide Curing Systems. *Polymer Science Series B*. 2019, **61**(6), 865-873. https://doi.org/10.1134/S1560090419060071

5. KVASNIČÁKOVÁ, A., KRUŽELÁK, J., MEDLENOVÁ, E., DOSOUDIL, R., HUDEC, I., and **GOŘALÍK, M**. Rubber magnets cured with peroxide and coagents. *Journal of Elastomers And Plastics*. 2020, **52**(3), 253-270. https://doi.org/10.1177/0095244319846176

6. JURČA, M., VILČÁKOVÁ, J., **GOŘALÍK, M**., MASAŘ, M., PONÍŽIL, P., KAZANTSEVA, N., FOULGER, S.H., and SÁHA, P. Reduced percolation threshold of conductive adhesive through nonuniform filler localization: Monte Carlo simulation and experimental study. *Composites Science and Technology*. 2021, **214**. doi: https://doi.org/10.1016/j.compscitech.2021.108964.

7. KRUŽELÁK, J., KVASNIČÁKOVÁ, A., HLOŽEKOVÁ, K., DOSOUDIL, R., **GOŘALÍK, M**., and HUDEC, I. Electromagnetic Interference Shielding and Physical-Mechanical Characteristics of Rubber Composites Filled with Manganese-Zinc Ferrite and Carbon Black. *Polymers*. 2021, **13** (4), 616. https://doi.org/10.3390/polym13040616

8. KRUŽELÁK, J., KVASNIČÁKOVÁ, A., BOCHKAREV, E.S., TUZHIKOV, O.O., **GOŘALÍK, M**., VILČÁKOVÁ, J., and HUDEC, I. Cross-linking, mechanical, dynamical, and EMI absorption shielding effectiveness of NBR based composites filled with combination on ferrite and carbon based fillers. *Polymers Advanced Technologies*. 2021, 1-11. https://doi.org/10.1002/pat.5305

9. KRUŽELÁK, J., KVASNIČÁKOVÁ, A., HLOŽEKOVÁ, K., PLAVES, R., DOSOUDIL, R., **GOŘALÍK, M**., VILČÁKOVÁ, J., and HUDEC, I. Mechanical, Thermal, Electrical Characteristics and EMI Absorption Shielding Effectiveness of Rubber Composites Based on Ferrite and Carbon Fillers. *Polymers*. 2021, **13** (17), 2937. https://doi.org/10.3390/polym13172937

OVERVIEW OF OTHER ACTIVITIES

Conference:

JURČA M., **GOŘALÍK M**., VILČÁKOVÁ J., FOULGER S.H., MASAŘ M., and KAZANTSEVA N. (2019), Enhanced electrical conductivity of immiscible blends filled with nickel particles. *ACS National Meeting* Orlando.

Studies abroad:

Doctoral study stays at the Institute of Natural and Synthetic Polymers at the Slovak University of Technology in Bratislava (Slovak Republic) 08/2021 - 09/2021

Vlastnosti polymerních kompozitů pohlcující elektromagnetické vlny

Electromagnetic wave absorbing properties of polymer composites

Doctoral Thesis